DOT/FAA/AR-10/36

Air Traffic Organization
NextGen & Operations Planning
Office of Research and
Technology Development
Washington, DC 20591

Fatigue Crack Initiation Test and Analysis of Corrosion Pits in Aluminum 7075-T7351, 4340 Steel, and D6AC Steel

June 2011

Final Report

This document is available to the U.S. public through the National Technical Information Service (NTIS), Springfield, Virginia 22161.

This document is also available from the Federal Aviation Administration William J. Hughes Technical Center at actlibrary.tc.faa.gov.

U.S. Department of Transportation
Federal Aviation Administration

NOTICE

This document is disseminated under the sponsorship of the U.S. Department of Transportation in the interest of information exchange. The United States Government assumes no liability for the contents or use thereof. The United States Government does not endorse products or manufacturers. Trade or manufacturer's names appear herein solely because they are considered essential to the objective of this report. The findings and conclusions in this report are those of the author(s) and do not necessarily represent the views of the funding agency. This document does not constitute FAA policy. Consult the FAA sponsoring organization listed on the Technical Documentation page as to its use.

This report is available at the Federal Aviation Administration William J. Hughes Technical Center's Full-Text Technical Reports page: actlibrary.tc.faa.gov in Adobe Acrobat portable document format (PDF).

Technical Report Documentation Page

1. Report No.	2. Government Accession No.	3. Recipient's Catalog No.
DOT/FAA/AR-10/36		

4. Title and Subtitle	5. Report Date
FATIGUE CRACK INITIATION TEST AND ANALYSIS OF CORROSION PITS IN ALUMINUM 7075-T7351, 4340 STEEL, AND D6AC STEEL	June 2011
	6. Performing Organization Code
7. Author(s)	8. Performing Organization Report No.
Daniel B. Garcia[1], Royce Forman[2], and David Shindo[2]	
9. Performing Organization Name and Address	10. Work Unit No. (TRAIS)
[1]Science Applications International Corporation 2450 NASA Parkway Houston, TX 77058 [2]Lyndon B. Johnson Space Center National Aeronautics and Space Administration 2101 NASA Parkway Houston, TX 77058-3696	
	11. Contract or Grant No.
12. Sponsoring Agency Name and Address	13. Type of Report and Period Covered
U.S. Department of Transportation Federal Aviation Administration Air Traffic Organization NextGen & Operations Planning Office of Research and Technology Development Washington, DC 20591	Final Report
	14. Sponsoring Agency Code ANE-111

15. Supplementary Notes

The Federal Aviation Administration Airport and Aircraft Safety R&D Division COTR was Cu Nguyen.

16. Abstract

The National Aeronautics and Space Administration Johnson Space Center (NASA-JSC) developed and executed a test program to evaluate the influence of hemispherical corrosion pits on the fatigue crack initiation and propagation properties in aluminum 7075-T7351, 4340 steel, and D6AC steel. In addition to the general corrosion pit influences, the effects of surface enhancements, such as shot peening and laser shock peening, were also studied. Once the fatigue test program was completed, an analysis effort was established with the objective of characterizing the test results with more accuracy than a typical surface crack model. In response to this objective, the NASA-JSC team developed a new NASGRO® software solution, called SC-31, which is based on a crack emanating from a hemispherical corrosion pit. This model was then used in the analysis to predict the test results.

The results specifically demonstrate that the aluminum and steel alloys behave differently with respect to fatigue crack initiation from hemispherical corrosion pits. The aluminum specimens were well characterized by the new fracture mechanics techniques and exhibited a general insensitivity to the residual stress field generated by shot peening. The steel specimens were better characterized by the endurance limit fatigue properties and exhibited sensitivities to residual stresses from shot peening or laser shock peening. This observation was particularly evident at lower applied load ratios. In addition to the predictions, the fracture surfaces were evaluated and documented so that correlations between the test results and analysis could be made.

17. Key Words	18. Distribution Statement
Corrosion pit, Fatigue, Initiation, Threshold, Aluminum, Steel	This document is available to the U.S. public through the National Technical Information Service (NTIS), Springfield, Virginia 22161. This document is also available from the Federal Aviation Administration William J. Hughes Technical Center at actlibrary.tc.faa.gov.

19. Security Classif. (of this report)	20. Security Classif. (of this page)	21. No. of Pages	22. Price
Unclassified	Unclassified	115	

Form DOT F 1700.7 (8-72) Reproduction of completed page authorized

ACKNOWLEDGEMENTS

The ability to complete this corrosion pit fatigue test and analysis program would not have been possible without the contributions of several individuals. The laboratory staff, particularly Frank Samonski, Ray Gonzalez, and Larry West, was responsible for performing the tests and acquiring the test results. Dr. Omar Hatamleh provided guidance and expertise regarding the specimen design and surface enhancements. The authors are also grateful to the members of the NASGRO development team, part of Jacobs Engineering Sciences Contract Group at the National Aeronautics and Space Administration Johnson Space Center (NASA-JSC) in Houston, Texas. Feng Yeh used a p-version finite element program to obtain the needed stress-intensity solution of a semi-circular crack from a hemispherical pit in a plate subjected separately to remote tension and bending. Yajun Guo developed the curve-fit solution, and Randall Christian programmed and incorporated the solution into the NASGRO fracture mechanics analysis software package. Finally, the authors would like to thank the NASA-JSC W. David Beverly Receiving Inspection and Test Facility for the use of their equipment and assistance during the fractographic examination.

TABLE OF CONTENTS

		Page
EXECUTIVE SUMMARY		xiii
1.	INTRODUCTION	1
1.1	Problem Statement and Motivation	1
1.2	Objective and Approach	1
2.	MATERIALS AND METHODS	2
2.1	Material Selection and Properties	2
2.2	Surface Enhancements	3
2.2.1	Al 7075-T7351 Residual Stress Measurements	3
2.2.2	4340 Steel Residual Stress Measurements	4
2.2.3	D6AC Steel Residual Stress Measurements	5
2.2.4	Summary of Residual Stress Measurements	5
2.3	Fatigue Properties	6
2.4	Fatigue Crack Growth Properties	9
2.5	Specimen Design	10
2.6	Fatigue Test Methods	12
3.	FATIGUE TESTS	15
3.1	Al 7075-T7351 Specimens	15
3.2	4340 Steel Specimens	18
3.3	D6AC Steel Specimens	20
4.	FATIGUE TEST RESULTS	21
4.1	Al 7075-T7351 Initiation Test Results	22
4.2	Al 7075-T7351 Fatigue Propagation Results	31
4.3	4340 Steel Initiation Test Results	32
4.4	4340 Steel Propagation Test Results	39
4.5	D6AC Steel Initiation Test Results	41
4.6	D6AC Steel Propagation Test Results	46
5.	ANALYSIS AND DISCUSSION	47
5.1	NASGRO Corrosion Pit Model	48
5.2	Corrosion Pit EIFS Fatigue Analysis	50
5.3	Al 7075-T7351 Corrosion Pit EIFS Predictions	51
5.4	4340 Steel Corrosion Pit EIFS Predictions	54

5.5 D6AC Steel Corrosion Pit EIFS Predictions 55
5.6 Fatigue Threshold Assessment 57
5.7 Al 7075-T7351 Threshold and Endurance Stress Predictions 58
5.8 4340 Steel Threshold and Endurance Stress Predictions 61
5.9 D6AC Steel Threshold and Endurance Stress Predictions 63
5.10 Fatigue Crack Propagation Assessment 65

6. FRACTOGRAPHIC OBSERVATIONS 70

6.1 Al 7075-T7351 Fractographic Observations 70
6.2 4340 Steel Fractographic Observations 72
6.3 D6AC Steel Fractographic Observations 74
6.4 Discussion of Fractographic Observations 75

7. SUMMARY AND CONCLUSIONS 75

8. REFERENCES 77

APPENDIX A—FATIGUE SPECIMEN FRACTURE SURFACES

LIST OF FIGURES

Figure		Page
1	Residual Stress Measurements for Al 7075-T7351	3
2	Residual Stress Measurements for 4340 Steel	4
3	Residual Stress Measurements for D6AC Steel	5
4	Residual Stress Measurements for all Three Materials and the Surface Treatments Used	6
5	The S-N Fatigue Properties for the Al and Steel Alloys	7
6	Notch Sensitivity of Al and Steel Alloys as a Function of Pit Radius	8
7	Fatigue Notch Factors as a Function of Pit Radius for Al and Steel Alloys	9
8	NASGRO Fatigue Crack Growth Curves for a Load Ratio of $R = 0.1$	10
9	Schematic of Dogbone Specimen and Corresponding Photograph	11
10	Corrosion Pit Process for Al Alloys Using the Electrochemical Process	11
11	Potential Drop Leads Shown on the Dogbone Specimens Loaded in the Test Frames	13
12	The Load Frames	14
13	Fatigue Crack Initiation and Propagation Test Process	14
14	Al 7075-T7351 Test Results for Bare and Nominal Shot-Peened Specimens, $R = 0.1$	29
15	Al 7075-T7351 Test Results for Bare and Nominal Shot-Peened Specimens, $R = 0.7$	29
16	Al 7075-T7351 Test Results for the Heavy-Peened Specimens, $R = 0.1$	30
17	Al 7075-T7351 Test Results for the Heavy-Peened Specimens, $R = 0.7$	30
18	Al 7075-T7351 Fatigue Crack Growth Comparisons From a Corrosion Pit	32
19	4340 Steel Fatigue Test Results for all Surface Conditions, $R = 0.1$	38
20	4340 Steel Fatigue Test Results for all Surface Conditions, $R = 0.7$	39
21	4340 Steel Fatigue Crack Growth Rate Data Compared to Corrosion Pit Data With Supporting Fracture Surface Images	40

22	D6AC Steel Bare and Shot-Peened Test Results for $R = 0.1$	46
23	D6AC Steel Bare and Shot-Peened Test Results for $R = 0.7$	46
24	D6AC Steel Fatigue Crack Growth Comparisons of a Corrosion Pit	47
25	A Comparison of Surface Crack and Corrosion Pit Crack Solutions	48
26	NASGRO SC-31 Solution and Generalized Threshold Stress Predictions	49
27	The EIFS Predictions for Al 7075-T7351, $R = 0.1$ and Reference Geometry	52
28	The EIFS Predictions for Al 7075-T7351, $R = 0.7$	52
29	The EIFS Predictions for Al 7075-T7351 Heavy Peen, $R = 0.1$	53
30	The EIFS Predictions for Al 7075-T7351 Heavy Peen, $R = 0.7$	53
31	The EIFS Predictions for 4340 Steel, $R = 0.1$	55
32	The EIFS Predictions for 4340 Steel, $R = 0.7$	55
33	The EIFS Predictions for D6AC Steel, $R = 0.1$	56
34	The EIFS Predictions for D6AC Steel, $R = 0.7$	56
35	Predicted Threshold Stress for Al 7075-T7351	58
36	Predicted Threshold Stress for Al 7075-T7351 Heavy Peen	59
37	Predicted Threshold Stress for all Al 7075-T7351 Test Results	59
38	Predicted Threshold Stresses at $R = 0.1$ Showing Endurance Limit Predictions	60
39	Predicted Threshold Stress for the 4340 Steel $R = 0.1$ Test Results	62
40	Predicted Threshold Stress for the 4340 Steel $R = 0.7$ Test Results	62
41	Predicted Threshold Stress for the D6AC Steel $R = 0.1$ Test Results	64
42	Predicted Threshold Stress for the D6AC Steel $R = 0.7$ Test Results	64
43	Comparison of NASGRO K_{max} Pedictions With Test Data	66
44	Mapping Procedure for 4340-PS-35 to Determine the Corrected K_{max}	67
45	Procedure to Correct for Crack Size and K_{max} for 4340-PS-LP-05	67
46	The K_{max} Corrected Test Results for 4340-PS-35 Compared to Original and NASGRO Data Sets	68

47 The K_{max} Corrected Test Results for 4340-PS-LP-05 Compared to Original and NASGRO Data Sets 69

48 Fracture Surface of 7075-PS-34 71

49 Fracture Surface of 7075-PS-SP-7 71

50 Fracture Surface of 7075-PS-SP2-7 72

51 Fracture Surface of 4340-PS-34 73

52 Fracture Surface of 4340-PS-LP-05 73

53 Fracture Surface of 4340-PS-SP-11 74

54 Fracture Surface of D6AC-PS2-18 74

55 Fracture Surface of D6AC-PS-SP-18 75

LIST OF TABLES

Table		Page
1	Material Properties and Surface Enhancement Method	2
2	Stress-Life Properties for the Al and Steel Alloys	6
3	NASGRO Equation Coefficients	10
4	High-Level Test Matrix for all Three Materials	15
5	Al 7075-T7351 Bare Specimens Tested at $R = 0.1$	16
6	Al 7075-T7351 Bare Specimens Tested at $R = 0.7$	16
7	Al 7075-T7351 Nominal Shot-Peened Specimens Tested at $R = 0.1$	17
8	Al 7075-T7351 Nominal Shot-Peened Specimens Tested at $R = 0.7$	17
9	Al 7075-T7351 Heavy-Peened Specimens Tested at $R = 0.1$	17
10	Al 7075-T7351 Heavy-Peened Specimens Tested at $R = 0.7$	18
11	4340 Steel Bare Specimens Tested at $R = 0.1$	18
12	4340 Steel Bare Specimens Tested at $R = 0.7$	19
13	4340 Steel Shot-Peened Specimens Tested at $R = 0.1$	19
14	4340 Steel Shot-Peened Specimens Tested at $R = 0.7$	19
15	4340 Steel Laser-Peened Specimens Tested at $R = 0.1$	20
16	4340 Steel Laser-Peened Specimens Tested at $R = 0.7$	20
17	D6AC Steel Shot-Peened Specimens Tested at $R = 0.1$	20
18	D6AC Steel Shot-Peened Specimens Tested at $R = 0.7$	21
19	D6AC Steel Bare Specimens Tested at $R = 0.1$	21
20	D6AC Steel Bare Specimens Tested at $R = 0.7$	21
21	Al 7075-T7351 Bare Fatigue Test Results for $R = 0.1$	23
22	Al 7075-T7351 Bare Fatigue Test Results for $R = 0.7$	24
23	Al 7075-T7351 Nominal Shot-Peened Fatigue Test Results for $R = 0.1$	25
24	Al 7075-T7351 Nominal Shot-Peened Fatigue Test Results for $R = 0.7$	26
25	Al 7075-T7351 Heavy-Peened Fatigue Test Results for $R = 0.1$	27
26	Al 7075-T7351 Heavy-Peened Fatigue Test Results for $R = 0.7$	28
27	4340 Steel Bare Fatigue Test Results for $R = 0.1$	33
28	4340 Steel Bare Fatigue Test Results for $R = 0.7$	34
29	4340 Steel Shot-Peened Fatigue Test Results for $R = 0.1$	35
30	4340 Steel Shot-Peened Fatigue Test Results for $R = 0.7$	35
31	4340 Steel Laser-Peened Fatigue Test Results for $R = 0.1$	36
32	4340 Steel Laser-Peened Fatigue Test Results for $R = 0.7$	37
33	D6AC Steel Bare Fatigue Test Results for $R = 0.1$	42
34	D6AC Steel Bare Fatigue Test Results for $R = 0.7$	43
35	D6AC Steel Shot-Peened Fatigue Test Results for $R = 0.1$	44
36	D6AC Steel Shot-Peened Fatigue Test Results for $R = 0.7$	45

LIST OF SYMBOLS AND ACRONYMS

ΔK	Stress-intensity factor range
Al	Aluminum
a/c	Radius/pit depth (crack aspect ratio)
a or c	Crack depth
K	Stress-intensity factor
K_f	Fatigue notch factor
$K_{\max}$	Maximum stress-intensity factor
K_t	Stress concentration factor
L	Longitudinal orientation
N_f	Number of cycles in current step
N_{step}	Number of cycles per step
q	Notch sensitivity
R	Load ratio
S_{eq}	Equivalent stress used in fatigue life calculations
$S_{\max}$	Maximum applied stress
EIFS	Equivalent initial flaw size
FCGR	Fatigue crack growth rate
FTA	Fatigue Technology Associates
MMPDS	Metallic Materials Properties Development Standardization
NASA-JSC	National Aeronautics and Space Administration Johnson Space Center
S-N	Stress-life
SIF	Stress-intensity factor
T-S	Transverse-short

EXECUTIVE SUMMARY

A test program was developed and executed by the National Aeronautics and Space Administration Johnson Space Center (NASA-JSC) to evaluate the influence of hemispherical corrosion pits on the fatigue crack initiation and propagation properties in aluminum 7075-T7351, 4340 steel, and D6AC steel. In addition to the general corrosion pit influences, the effects of surface enhancements, such as shot peening and laser shock peening, were also studied. Once the fatigue test program was completed, an analysis effort was established with the objective of characterizing the test results with more accuracy than a typical surface crack model. In response to this objective, the NASA-JSC team developed a new NASGRO® solution called SC-31 that is based on a crack emanating from a hemispherical corrosion pit. The model takes a first order approximation by modeling a crack emanating from a hemispherical notch in a concentric fashion. This model was then used in the analysis to predict the test results by using a threshold-based assessment or a life prediction assessment.

The aluminum specimens exhibited a relative insensitivity to the surface enhancements for crack initiation in pits ranging from 0.01-0.08 inch, and localized yielding was only a factor for smaller pits operated at an elevated load ratio. Residual stresses created by the surface enhancements, as well as localized yielding, improved the crack initiation behavior from the base of the pits for both the 4340 and D6AC steel specimens. This behavior was evident at high and low load ratios. In particular, laser shock peening-induced residual stresses produced a significant increase in the crack initiation stress even when localized yielding was not a factor.

The aluminum specimen test results were well characterized by the new fracture mechanics techniques implemented in the new NASGRO SC-31 model, but the steel specimens were better characterized by the endurance limit fatigue properties. This endurance limit approach was overly conservative for the aluminum tests, but provided a reasonably conservative estimate for the steels. This behavior is due to the notch behavior and reflects the condition where the notch fatigue concentration factor is similar to the quasi-static stress concentration factor.

In addition to the predictions, the fracture surfaces were evaluated and documented so that correlations between the test results and analysis could be made. Fracture surface examinations revealed the majority of cracks initiated from the base of the pits and propagated as a surface crack simultaneously into the depth and around the pit circumference. At this point, surface compressive residual stresses acted to constrain the growth. This resulted in cracks with the widest region located subsurface rather than on the surface.

1. INTRODUCTION.

A test program was performed at the National Aeronautics and Space Administration Johnson Space Center (NASA-JSC) in support of the Federal Aviation Administration to examine fatigue crack initiation and propagation from corrosion pits in aluminum (Al) and steel alloys used in aerospace applications. A total of 149 fatigue initiation and propagation fatigue tests were performed on three aerospace alloys with corrosion pits and a subsequent analytical effort was established to characterize the results. The testing also incorporated two forms of surface enhancements that included shot peening and laser shock peening. This report documents the motivation behind the test program and details the testing and analytical efforts that support the observations and conclusions.

1.1 PROBLEM STATEMENT AND MOTIVATION.

Aerospace structural materials such as Al 7075-T7351, 4340 steel, and D6AC steel are susceptible to pitting when operated in a corrosive environment. Corrosion pits can readily act as crack initiation regions because of the metallurgical damage as well as the stress concentration influence. Throughout this report, the term initiation refers to the process by which a fatigue crack is formed and reaches a sufficient size, at which time it can be characterized by fracture mechanics methods. Current fracture mechanics tools like NASGRO® [1] and AFGROW [2] do not capture the geometry of the corrosion pit with standard surface crack solutions, so the influences of the corrosion pit on the fatigue crack growth and the initiation/nucleation properties are not evident. The primary motivation of this project was to enhance the fracture mechanics understanding of crack initiation and propagation from a corrosion pit.

Surface treatment methods, such as shot peening and laser shock peening, can be implemented to enhance the fatigue initiation resistance and improve fatigue crack growth behavior in materials. For this reason, surface enhancements, such as shot peening and laser shock peening (also referred to as laser peening), were also evaluated during this project. The results from all three surface conditions were assessed and compared with particular emphasis placed on the fatigue crack initiation and propagation from the corrosion pit.

1.2 OBJECTIVE AND APPROACH.

This project was initiated because fatigue crack initiation and propagation associated with corrosion pits cannot be modeled effectively with standard fracture mechanics solutions. The objective of this project was to advance the fundamental understanding of the mechanics of fatigue crack initiation and propagation processes from corrosion pits in Al 7075-T7351, 4340 steel, and D6AC steel with a variety of surface conditions. The three surface conditions chosen for this project were bare (no treatment), shot peened, and laser peened.

The approach consisted of two aspects: testing and analysis. The experimental program incorporated mechanical fatigue crack initiation and propagation testing that encompassed three alloys, three different surface treatment conditions, multiple corrosion pit sizes, and two applied load ratios. Analytically, the approach included implementing fracture mechanics software (i.e., NASGRO) and techniques to characterize and/or predict the behavior of cracks initiating and propagating from corrosion pits. This also included the creation of a new corrosion pit solution

for NASGRO. The entire corrosion pit fatigue test program, subsequent analysis, and specific conclusions obtained during both the experimental and analytical phases are detailed in this report.

2. MATERIALS AND METHODS.

To satisfy the objectives of the investigation, three materials were evaluated that included one Al alloy and two steel alloys. During the program, knowledge of the fatigue, fracture, and notch properties were necessary to interpret the results, and these properties are discussed in detail. In this report, the term notch is used synonymously with the term pit (as in corrosion pit). In addition to the materials, the specimen fabrication, identification, and corrosion pitting methods are also discussed. Finally, the fatigue testing procedures are highlighted.

2.1 MATERIAL SELECTION AND PROPERTIES.

The three aerospace materials chosen for the test program were Al 7075-T7351, 4340 steel, and DCAC steel. The raw material for the program was originally obtained from plate stock in the appropriate heat-treat condition. All specimens were tested in the transverse-short (T-S) orientation under a variety of surface conditions that included bare (no treatment), shot peened, and laser shock peened. The general tensile properties and surface conditions are listed for reference in table 1.

Table 1. Material Properties and Surface Enhancement Method

Material	Yield (ksi)	Ultimate (ksi)	Orientation Tested	Surface Condition Tested	Surface Enhancement Parameters
Al 7075-T7351	63	73	T-S	Bare	NA
				Nominal shot peen	0.0023″ glass shot, 8-12 almen, 100% coverage repeated 2 times
				Heavy peen	0.125″ shot, 5-7 Y2 almen, 100% coverage, repeated 5 times
4340 Steel	175	190	T-S	Bare	NA
				Shot peen	8-12 almen 100% coverage
				Laser peen	Power density 8GW/cm^2, 18-ns pulse, 16J laser energy, 3 layers, 3.33- x 3.33-mm spot size
D6AC Steel	80	160	T-S	Bare	NA
				Shot peen	S-230 (steel 0.023″), 8-12 almen, 100% coverage

NA = Not applicable

2.2 SURFACE ENHANCEMENTS.

The surface enhancements generated residual stress fields in the specimens, and it was important to understand each respective stress field to determine how they influence the corrosion pit fatigue tests. Specific surface enhancement parameters for the various surface conditions are also provided in table 1. From each set of specimens selected for the fatigue tests, one was chosen for residual stress measurements, which was performed using the slitting method [3 and 4]. This technique is destructive, so the selected specimen could not be used for further fatigue testing. For reference, none of the bare specimens from any of the three materials were selected for residual stress measurements.

2.2.1 Al 7075-T7351 Residual Stress Measurements.

As shown in table 1, Al 7075-T7351 had two forms of shot peening performed, a nominal shot peen and a heavy shot peen (or heavy peen). The results from the residual stress measurements in the Al specimens are shown in figure 1. It is apparent that the heavy-peened specimen had a larger magnitude peak compressive stress but a steeper stress gradient compared to the nominal shot peen condition. For both specimens, the residual stress field became tensile at approximately 0.050″ into the depth of the specimen.

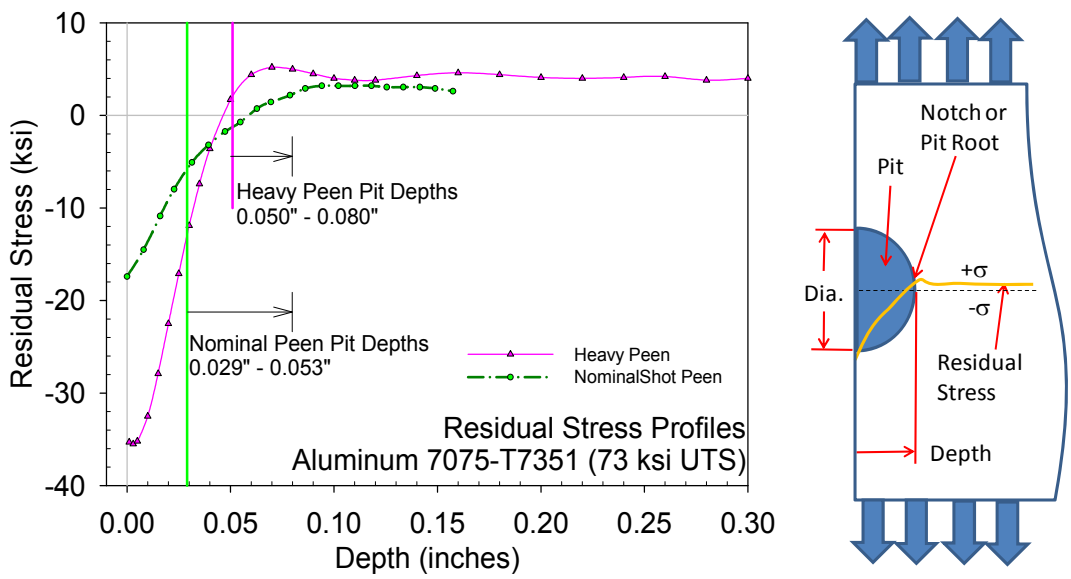

Figure 1. Residual Stress Measurements for Al 7075-T7351

As an additional reference, the ranges of corrosion pit depths are also shown in figure 1 for the nominal shot peen and heavy peen, respectively. For completeness, a schematic of the sectioned pit geometry with respect to the residual stress field is shown in figure 1 next to the residual stress plot. The smaller pits in the nominal shot-peened specimens were completely encompassed by the compressive residual stress field, but the root depths of the larger pits crossed into the tensile region. The root depth for all the heavy-peened specimens crossed into the tensile region. This implies that the effect of the residual stress was more pronounced at the surfaces of the corrosion pits than at the root of the pits.

2.2.2 4340 Steel Residual Stress Measurements.

The 4340 steel was the only material that implemented the laser-peened specimens in addition to the conventional shot-peened specimens. Laser peening can generate very high magnitude residual compressive stresses with gradual stress gradients. The laser-peened residual stress profile is compared to the shot-peened residual stress profile in figure 2 for the 4340 steel.

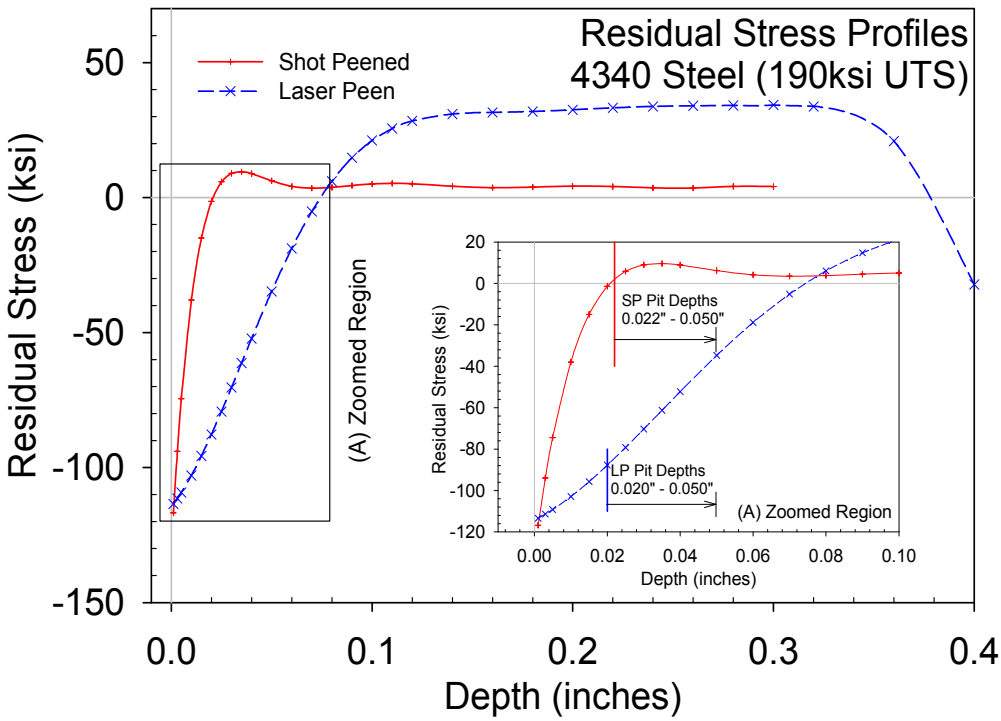

Figure 2. Residual Stress Measurements for 4340 Steel

The inset in figure 2 shows the compressive region in greater detail. Although the surface residual stress for the two methods was approximately the same (~ -120 ksi), the laser-peened residual stress remained compressive up to a depth of approximately 0.080″ while the shot-peened residual stress turned positive at approximately 0.020″. These results show that the laser-peened residual stress remained compressive over a distance of four times that of the shot-peened surface. It should also be noted that the laser-peened resultant tensile field was also approximately four times greater than the shot-peened resultant tensile field. This observation is consistent with expectations based on equilibrium.

Within the inset are the ranges of corrosion pit depths tested for this program on the 4340 steel. The depth of the notch root for the smallest pit tested in the shot-peened condition corresponds with zero residual stress, but the larger pit sizes had depths that spanned into the residual tensile stress field. All the laser-peened specimens had corrosion pits that were encompassed by the compressive residual stress field generated by the laser peening.

2.2.3 D6AC Steel Residual Stress Measurements.

The D6AC steel material was only tested in the bare and shot-peened conditions, and the results of the shot-peening residual stress measurements are shown in figure 3. For reference, the pit depth ranges for the shot-peened specimens are shown, and it is apparent that the root of the smallest pit depth crossed into the tensile residual stress region. All shot-peened D6AC steel specimens had corrosion pits in which some region of the pit crossed into the tensile residual stress field.

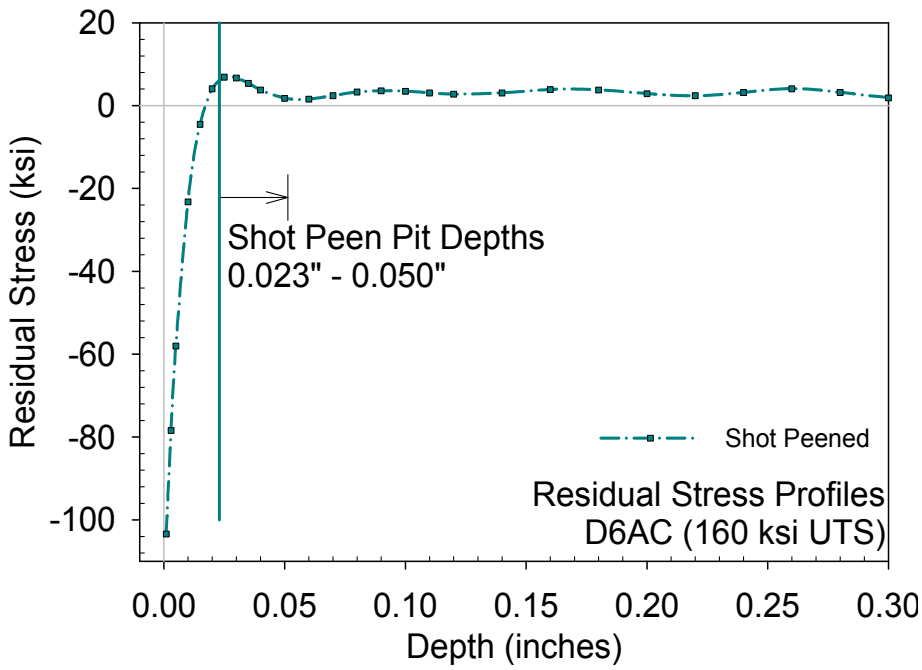

Figure 3. Residual Stress Measurements for D6AC Steel

2.2.4 Summary of Residual Stress Measurements.

To be complete, the residual stresses for all three materials are shown in figure 4 for comparison. The measurements show that the shot peening on the D6AC and 4340 steels generated very similar residual stress profiles. The magnitude of the residual stress profiles on the steels was much greater than the Al, and the laser-peened surface enhancement method generated the most gradual stress gradient of the methods shown.

Comparing the residual stress measurements to the corrosion pit depths used for this study, it is interesting to note that the root of the majority of corrosion pit depths crossed into the tensile residual stress region. The laser-peened 4340 steel was the only specimen in which the residual stress field encompassed the entire corrosion pit. Throughout this report, any correlation regarding the residual stress field and its effect on the corrosion pit during the fatigue crack initiation and propagation processes will be discussed.

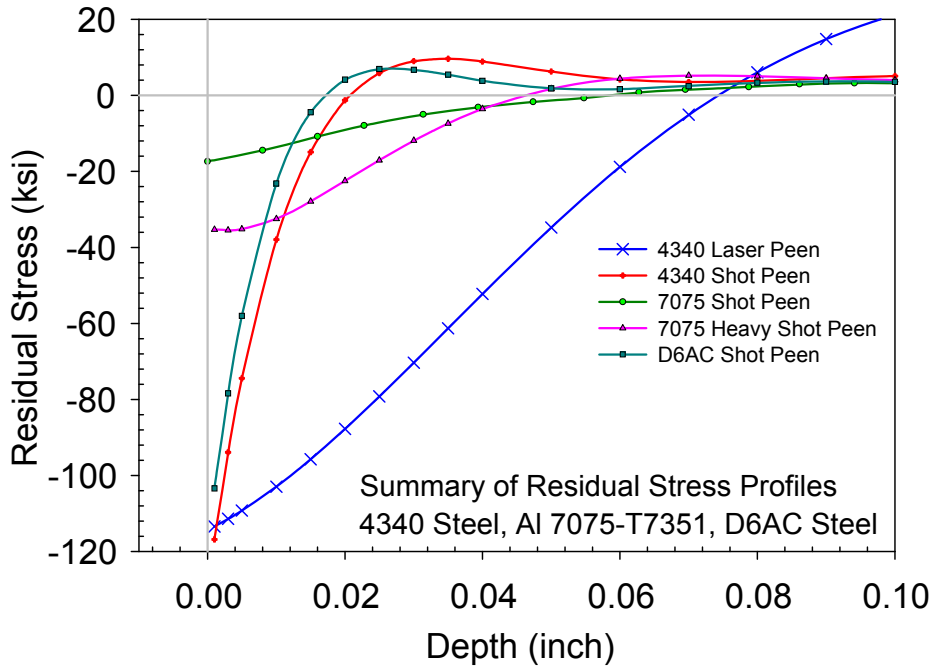

Figure 4. Residual Stress Measurements for all Three Materials and the Surface Treatments Used

2.3 FATIGUE PROPERTIES.

For reference, the fatigue properties (stress life (S-N)) for each of the materials used in this study are provided in table 2 and shown graphically in figure 5. Specific fatigue data for the Al 7075-T7351 material was not available, so the Al 7075-T6 values and equations from Metallic Materials Properties Development Standardization (MMPDS) were used as a reference (although the temper was T6 rather than T7351) [5]. The 4340 steel was also obtained from MMPDS in the correct condition. The D6AC steel fatigue initiation properties were obtained from a literature survey, but the fatigue data corresponds to D6AC steel with a strength of 270 ksi instead of the appropriate 160 ksi used for this program [6]. It should also be noted that the fatigue data represents longitudinally oriented specimens, whereas the specimens tested were transversely oriented.

Table 2. Stress-Life Properties for the Al and Steel Alloys

Material (orientation)	Fatigue Data		
	Life Equation $K_t = 1.0$ [5 and 6]	S_{eq} (ksi)	Notch Sensitivity Parameter, α (in.)
Al 7075-T6 (L)	Log $N_f = 18.22\text{-}7.77 \log (S_{eq}\text{-}10.15)$	$S_{eq} = S_{max} (1\text{-}R)^{0.62}$	0.02
4340 steel (L)	Log $N_f = 9.31\text{-}2.73 \log (S_{eq}\text{-}83.4)$	$S_{eq} = S_{max} (1\text{-}R)^{0.59}$	0.0023
D6AC steel (L)	No equation		0.0031

L = Longitudinal

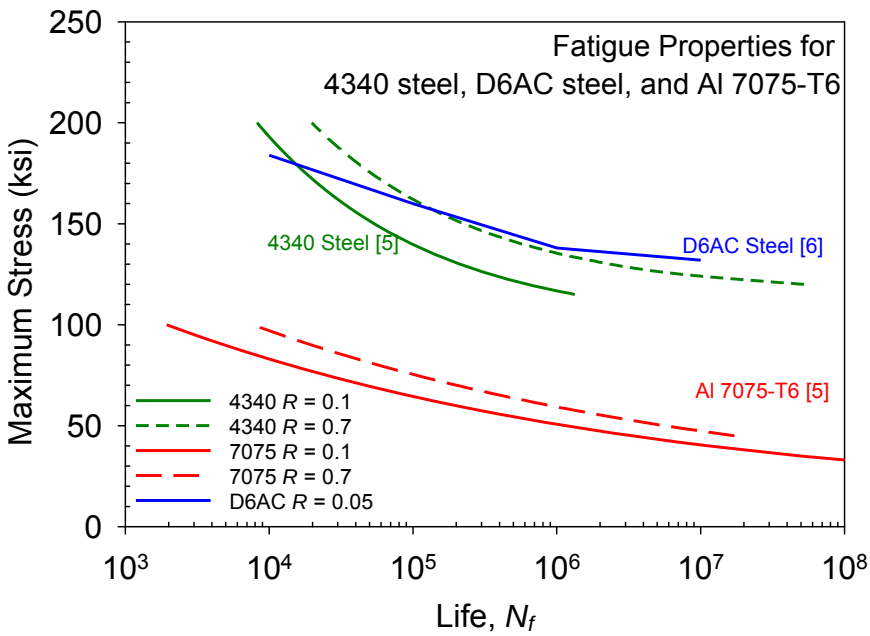

Figure 5. The S-N Fatigue Properties for the Al and Steel Alloys

As stated in the objective, the fatigue and fracture characteristics of cracks emanating from corrosion pits was the primary area of concentration; therefore, to fully explore the fatigue and fracture mechanics aspects of the problem, the influence of the notches needs to be discussed. The notches or stress concentrators used in this program can actually be generalized as hemispherical pits. This assumption was based on the corrosion pit processing approach, and details regarding the processes are provided in section 2.5.

A hemispherical pit should not be confused with a semi-circular notch because the boundary conditions are different. A hemispherical pit is a three-dimensional feature and cannot be generalized in two dimensions like a hole in a plate. The added dimensional constraint in three dimensions essentially lowers the stress concentration. The analytical stress concentration factor for a hole in an infinite plate is $K_t = 3.0$. The stress concentration factor, K_t, for a hemispherical pit in a plate is quoted as $K_t = 2.15\text{-}2.23$ [7 and 8]. The lower bound is from an empirical fit of a finite element model and the larger value is an analytical solution. For the remainder of this document, the K_t at a hemispherical pit is assumed to be 2.23.

In the mechanics of fatigue, materials are sensitive to the stress concentrator in a variety of ways. Al alloys are less sensitive to stress concentrators than steels under cyclic loading, and smaller pits are less sensitive to fatigue than larger pits. The notch sensitivity, q, is shown in equation 1 to be a function of the stress concentrator, K_t, and the fatigue notch factor, K_f [9 and 10]. This value was also determined empirically with equation 2, where α is the notch sensitivity parameter for a given material, and ρ is the radius of the notch.

$$q = \frac{K_f - 1}{K_t - 1} \tag{1}$$

$$q = \frac{1}{1 + \frac{\alpha}{\rho}} \tag{2}$$

Equation 1 and figure 6 show that as the notch sensitivity, q, increases and approaches 1.0, the fatigue notch factor, K_f, approaches the stress concentration factor, K_t. This means that larger pit sizes have greater influence on the fatigue life. As the notch sensitivity approaches zero, the notch fatigue factor approaches 1.0. This means that the effect of the pit on fatigue life becomes negligible as the pit size decreases.

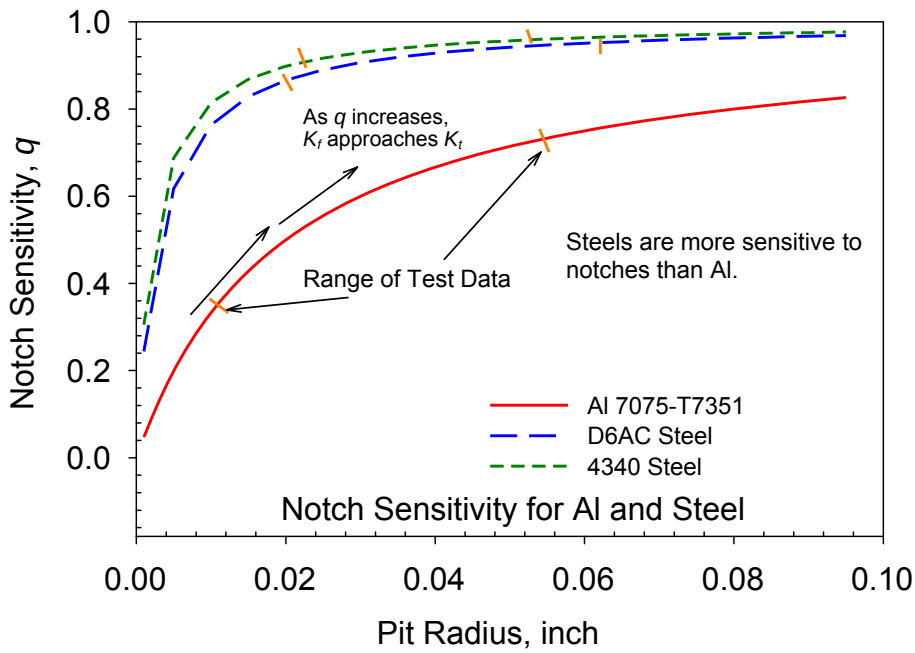

Figure 6. Notch Sensitivity of Al and Steel Alloys as a Function of Pit Radius

For reference, the notch sensitivity parameter, α, is provided in table 2, and the notch sensitivity as a function of pit depth is shown in figure 6 [9 and 10]. The fatigue notch factor, K_f, is shown as a function of pit depth in figure 7. The data shown in figures 6 and 7 demonstrate that the fatigue notch factors in Al alloys are much less sensitive to notches than the steel alloys. For example, a hemispherical notch between 0.02″ and 0.06″ in Al will have a fatigue notch factor between 40% and 85% of the stress concentration factor, but the same pit size in steels will have a notch fatigue factor that is greater than 90% of the stress concentrator.

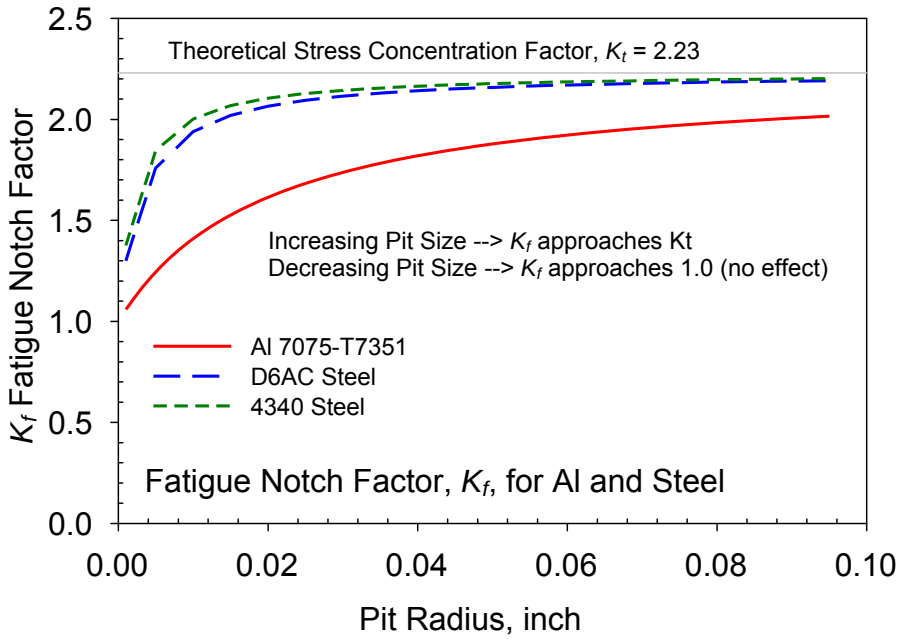

Figure 7. Fatigue Notch Factors as a Function of Pit Radius for Al and Steel Alloys

In summary, this section discusses the fatigue properties of Al 7075-T7351, 4340 steel, and D6AC steel with particular emphasis on fatigue notch properties. A few key points are reiterated below for quick reference:

- Notches in steels have more influence on fatigue life than Al alloys. This implies that notches reduce the fatigue life more in steels than Al alloys.

- The notch fatigue factor, K_f, increases and eventually approaches the stress concentration factor, K_t, as the pit size increases.

- As the pit size decreases, the notch fatigue factor approaches 1.0. This means that the influence of the pit on fatigue life is negligible for small pits (i.e., less than 0.01″).

2.4 FATIGUE CRACK GROWTH PROPERTIES.

For this effort, the NASGRO [1] software program was used for fatigue crack propagation evaluations. Within NASGRO, a database of materials, fatigue crack growth material properties, and coefficients exists that are used as inputs into the NASGRO equation. More information regarding the NASGRO equation can be found with the software, but the coefficients used for this study are provided in table 3 and shown graphically in figure 8 for a load ratio of $R = 0.1$. For reference, these coefficients are actually the results of new curve fits of the data and do not currently appear in the latest release of NASGRO. The older Al 7075-T7351 coefficients were also used during this evaluation.

Table 3. NASGRO Equation Coefficients

Material (Orientation)	NASGRO Equation Coefficients [1]											
	C	n	P	Q	SR	α	K_c	K_{Ic}	A_k	B_k	$DK1$	C_{th}
Al 7075-T7351 (T-L)	1.5E-8	3.3	0.75	0.75	0.3	2.0	44.3	25.0	1.0	1.0	0.95	0.0
4340 steel (T-L)	3.0E-9	2.4	0.25	0.25	0.3	2.5	132.7	90.0	0.75	0.5	2.8	0.0
D6AC steel (Forging)	6.0E-9	2.5	0.5	0.5	0.3	2.0	112.5	90.0	0.5	0.25	1.60	0.0

T-L = Transverse long

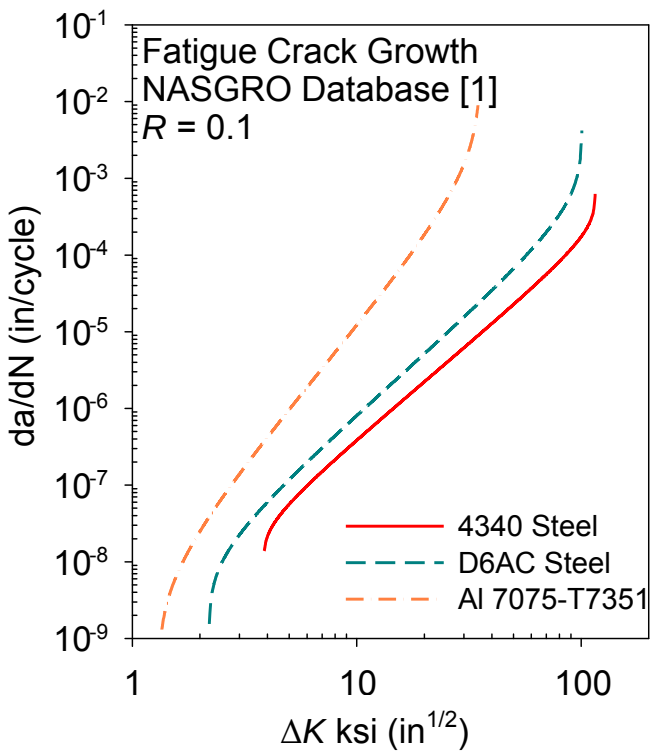

Figure 8. NASGRO Fatigue Crack Growth Curves for a Load Ratio of $R = 0.1$

2.5 SPECIMEN DESIGN.

The general approach for developing the fatigue test was to incorporate a dogbone-shaped specimen design. This implies that the grip section is wide and tapered to the gage section so that the highest stresses are in the gage section. This design forces the failure to the center of the specimen away from the grips. For each material used, the nominal gage thickness varied between 0.4″ and 0.5″ and the width was approximately 0.9″. All specimens were manufactured in the T-S orientation. A schematic and a photograph of a representative dogbone specimen are

provided in figure 9. After machining, a set of specimens from each material were either shot peened or laser shock peened. (The surface treatment process was discussed in section 2.2.)

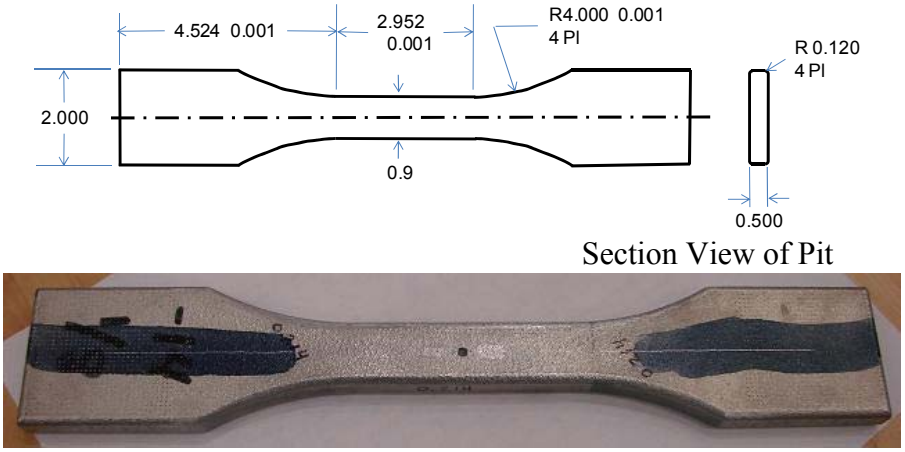

Figure 9. Schematic of Dogbone Specimen and Corresponding Photograph

After the surface treatments were applied, the specimens were prepared for the corrosion pit process. Within each specimen, a single hemispherical pit was centrally located, and each pit varied in diameter. The pit was created by drilling a hemispherical notch into the specimen and then corroding the hemispherical region later. It should be noted that this is a controlled method for generating a single, centrally located corrosion pit. In other words, the corrosion process was specifically isolated to the pit and the remaining surfaces of the specimen were not allowed to corrode. The process for each material is discussed separately, and figure 10 clarifies the explanation.

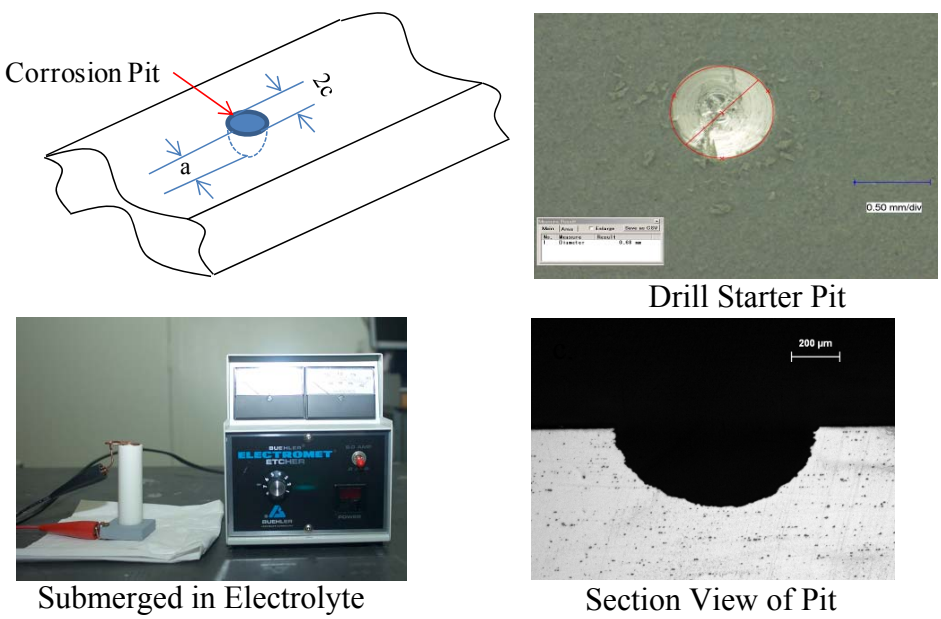

Figure 10. Corrosion Pit Process for Al Alloys Using the Electrochemical Process

The pitting process for the 7075-T7351 Al specimens required the use of a corrosion cell and electrolyte. The process for generating the corrosion pit included the following steps:

1. The specimen was polished, coated with primer, and then multiple coats of acrylic clear coat were applied.

2. The hemispherical notch was drilled into the specimen, which was centrally located on the specimen face.

3. A corrosion cell was created by attaching a small PVC (polyvinyl chloride) pipe to the specimen over the starter pit using wax, and then the pipe was filled with the electrolyte. The following chemistry was used to make the pitting electrolyte: 250-mL de-ionized water, 1.6-mL HNO3 (nitric acid), and 0.8-g NaCl (sodium chloride, or salt).

4. A copper electrode was used as the cathode, and a small direct current rectifier was used to apply 2.5 V to the corrosion pit for 10 minutes to 1 hour, depending on desired pit size.

5. After pitting, the corrosion cell was removed and the specimen was thoroughly rinsed. The coating was then removed using a solvent such as methanol or acetone.

The corrosion pitting process for the 4340 and D6AC steel specimens included the following steps:

1. The specimen was polished, primed, and then coated with multiple coats of acrylic clear coat.

2. A small drill bit was used to create the hemispherical starter pit in the material, which was centrally located on the specimen face.

3. Four drops of the electrolyte solution were placed on the starter pit and allowed to react for 45 minutes. The electrolyte consisted of 60% de-ionized water and 40% concentrated nitric acid.

4. After pitting, the specimen was rinsed, and the coating was removed using a solvent such as acetone or methanol.

2.6 FATIGUE TEST METHODS.

Once the specimens were machined and the corrosion pits were generated, they were measured and instrumented for data acquisition. Each corrosion pit was measured in the depth and surface width in addition to the general dogbone width and thickness. The Fatigue Technology Associates (FTA) data acquisition system was used for the test with the surface crack parameter selected. For the FTA to interpret the surface crack propagation, the specimens were instrumented for potential drop, as shown in figure 11. Although the notches were not true surface cracks, surface cracks did initiate from these notches, and the potential drop method could detect the crack propagation through the change in electric potential. The use of the direct

current potential drop method is preferred because it is a nondestructive method for monitoring crack propagation in a specimen.

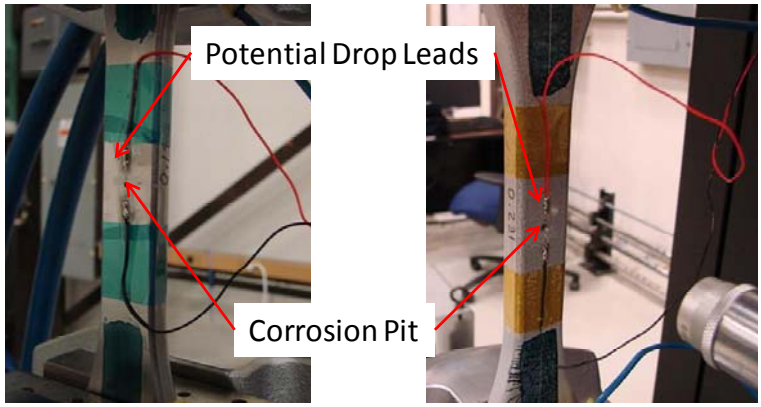

Figure 11. Potential Drop Leads Shown on the Dogbone Specimens Loaded in the Test Frames

After the specimens were instrumented, fatigue tests were performed on site at NASA-JSC. The test frames used for the experiments included the 22-kip load frame #2, 55-kip load frame #3, 110-kip load frame #4, and the 55-kip load frame #11. Photographs of each test frame are shown in figure 12.

The process for performing the corrosion pit initiation and propagation tests is shown in figure 13. At the beginning of the test phase, the specimens were cycled at a given starter load and load ratio, $R = 0.1$ or $R = 0.7$, until a crack was detected or 3 million cycles was reached. Each test machine was operated at the maximum capable frequency to ensure that the loads were reached and that the system avoided natural frequencies. If the FTA detected a crack of sufficient size, it was visually confirmed, or the test was continued until a visual crack was detected. If 3 million cycles was reached prior to detecting a crack, the load was increased approximately 10%, and the test was started again until a crack was detected or 3 million cycles was reached. This process, known as step testing, is used to determine a threshold load or endurance limit, depending on the critical parameter. The process was repeated until a crack was detected in the pit or anywhere else on the specimen.

After the test was started, the initial crack detection limiting parameter was set at a depth of 0.010″. This implies that the FTA interpreted the surface crack fatigue propagation from the pit to be approximately 0.010″ and then automatically stopped the test. The initial growth is referred to as the initiation phase in this study. Because the cracks did not grow uniformly out of the pits, the initial growth was measured and photodocumented after the test. To measure the initial growth, the fracture surface was marked either by changing the load ratio from $R = 0.7$ to $R = 0.1$ or increasing the load if the load ratio during the initial test was $R = 0.1$.

Once the crack marking occurred, the FTA stopped the test after the crack reached 0.15″ in depth. This step indicates the propagation phase, and the fatigue crack growth data was also acquired. After the crack propagated to 0.15″, the test was stopped, and the specimen was fractured to expose the crack face. Immediately after the fracture surfaces were exposed, the pit dimensions, initial growth, and final growth were measured and documented.

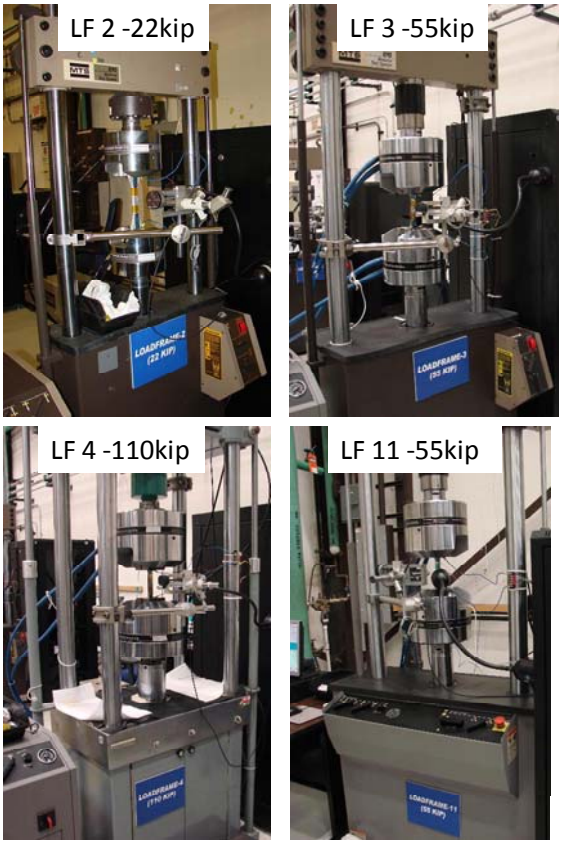

Figure 12. The Load Frames

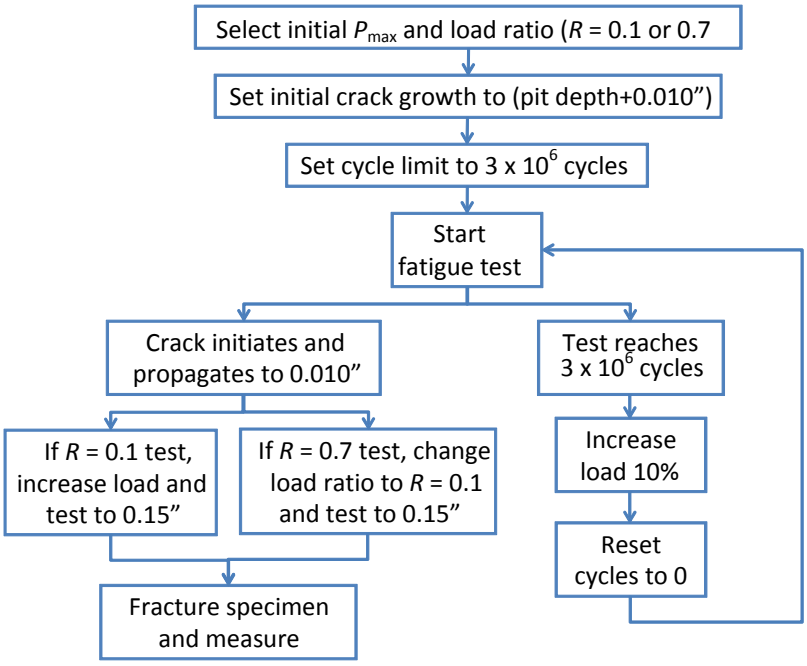

Figure 13. Fatigue Crack Initiation and Propagation Test Process

3. FATIGUE TESTS.

A total of 149 fatigue tests were performed on all three materials. A high-level test matrix is provided in table 4 showing the number of tests for each material, surface condition, and load ratio. In this section, each specific specimen tested and corresponding test condition are discussed for each material. The fatigue test process, discussed previously in section 2.6, was implemented for all three materials under a variety of conditions.

Table 4. High-Level Test Matrix for all Three Materials

Specimen Identifier	Load Ratio, *R*	Number of Tests
7075-PS	0.1	14
	0.7	12
7075-PS-SP	0.1	11
	0.7	4
7075-PS-SP2	0.1	12
	0.7	10
4340-PS	0.1	9
	0.7	8
4340-PS-SP	0.1	9
	0.7	5
4340-PS-LP	0.1	5
	0.7	6
D6AC-PS-SP	0.1	8
	0.7	8
D6AC-PS2	0.1	9
	0.7	9

To capture each condition and track each test accordingly, an identification scheme was implemented that incorporated the material, specimen type, and surface enhancement. The scheme was AAAA-PS-BB-##, where AAAA indicates the four-letter or -number material identifier such as 7075, 4340, or D6AC. The PS indicates a surface crack dogbone test that is used primarily for input into the FTA system. The BB indicates the surface enhancement, which may have an associated number if the surface enhancement method had two types. These identifiers are as follows: SP for shot peened, LP for laser peened, SP2 for heavy peened. The final indicator is the specimen number.

3.1 Al 7075-T7351 SPECIMENS.

A total of 63 Al specimens were tested. The test specimens consisted of three surface conditions: bare, nominal shot peen, and heavy shot peen. Within each condition, a variety of corrosion pit depths, ranging from 0.011″ to 0.080″, were also tested. Larger pit sizes (0.050″ to 0.080″) were tested for the heavy peen specimens because experience from previous programs

demonstrated that crack initiation from the pit would be difficult to control for smaller pits. That is, the notch effect was so negligible for smaller pits that the cracks would most likely initiate at the spot welds or taper.

To assist with the geometry, refer to figure 10, which demonstrates the pit dimensions where "2c" is the surface diameter of the pit and "a" is the pit depth. The specific measurements for each Al specimen are included in tables 5 through 10 with the corresponding pit aspect ratio (a/c) and applied load ratio (*R*).

Table 5. Al 7075-T7351 Bare Specimens Tested at $R = 0.1$

Specimen ID	Width (inch)	Thickness (inch)	Depth a (inch)	Surface 2c (inch)	a/c
7075-PS-1	0.90	0.48	0.011	0.033	0.67
7075-PS-2	0.90	0.48	0.011	0.033	0.67
7075-PS-3	0.90	0.48	0.012	0.031	0.77
7075-PS-4	0.90	0.48	0.011	0.030	0.73
7075-PS-5	0.91	0.49	0.013	0.033	0.79
7075-PS-20	0.90	0.49	0.030	0.065	0.92
7075-PS-23	0.90	0.49	0.028	0.054	1.04
7075-PS-30	0.91	0.46	0.028	0.071	0.79
7075-PS-35	0.90	0.49	0.049	0.100	0.98
7075-PS-36	0.90	0.49	0.048	0.098	0.98
7075-PS-39	0.90	0.49	0.032	0.079	0.81
7075-PS-40	0.90	0.49	0.049	0.100	0.98
7075-PS-41	0.91	0.49	0.030	0.073	0.82
7075-PS-43	0.90	0.49	0.050	0.116	0.86

Table 6. Al 7075-T7351 Bare Specimens Tested at $R = 0.7$

Specimen ID	Width (inch)	Thickness (inch)	Depth a (inch)	Surface 2c (inch)	a/c
7075-PS-21	0.90	0.49	0.028	0.059	0.95
7075-PS-22	0.90	0.49	0.026	0.058	0.90
7075-PS-24	0.90	0.49	0.030	0.074	0.81
7075-PS-27	0.91	0.49	0.031	0.090	0.69
7075-PS-28	0.91	0.49	0.030	0.075	0.80
7075-PS-31	0.90	0.49	0.047	0.100	0.94
7075-PS-34	0.90	0.49	0.046	0.099	0.93
7075-PS-37	0.90	0.49	0.045	0.104	0.87
7075-PS-42	0.90	0.49	0.046	0.104	0.88
7075-PS-44	0.90	0.49	0.028	0.072	0.78
7075-PS-45	0.90	0.49	0.054	0.111	0.97
7075-PS-46	0.90	0.51	0.034	0.075	0.90

Table 7. Al 7075-T7351 Nominal Shot-Peened Specimens Tested at $R = 0.1$

Specimen ID	Width (inch)	Thickness (inch)	Depth a (inch)	Surface 2c (inch)	a/c
7075-PS-SP-5	0.92	0.49	0.033	0.073	0.90
7075-PS-SP-6	0.92	0.49	0.029	0.078	0.74
7075-PS-SP-7	0.92	0.49	0.037	0.083	0.89
7075-PS-SP-10	0.90	0.49	0.034	0.070	0.97
7075-PS-SP-11	0.90	0.49	0.050	0.114	0.88
7075-PS-SP-12	0.90	0.49	0.047	0.115	0.82
7075-PS-SP-13	0.90	0.49	0.029	0.066	0.88
7075-PS-SP-14	0.90	0.49	0.028	0.067	0.84
7075-PS-SP-15	0.90	0.49	0.026	0.055	0.95
7075-PS-SP-16	0.90	0.49	0.027	0.074	0.73
7075-PS-SP-19	0.90	0.49	0.049	0.127	0.77

Table 8. Al 7075-T7351 Nominal Shot-Peened Specimens Tested at $R = 0.7$

Specimen ID	Width (inch)	Thickness (inch)	Depth a (inch)	Surface 2c (inch)	a/c
7075-PS-SP-8	0.92	0.49	0.034	0.061	1.11
7075-PS-SP-9	0.90	0.49	0.035	0.083	0.84
7075-PS-SP-17	0.90	0.49	0.049	0.121	0.81
7075-PS-SP-18	0.90	0.49	0.053	0.121	0.88

Table 9. Al 7075-T7351 Heavy-Peened Specimens Tested at $R = 0.1$

Specimen ID	Width (inch)	Thickness (inch)	Depth a (inch)	Surface 2c (inch)	a/c
7075-PS-SP2-7	0.90	0.50	0.068	0.121	0.84
7075-PS-SP2-8	0.90	0.50	0.067	0.138	0.97
7075-PS-SP2-14	0.91	0.50	0.068	0.129	1.05
7075-PS-SP2-15	0.91	0.50	0.071	0.141	1.01
7075-PS-SP2-16	0.91	0.50	0.069	0.147	0.94
7075-PS-SP2-18	0.91	0.50	0.069	0.148	0.93
7075-PS-SP2-19	0.91	0.50	0.051	0.121	0.84
7075-PS-SP2-20	0.90	0.51	0.052	0.123	0.84
7075-PS-SP2-21	0.91	0.51	0.055	0.114	0.96
7075-PS-SP2-22	0.90	0.50	0.053	0.124	0.85
7075-PS-SP2-25	0.90	0.50	0.056	0.111	1.01
7075-PS-SP2-27	0.90	0.50	0.051	0.100	1.02

Table 10. Al 7075-T7351 Heavy-Peened Specimens Tested at $R = 0.7$

Specimen ID	Width (inch)	Thickness (inch)	Depth a (inch)	Surface 2c (inch)	a/c
7075-PS-SP2-10	0.90	0.50	0.080	0.131	1.22
7075-PS-SP2-11	0.90	0.50	0.070	0.130	1.08
7075-PS-SP2-12	0.90	0.50	0.072	0.127	1.13
7075-PS-SP2-13	0.90	0.50	0.071	0.136	1.04
7075-PS-SP2-17	0.90	0.51	0.067	0.130	1.03
7075-PS-SP2-23	0.90	0.50	0.055	0.110	1.00
7075-PS-SP2-24	0.90	0.50	0.057	0.114	1.00
7075-PS-SP2-26	0.90	0.50	0.056	0.112	1.00
7075-PS-SP2-28	0.90	0.50	0.053	0.105	1.01
7075-PS-SP2-29	1.01	0.506	0.055	0.128	0.86

3.2 4340 STEEL SPECIMENS.

A total of forty-two 4340 steel specimens were tested. These specimens were the only set that included laser peening as one of the surface parameters in addition to shot peening. The pit depths for the 4340 steel specimens varied from 0.020″ to 0.050″. The general dimensions and pit dimensions for the 4340 steel specimens are provided in tables 11 through 16 with the corresponding pit aspect ratio (a/c) and applied load ratio (R).

Table 11. 4340 Steel Bare Specimens Tested at $R = 0.1$

Specimen ID	Width (inch)	Thickness (inch)	Depth a (inch)	Surface 2c (inch)	a/c
4340-PS-28	0.90	0.45	0.039	0.085	0.92
4340-PS-30	0.90	0.45	0.037	0.076	0.97
4340-PS-31	0.90	0.45	0.036	0.047	1.53
4340-PS-32	0.90	0.45	0.061	0.100	1.22
4340-PS-33	0.91	0.45	0.053	0.096	1.10
4340-PS-35	0.91	0.45	0.062	0.101	1.23
4340-PS-37	0.90	0.44	0.025	0.072	0.69
4340-PS-38	0.90	0.44	0.023	0.070	0.66
4340-PS-40	0.91	0.44	0.023	0.081	0.57

Table 12. 4340 Steel Bare Specimens Tested at $R = 0.7$

Specimen ID	Width (inch)	Thickness (inch)	Depth a (inch)	Surface 2c (inch)	a/c
4340-PS-29	0.90	0.45	0.038	0.094	0.81
4340-PS-34	0.90	0.44	0.058	0.098	1.18
4340-PS-36	0.90	0.44	0.027	0.052	1.04
4340-PS-39	0.90	0.44	0.026	0.072	0.72
4340-PS-41	0.90	0.44	0.039	0.076	1.03
4340-PS-42	0.90	0.45	0.023	0.046	1.00
4340-PS-43	0.90	0.45	0.027	0.076	0.71
4340-PS-44	0.90	0.45	0.027	0.084	0.64

Table 13. 4340 Steel Shot-Peened Specimens Tested at $R = 0.1$

Specimen ID	Width (inch)	Thickness (inch)	Depth a (inch)	Surface 2c (inch)	a/c
4340-PS-SP-01	0.90	0.45	0.050	0.100	1.00
4340-PS-SP-02	0.90	0.45	0.050	0.100	1.00
4340-PS-SP-03	0.90	0.45	0.048	0.097	0.98
4340-PS-SP-04	0.90	0.45	0.046	0.094	0.98
4340-PS-SP-06	0.90	0.45	0.049	0.097	1.01
4340-PS-SP-09	0.90	0.45	0.028	0.076	0.74
4340-PS-SP-11	0.90	0.45	0.023	0.054	0.85
4340-PS-SP-12	0.90	0.45	0.022	0.046	0.96
4340-PS-SP-13	0.9	0.45	0.023	0.049	0.94

Table 14. 4340 Steel Shot-Peened Specimens Tested at $R = 0.7$

Specimen ID	Width (inch)	Thickness (inch)	Depth a (inch)	Surface 2c (inch)	a/c
4340-PS-SP-05	0.90	0.448	0.047	0.097	0.97
4340-PS-SP-07	0.90	0.448	0.046	0.081	1.14
4340-PS-SP-08	0.90	0.448	0.045	0.093	0.97
4340-PS-SP-10	0.90	0.451	0.031	0.071	0.87
4340-PS-SP-14	0.90	0.450	0.024	0.048	1.00

Table 15. 4340 Steel Laser-Peened Specimens Tested at $R = 0.1$

Specimen ID	Width (inch)	Thickness (inch)	Depth a (inch)	Surface 2c (inch)	a/c
4340-PS-LP-01	0.90	0.45	0.048	0.102	0.94
4340-PS-LP-02	0.90	0.45	0.046	0.101	0.91
4340-PS-LP-03	0.90	0.45	0.049	0.104	0.94
4340-PS-LP-08	0.90	0.43	0.031	0.096	0.64
4340-PS-LP-09	0.90	0.430	0.028	0.077	0.73

Table 16. 4340 Steel Laser-Peened Specimens Tested at $R = 0.7$

Specimen ID	Width (inch)	Thickness (inch)	Depth a (inch)	Surface 2c (inch)	a/c
4340-PS-LP-04	0.90	0.45	0.047	0.100	0.94
4340-PS-LP-05	0.90	0.45	0.050	0.100	1.00
4340-PS-LP-06	0.90	0.45	0.048	0.101	0.95
4340-PS-LP-07	0.90	0.45	0.025	0.072	0.69
4340-PS-LP-10	0.90	0.45	0.023	0.053	0.81
4340-PS-LP-11	0.90	0.43	0.020	0.051	0.78

3.3 D6AC STEEL SPECIMENS.

A total of 44 D6AC steel specimens were tested in the shot-peened and bare conditions. The pit depths for the D6AC steel specimens varied from 0.023″ to 0.052″. The dimensions for the D6AC steel specimens are provided in tables 17 through 20 with the corresponding pit aspect ratio and applied load ratio.

Table 17. D6AC Steel Shot-Peened Specimens Tested at $R = 0.1$

Specimen ID	Width (inch)	Thickness (inch)	Depth a (inch)	Surface 2c (inch)	a/c
D6AC-PS-SP-16	0.90	0.45	0.046	0.094	0.98
D6AC-PS-SP-17	0.90	0.42	0.047	0.096	0.98
D6AC-PS-SP-18	0.90	0.44	0.045	0.095	0.95
D6AC-PS-SP-32	0.90	0.44	0.050	0.103	0.97
D6AC-PS-SP-33	0.90	0.41	0.048	0.113	0.85
D6AC-PS-SP-34	0.90	0.45	0.046	0.095	0.97
D6AC-PS-SP-38	0.90	0.45	0.028	0.091	0.62
D6AC-PS-SP-42	0.91	0.45	0.024	0.055	0.87

Table 18. D6AC Steel Shot-Peened Specimens Tested at $R = 0.7$

Specimen ID	Width (inch)	Thickness (inch)	Depth a (inch)	Surface 2c (inch)	a/c
D6AC-PS-SP-14	0.90	0.44	0.049	0.094	1.04
D6AC-PS-SP-15	0.90	0.44	0.045	0.089	1.01
D6AC-PS-SP-35	0.90	0.45	0.047	0.098	0.96
D6AC-PS-SP-36	0.90	0.45	0.048	0.094	1.02
D6AC-PS-SP-37	0.90	0.45	0.024	0.089	0.54
D6AC-PS-SP-39	0.90	0.45	0.025	0.052	0.96
D6AC-PS-SP-40	0.90	0.45	0.023	0.048	0.96
D6AC-PS-SP-41	0.90	0.44	0.023	0.048	0.96

Table 19. D6AC Steel Bare Specimens Tested at $R = 0.1$

Specimen ID	Width (inch)	Thickness (inch)	Depth a (inch)	Surface 2c (inch)	a/c
D6AC-PS2-07	0.90	0.40	0.024	0.068	0.70
D6AC-PS2-08	0.90	0.31	0.023	0.065	0.71
D6AC-PS2-09	0.90	0.35	0.025	0.078	0.34
D6AC-PS2-10	0.90	0.39	0.046	0.100	0.92
D6AC-PS2-11	0.90	0.40	0.045	0.099	0.91
D6AC-PS2-12	0.90	0.39	0.041	0.115	0.71
D6AC-PS2-13	0.90	0.39	0.046	0.104	0.88
D6AC-PS2-14	0.90	0.38	0.046	0.110	0.84
D6AC-PS2-17	0.90	0.40	0.046	0.104	0.88

Table 20. D6AC Steel Bare Specimens Tested at $R = 0.7$

Specimen ID	Width (inch)	Thickness (inch)	Depth a (inch)	Surface 2c (inch)	a/c
D6AC-PS2-01	0.90	0.38	0.023	0.058	0.79
D6AC-PS2-02	0.90	0.40	0.022	0.067	0.66
D6AC-PS2-03	0.90	0.40	0.026	0.066	0.79
D6AC-PS2-04	0.90	0.39	0.025	0.062	0.81
D6AC-PS2-05	0.90	0.39	0.024	0.064	0.75
D6AC-PS2-06	0.90	0.39	0.025	0.062	0.81
D6AC-PS2-15	0.90	0.40	0.052	0.114	0.91
D6AC-PS2-16	0.90	0.40	0.048	0.111	0.86
D6AC-PS2-18	0.90	0.41	0.047	0.104	0.90

4. FATIGUE TEST RESULTS.

The fatigue test program incorporated a step-test methodology to determine the threshold or initiation properties. The terms threshold and initiation are used in this context because it is

unclear if the initial crack process is dominated by fracture mechanics (threshold) or fatigue (initiation). One advantage of this test approach is that the threshold behavior can be determined rather rapidly if the initial loads are appropriately chosen. The disadvantage is that the initial predictions may be too high, resulting in a first-step initiation, or too low, resulting in several steps and cycles required to reach threshold. Early in this test program, the initial load was essentially an estimate that sometimes proved to be incorrect, either conservatively or nonconservatively. As the test program progressed for each material and surface condition, the load predictions were more accurate and the testing pace increased.

For each material, the test results were documented in tabular form and graphically. The test results included the initial test parameters, final test results, pit measurement, and crack measurements. Any nuances, such as a first-step failure or a failure in the tack weld, were documented.

4.1 Al 7075-T7351 INITIATION TEST RESULTS.

The test results for each surface condition and load ratio are included in tables 21 through 26 for the Al specimens. Several of the initial tests performed were used to understand the process, so these tests failed in the spot weld or exhibited some other problem during the test. In general, the primary nuances experienced during these tests included first-step failures and a few spot weld crack initiations.

This test program is the combination of two separate test projects. One project included the bare and nominal shot peen and the other project included the heavy peen. For this reason, the results are separated in the figures. The results from the bare and nominal shot-peened specimens are shown in figures 14 and 15, and the results from the heavy-peened specimens are shown in figures 16 and 17. It is important to note that none of the test data have been postprocessed to account for residual stress. For simplicity, the test results are organized in bins within the figures to represent pit sizes. There are three bin sizes used to characterize the test results: 0.010″, 0.030″, and 0.047″. The 0.010″ data represents all test results between 0.010″ and the next bin size (i.e., 0.030″). The data between 0.030″ and 0.047″ is represented by the 0.030″ bin, and everything larger than 0.047″ is represented by the 0.047″ bin. The data are also shown with the S-N curve fit of Al 7075-T6 with $K_f = 1.8$, which is in the same range as the test data ($K_f = 1.4$-1.9).

In addition to the fatigue curve, the threshold stress corresponding to a semicircular surface crack based on an initial flaw size and threshold stress-intensity factor (SIF) range is also shown for reference. This value can be calculated with equation 3; where σ_{th} is the threshold stress, ΔK_{th} is the threshold SIF range, R is the load ratio, β is the dimensionless shape factor obtained from NASGRO, and a is the pit diameter.

$$\sigma_{th} = \frac{\Delta K_{th}}{(1-R)\beta\sqrt{\pi a}} \tag{3}$$

Table 21. Al 7075-T7351 Bare Fatigue Test Results for $R = 0.1$

Specimen ID	Initial Test Parameters					Final Test Parameters			Measurements			
									Pit Measurement		Pit + Crack Initiation Measurement	
	P_{max} (lb)	S_{max} (ksi)	No. of Load Steps	Maximum Loads (kip) $R = 0.1$	Cycles Per Step (10^6)	Final P_{max} (lb)	Final S_{max} (ksi)	Cycles in Final Step	a (inch)	2c (inch)	a (inch)	2c (inch)
7075-PS-1**	NA	NA	NA	NA	NA	NA	NA	NA	0.011	0.033	NA	NA
7075-PS-2**	NA	NA	NA	NA	NA	NA	NA	NA	0.011	0.033	NA	NA
7075-PS-3	8,533	20.13	4	8.5, 9.7, 10.9, and 12	2	12,025	28.37	129,310	0.012	0.031	NA	NA
7075-PS-4*	11,281	26.63	1	11.3	NA	11,281	26.63	127,822	0.011	0.030	NA	NA
7075-PS-5*	11,062	25.63	1	11.1	NA	11,063	25.63	485,498	0.013	0.033	NA	NA
7075-PS-20	6,744	15.83	4	6.7, 7.1, 7.4, and 7.8	3	8,015	18.81	34,936	0.030	0.065	NA	NA
7075-PS-23*	7,500	17.35	1	7.5	3	7,500	17.35	470,751	0.028	0.054	0.041	0.08
7075-PS-30*	7,000	16.08	1	7	NA	7,000	16.08	186,126	0.028	0.071	0.049	0.108
7075-PS-35	4,000	9.33	5	4, 5, 6, 7, and 8	3	8,000	18.66	172,309	0.049	0.100	0.067	0.152
7075-PS-36	5,000	11.62	3	5, 6, and 7	3	7,000	16.26	395,825	0.048	0.098	0.082	0.186
7075-PS-39	6,000	13.96	4	6, 7, 8, and 9	3	9,000	20.94	1373,845	0.032	0.079	0.047	0.111
7075-PS-40	5,000	11.68	3	5, 6, and 7	3	7,000	16.35	361,893	0.049	0.100	0.073	0.159
7075-PS-41*	6,000	13.85	1	6	NA	6,000	13.85	272,356	0.030	0.073	0.055	0.117
7075-PS-43	6,000	13.97	2	6 and 8	3	8,000	18.62	228,735	0.050	0.116	0.064	0.136

*First-step initiation
**Spot weld initiation

Table 22. Al 7075-T7351 Bare Fatigue Test Results for $R = 0.7$

Specimen ID	Initial Test Parameters					Final Test Parameters			Measurements			
									Pit Measurement		Pit + Crack Initiation Measurement	
	P_{max} (lb)	S_{max} (ksi)	No. of Load Steps	Maximum Loads (kip) $R = 0.7$	Cycles Per Step (10^6)	Final P_{max} (lb)	Final S_{max} (ksi)	Cycles in Final Step	a (inch)	2c (inch)	a (inch)	2c (inch)
7075-PS-21	14,273	33.19	4	14.3, 15.7, 17.3, and 19	3	19,000	44.18	229,299	0.028	0.059	NA	NA
7075-PS-22*	18,000	42.12	1	18	NA	18,000	42.12	303,069	0.026	0.058	0.034	0.070
7075-PS-24*	16,500	37.77	1	15.5	NA	16,500	37.77	140,209	0.030	0.074	0.060	0.123
7075-PS-27*	15,750	36.44	1	15.8	NA	15,750	36.44	217,381	0.031	0.090	0.053	0.125
7075-PS-28*	16,250	37.44	1	16.2	NA	16,250	37.44	202,976	0.030	0.075	0.036	0.083
7075-PS-31	4,000	9.32	10	4, 5, 6, 7, 8, 9, 10, 12, and 14	2	14,000	32.62	505,025	0.047	0.100	0.063	0.152
7075-PS-34	12,000	27.97	2	12 and 13	2	13,000	30.30	449,915	0.046	0.099	0.061	0.080
7075-PS-37	11,000	25.56	4	11, 13, 14, and 15	3	15,000	34.85	944,166	0.045	0.104	0.061	0.162
7075-PS-42	12,000	28.00	2	12 and 14	3	14,000	32.66	994,876	0.046	0.104	0.071	0.078
7075-PS-44*	15,000	34.92	1	15	NA	15,000	34.92	425,378	0.028	0.072	0.061	0.114
7075-PS-45	10,000	23.30	2	10 and 12	3	12,000	27.96	1,660,282	0.054	0.111	0.073	0.174
7075-PS-46*	13,000	29.53	1	13	NA	13,000	29.53	1,037,016	0.034	0.075	0.155	0.275

*First-step initiation

Table 23. Al 7075-T7351 Nominal Shot-Peened Fatigue Test Results for $R = 0.1$

Specimen ID	Initial Test Parameters					Final Test Parameters			Measurements			
									Pit Measurement		Pit + Crack Initiation Measurement	
	P_{max} (lb)	S_{max} (ksi)	No. of Load Steps	Maximuim Loads (kips) $R = 0.1$	Cycles Per Step (10^6)	Final P_{max} (lb)	Final S_{max} (ksi)	Cycles in Final Step	a (inch)	2c (inch)	a (inch)	2c (inch)
7075-PS-SP-5*	9,000	20.56	1	9	NA	9,000	20.56	89,045	0.033	0.073	0.078	0.165
7075-PS-SP-6*	10,000	22.82	1	10	NA	10,000	22.82	77,107	0.029	0.078	0.073	0.168
7075-PS-SP-7*	6,000	13.7	1	6	NA	6,000	13.7	251,863	0.037	0.083	0.063	0.124
7075-PS-SP-10	4,000	9.24	3	4, 5, and 6	3	6,000	13.86	6,377,641	0.034	0.07	0.059	0.119
7075-PS-SP-11*	4,000	9.3	1	4	NA	4,000	9.3	276,391	0.05	0.114	0.061	0.144
7075-PS-SP-12*	3,000	6.98	1	3	NA	3,000	6.98	49,893	0.047	0.115	0.079	0.153
7075-PS-SP-13	5,000	11.6	5	5, 6, 7, 8, and 9	3	9,000	20.89	262,497	0.029	0.066	0.066	0.119
7075-PS-SP-14	4,000	9.26	5	4, 5, 6, 7, and 8	3	8,000	18.53	392,494	0.028	0.067	0.042	0.097
7075-PS-SP-15	6,000	13.92	2	6 and 7	3	7,000	15.76	498,885	0.026	0.055	0.033	0.07
7075-PS-SP-16	6,000	14.0	3	6, 7, and 8	3	8,000	18.68	523,297	0.027	0.074	0.095	0.228
7075-PS-SP-19	4,000	9.31	3	4, 5, and 6	3	6,000	13.96	573,200	0.049	0.127	0.118	0.192

*First-step initiation

Table 24. Al 7075-T7351 Nominal Shot-Peened Fatigue Test Results for $R = 0.7$

Specimen ID	Initial Test Parameters					Final Test Parameters			Measurements			
									Pit Measurement		Pit + Crack Initiation Measurement	
	P_{max} (lb)	S_{max} (ksi)	No. of Load Steps	Maximum Loads (kip) $R = 0.7$	Cycles PerStep (10^6)	Final P_{max} (lb)	Final S_{max} (ksi)	Cycles in Final Step	a (inch)	2c (inch)	a (inch)	2c (inch)
7075-PS-SP-8	5000	11.65	8	5, 6, 7, 8, 9, 10, 11, and 12	2	12,000	27.96	796,450	0.034	0.061	0.046	0.088
7075-PS-SP-9	8000	19.15	5	8, 9, 10, 11, and 12	2	12,000	28.19	616,643	0.035	0.083	0.063	0.133
7075-PS-SP-17	8000	18.76	3	8, 10, and 12	3	12,000	28.14	3,000,000	0.049	0.121	0.104	0.178
7075-PS-SP-18	8000	18.55	3	8, 10, and 12	3	12,000	27.82	418,230	0.053	0.121	0.083	0.171

Table 25. Al 7075-T7351 Heavy-Peened Fatigue Test Results for $R = 0.1$

Specimen ID	Initial Test Parameters					Final Test Parameters			Measurements			
									Pit Measurement		Pit + Crack Initiation Measurement	
	P_{max} (lb)	S_{max} (ksi)	Number of Load Steps	Maximum Loads (kip) $R = 0.1$	Cycles Per Step (10^6)	Final P_{max} (lb)	Final S_{max} (ksi)	Cycles in Final Step	a (inch)	2c (inch)	a (inch)	2c (inch)
7075-PS-SP2-7*	5000	11.29	1	5	3	5000	11.29	582,909	0.068	0.121	0.152	0.157
7075-PS-SP2-8	3000	6.79	4	3, 4, 5, and 6	3	6000	13.57	373,952	0.067	0.138	0.157	0.17
7075-PS-SP2-14	4000	8.99	2	4 and 5	3	5000	11.24	1,044,904	0.068	0.129	0.192	0.217
7075-PS-SP2-15	4000	8.99	2	4 and 5	3	5000	11.24	439,232	0.071	0.141	0.184	0.201
7075-PS-SP2-16	4000	8.99	2	4 and 5	3	5000	11.24	611,853	0.069	0.147	0.165	0.16
7075-PS-SP2-18	2000	4.5	6	2, 3, 4, 5, 6, and 7	3	7000	15.73	244,487	0.069	0.148	0.136	0.13
7075-PS-SP2-19	4000	8.99	5	4, 5, 6, 7, and 8	3	8000	17.98	305,803	0.051	0.121	0.127	0.148
7075-PS-SP2-20*	7000	15.76	1	4	3	7000	15.76	244,192	0.052	0.123	0.116	0.152
7075-PS-SP2-21	6000	13.44	3	6, 7, and 8	3	5000	11.20	261,658	0.055	0.114	0.171	0.237
7075-PS-SP2-22	6000	13.57	2	6 and 7	3	7000	15.84	784,017	0.053	0.124	0.142	0.130
7075-PS-SP2-25	6000	13.60	2	6 and 7	3	7000	15.87	340,689	0.056	0.111	0.156	0.158
7075-PS-SP2-27	6000	13.60	3	6, 7, and 8	3	8000	18.14	325,466	0.051	0.100	0.151	0.154

*First-step initiation

Table 26. Al 7075-T7351 Heavy-Peened Fatigue Test Results for $R = 0.7$

Specimen ID	Initial Test Parameters					Final Test Parameters			Measurements			
									Pit Measurement		Pit + Crack Initiation Measurement	
	P_{max} (lb)	S_{max} (ksi)	No. of Load Steps	Maximum Loads (kip) $R = 0.1$	Cycles Per Step (10^6)	Final P_{max} (lb)	Final S_{max} (ksi)	Cycles in Final Step	a (inch)	2c (inch)	a (inch)	2c (inch)
7075-PS-SP2-10	7,000	15.8	6	7, 8, 9, 10, and 11, 13	3	13,000	29.35	612,040	0.080	0.131	0.090	
7075-PS-SP2-11	9,000	18.66	2	9 and 10	3	10,000	22.58	2,280,781	0.070	0.130	0.127	0.169
7075-PS-SP2-12	9,000	18.66	3	9, 10, and 11	3	10,000	22.58	848,822	0.072	0.127	0.135	0.193
7075-PS-SP2-13	9,000	18.66	2	9 and 10	3	10,000	22.58	1,133,015	0.071	0.136	0.116	0.187
7075-PS-SP2-17	9,000	20.21	3	9, 10, and 11	3	11,000	24.99	1,119,531	0.067	0.130	0.113	0.181
7075-PS-SP2-23	8,500	19.23	2	8.5 and 9.5	3	9,500	21.49	1,530,802	0.055	0.110	0.138	0.135
7075-PS-SP2-24	10,000	22.62	2	10 and 11	3	11,000	24.89	679,779	0 .057	0.114	0.104	0.101
7075-PS-SP2-26	10,000	22.67	2	10 and 11	2	11,000	24.94	1,369,454	0.056	0.112	0.095	0.088
7075-PS-SP2-28	10,000	22.67	5	10, 11, 12, and 13, 15	5	15,000	34.0	440,039	0.053	0.105	0.137	0.159
7075-PS-SP2-29	11,000	22.18	1	11	3	11,000	22.18	2,219,412	0.055	0.128	0.118	0.139

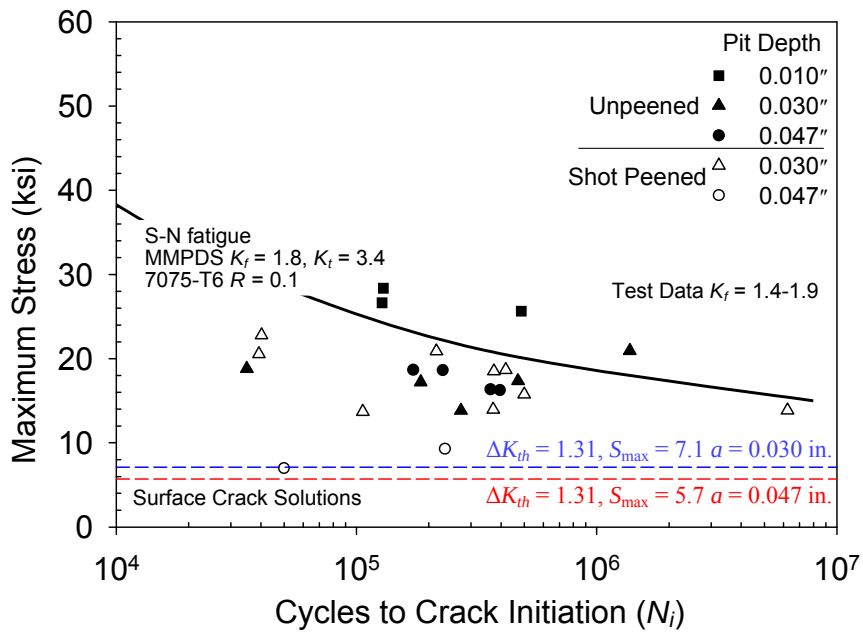

Figure 14. Al 7075-T7351 Test Results for Bare and Nominal Shot-Peened Specimens, R = 0.1

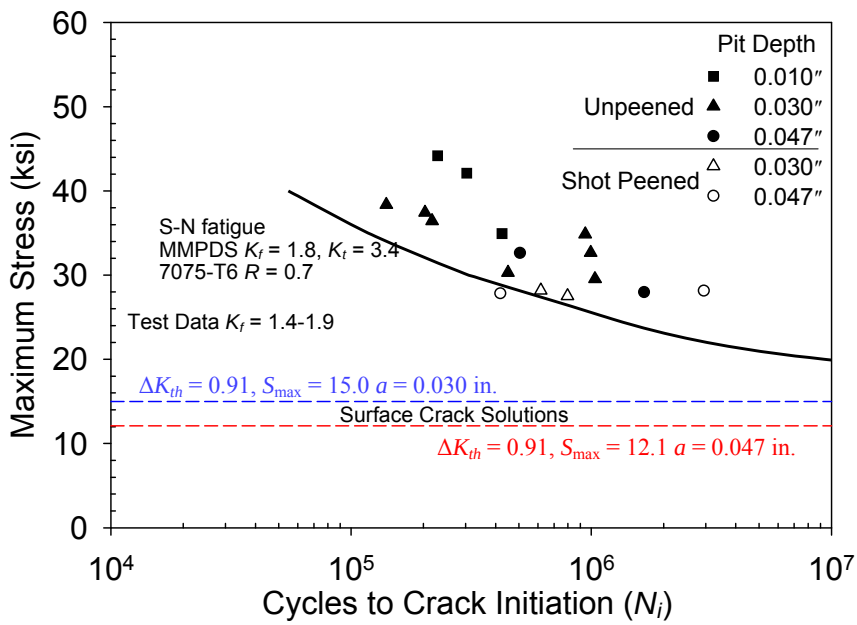

Figure 15. Al 7075-T7351 Test Results for Bare and Nominal Shot-Peened Specimens, R = 0.7

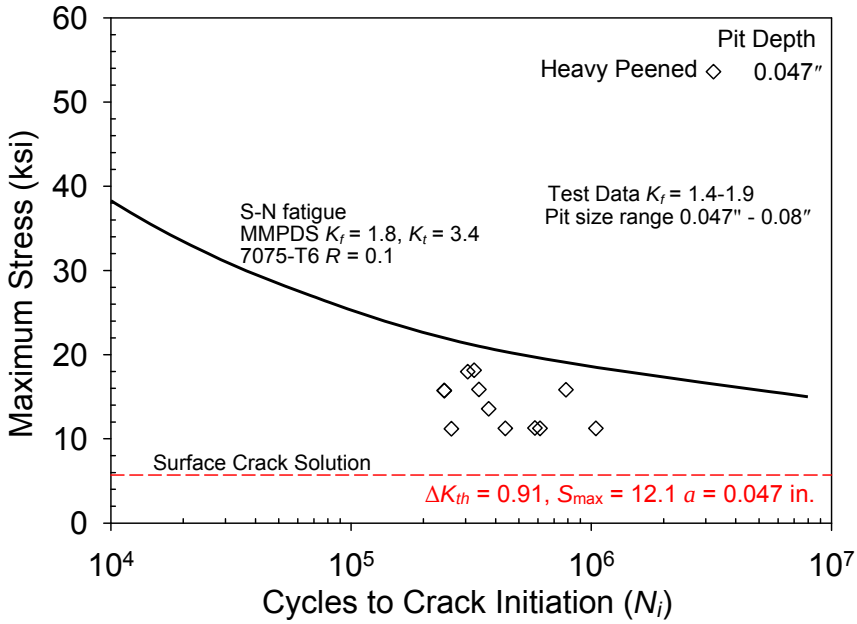

Figure 16. Al 7075-T7351 Test Results for the Heavy-Peened Specimens, $R = 0.1$

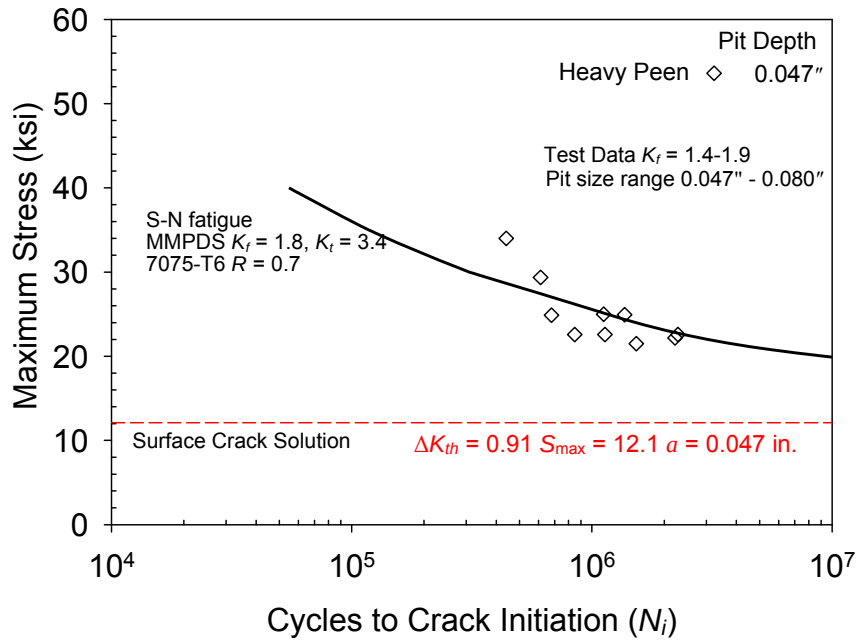

Figure 17. Al 7075-T7351 Test Results for the Heavy-Peened Specimens, $R = 0.7$

Upon initial observation, all the $R = 0.1$ nominal shot peen and heavy peen test results have lower initiation stresses compared to the MMPDS curve. This includes both the shot peen and heavy peen test results. In addition, the threshold stress based on a surface crack fracture model is conservative compared to all test results. These results imply that the $R = 0.1$ test results are essentially bound by the threshold stress and fatigue curve.

The $R = 0.7$ shot peen test results appear to be well characterized by the MMPDS curve for both shot peening cases. This initial result suggests that shot peening does not influence the initiation life of corrosion pits for Al 7075-T7351 and that the propagation life is negligible compared to the initiation life. The MMPDS data appear to be conservative compared to all the $R = 0.7$ data in the bare condition, but there are a few shot-peened and heavy-peened tests in which the MMPDS curve is nonconservative. Again, the threshold stress for a surface flaw is very conservative compared to the $R = 0.7$ test results, but it provides a lower bound estimate of the results. These aspects will be discussed in greater detail in section 5. The following list details the key observations:

- The MMPDS notch fatigue curve (S-N curve) generally characterizes the Al corrosion pit fatigue crack initiation test results effectively. This is particularly effective for the $R = 0.7$ test results. The MMPDS curve is conservative for the $R = 0.7$ test results and nonconservative for the $R = 0.1$ test results.

- The surface crack-based threshold stress is an overly conservative assessment of all the test results.

- Initial observation of the test results suggest that the residual stress from shot peening or heavy peening does not influence the fatigue initiation life of a crack emanating from a corrosion pit in Al 7075-T7351.

4.2 Al 7075-T7351 FATIGUE PROPAGATION RESULTS.

After the initiation portion of the test, the specimen fracture surface was marked by increasing the load or changing the load ratio and then continuing the test until the crack reached 0.15″ in depth. (This process was discussed in section 2.5.) Once the crack was grown to a depth of approximately 0.15″, the test was complete, and the specimen was fractured. As part of the data acquisition, the fatigue crack growth rates were recorded throughout the test, but they were not used in further analysis. For reference, the growth rates from three Al specimens are shown in figure 18 with a comparison to the NASGRO data.

In general, the tests' growth rates correspond well with the NASGRO fatigue crack growth data. This result suggests that the residual stress from shot peening does not affect the propagation of the crack and that there are no apparent load history (i.e., crack retardation) effects. It also suggests that the surface crack geometry assumed by the FTA data acquisition and analysis software is reasonable for the Al 7075-T7351 specimens. There is some deviation at the lower growth rates, but this is believed to be a function of geometry rather than residual stress. This observation will be discussed further in section 5.10.

To summarize the observations from the fatigue crack growth tests, the following list highlights the pertinent information.

- The fatigue crack propagation from a corrosion pit does not appear to be influenced by the residual stress induced by nominal shot peening or heavy peening. The crack propagation curves from the shot-peened, heavy-peened, and bare surface conditions all correspond well with each other and the NASGRO data.

- The surface crack assumption used by the FTA appears to reasonably capture the fatigue crack propagation from a corrosion pit for cracks that are between 0.010″ and 0.15″.

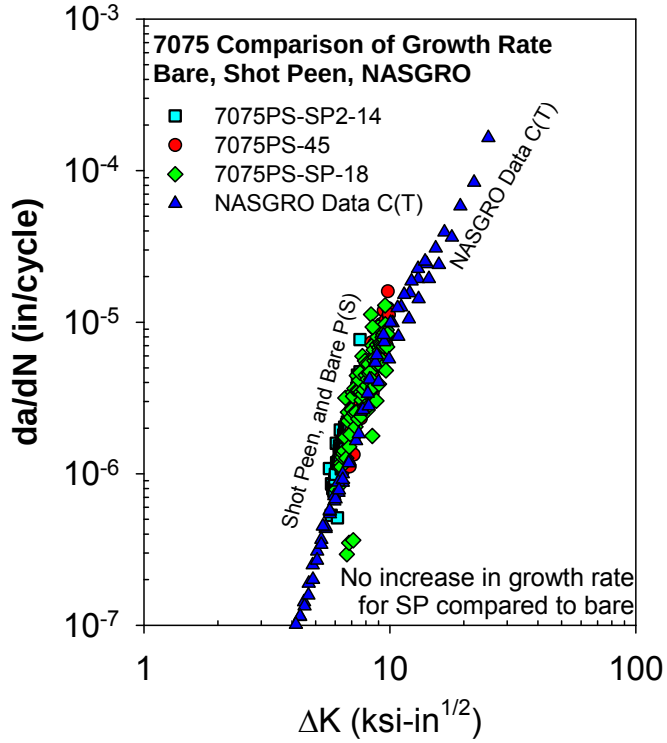

C(T) = Compact tension
SP = Shot peened

Figure 18. Al 7075-T7351 Fatigue Crack Growth Comparisons From a Corrosion Pit

4.3 4340 STEEL INITIATION TEST RESULTS.

The test results for each surface condition and load ratio are included in tables 27 through 32 for the 4340 steel specimens. For reference, the steel specimens consisted of bare, shot-peened, and laser-peened surface conditions. In several laser-peened tests, it was difficult to nucleate a crack within the pit. This result should be noted because the pit in 4340 steel had a fatigue notch factor of K_f = 2.1-2.18, which is very similar to the stress concentration factor of K_t = 2.2. This implies that although the stress concentration effect was not drastically reduced in the steel alloys under cyclic loading, there were still problems nucleating a crack in the pit.

Table 27. 4340 Steel Bare Fatigue Test Results for $R = 0.1$

Specimen ID	Initial Test Parameters					Final Test Parameters			Measurements			
									Pit Measurement		Pit + Crack Initiation Measurement	
	P_{max} (lb)	S_{max} (ksi)	No. of Load Steps	Maximum Loads (kip) $R = 0.1$	Cycles Per Step E6	Final P_{max} (lb)	Final S_{max} (ksi)	Cycles in Final Step	a (inch)	2c (inch)	a (inch)	2c (inch)
4340-PS-28*	25,000	63.5	1	25	NA	25,000	63.5	491,560	0.039	0.085	0.05	0.137
4340-PS-30*	22,500	57.6	1	22.5	NA	22,500	57.6	237,177	0.037	0.076	0.063	0.125
4340-PS-31**	18,000	45.97	4	18, 20, 22, and 24	2	24,000	61.29	405,660	0.036	0.047	0.042	0.06
4340-PS-32	20,000	51.08	4	20, 23, 26, and 29	2	29,000	74.06	88,400	0.061	0.1	0.071	0.153
4340-PS-33	23,000	59.54	3	23, 26, and 29	2	29,000	75.07	76,264	0.053	0.096	0.075	0.166
4340-PS-35	20,000	51.77	3	20, 23, and 26	2	26,000	67.3	155,389	0.062	0.101	0.063	0.154
4340-PS-37+	20,000	52.3	3	20, 22, and 25	3	25,000	65.38	935,503	0.025	0.072	NA	NA
4340-PS-38	20,000	51.89	3	20, 22, and 25	3	25,000	64.86	1,464,655	0.023	0.07	0.054	0.128
4340-PS-40	20,000	51.65	4	20, 22, 25, and 28	2	28,000	72.31	285,149	0.023	0.081	0.046	0.128

*First-step initiation
**Multiple initiation sites
+Spot weld initiation

Table 28. 4340 Steel Bare Fatigue Test Results for $R = 0.7$

Specimen ID	Initial Test Parameters					Final Test Parameters			Measurements			
									Pit Measurement		Pit + Crack Initiation Measurement	
	P_{max} (lb)	S_{max} (ksi)	No. of Load Steps	Maximum Loads (kip) $R = 0.7$	Cycles Per Step 10^6	Final P_{max} (lb)	Final S_{max} (ksi)	Cycles in Final Step	a (inch)	2c (inch)	a (inch)	2c (inch)
4340-PS-29	28,000	72.08	4	28, 32, 35, and 38	3	38,000	97.82	285,076	0.038	0.094	0.056	0.141
4340-PS-34	32,000	82.83	7	32, 35, 38, 42, 46, 50, and 54.5	2	54,500	141.08	1,747,582	0.058	0.098	0.099	0.128
4340-PS-36*	33,000	85.62	6	33, 37, 41, 45, 49, and 54	2	54,000	140.1	207,141	0.027	0.052	NA	NA
4340-PS-39**	32,000	83.31	6	32, 35, 38, 42, 45, and 48	3	48,000	124.82	1,014,403	0.026	0.072	NA	NA
4340-PS-41***	35,000	90.7	4	35, 38, 41, and 45	2	45,000	116.62	427,981	0.039	0.076	NA	NA
4340-PS-42	40,000	101.7	4	40, 44, 48, and 53	2	53,000	134.75	219,982	0.023	0.046	0.056	0.068
4340-PS-43	40,000	103.42	4	40, 44, 48, and 52	3	52,000	134.45	198,006	0.027	0.076	0.043	0.088
4340-PS-44	36,000	91.64	4	36, 40, 46, and 50	2	50,000	127.28	429,015	0.027	0.084	0.065	0.134

*Spot weld initiation
**No precrack, specimen propagated to fracture
***Hydraulic overload event

Table 29. 4340 Steel Shot-Peened Fatigue Test Results for $R = 0.1$

Specimen ID	Initial Test Parameters					Final Test Parameters			Measurements			
									Pit Measurement		Pit + Crack Initiation Measurement	
	P_{max} (lb)	S_{max} (ksi)	No. of Load Steps	Maximum Loads (kip) $R = 0.1$	Cycles Per Step 10^6	Final P_{max} (lb)	Final S_{max} (ksi)	Cycles in Final Step	a (inch)	2c (inch)	a (inch)	2c (inch)
4340-PS- SP-1	24,000	61.36	4	24, 27, 30, and 33	2	33,000	84.38	109,104	0.05	0.1	0.079	0.161
4340-PS- SP-2*	30,000	76.7	1	30	NA	30,000	76.7	115,860	0.05	0.1	0.076	0.151
4340-PS- SP-3*	30,000	76.7	1	30	NA	30,000	76.7	98,776	0.048	0.097	0.076	0.045
4340-PS- SP-4	22,000	56.25	5	22, 24, 26, 28, and 31	2	31,000	79.26	435,489	0.046	0.094	0.079	0.144
4340-PS- SP-6*	33,000	83.71	1	33	NA	33,000	83.71	104,055	0.049	0.097	0.067	0.138
4340-PS- SP-9*	40,000	101.5	1	40	NA	40,000	101.5	40,957	0.028	0.076	0.067	0.098
4340-PS- SP-11	30,000	76.7	3	30, 33, and 36	2	36,000	92.05	69,648	0.023	0.054	0.067	0.089
4340-PS- SP-12	30,000	76.7	2	30 and 33	3	33,000	84.38	161,259	0.022	0.046	0.052	0.071
4340-PS- SP-13**	30,000	76.7	1	30	NA	30,000	76.7	548,291	0.023	0.049	NA	NA

*Firsts-step initiation
**Spot weld initiation

Table 30. 4340 Steel Shot-Peened Fatigue Test Results for $R = 0.7$

Specimen ID	Initial Test Parameters					Final Test Parameters			Measurements			
									Pit Measurement		Pit + Crack Initiation Measurement	
	P_{max} (lb)	S_{max} (ksi)	No. of Load Steps	Maximum Loads (kip) $R = 0.7$	Cycles Per Step 10^6	Final P_{max} (lb)	Final S_{max} (ksi)	Cycles in Final Step	a (inch)	2c (inch)	a (inch)	2c (inch)
4340-PS-SP-5	38,000	97.16	7	38, 42, 46, 50, 55, 60, and 65	2	65,000	166.2	90,243	0.047	0.097	0.065	0.109
4340-PS-SP-7	46,000	117.62	3	46, 50, and 55	2	55,000	140.63	348,067	0.046	0.081	0.073	0.081
4340-PS-SP-8	46,000	117.62	4	46, 50, 55, and 60	2	60,000	153.41	438,06	0.045	0.093	0.085	0.116
4340-PS-SP-10	40,000	101.25	2	40 and 44	2	44,000	111.37	1,965,058	0.031	0.071	NA	NA
4340-PS-SP-14	50,000	127.84	3	50, 55, and 60	2	60,000	153.41	318,476	0.024	0.048	0.042	0.055

Table 31. 4340 Steel Laser-Peened Fatigue Test Results for $R = 0.1$

Specimen ID	Initial Test Parameters					Final Test Parameters			Measurements			
									Pit Measurement		Pit + Crack Initiation Measurement	
	P_{max} (lb)	S_{max} (ksi)	No. of Load Steps	Maximum Loads (kip) $R = 0.1$	Cycles Per Step 10^6	Final P_{max} (lb)	Final S_{max} (ksi)	Cycles in Final Step	a (inch)	2c (inch)	a (inch)	2c (inch)
4340-PS-LP-01	20,000	51.14	7	20, 22, 25, 28, 31, 34, and 38	2	38,000	97.16	172,034	0.048	0.102	0.081	0.15
4340-PS-LP-02*	40,000	102.27	1	40	NA	40,000	102.27	731,953	0.046	0.101	0.139	0.181
4340-PS-LP-03[+]	34,000	86.93	2	34 and 38	2	38,000	97.16	313,443	0.049	0.104	NA	NA
4340-PS-LP-08*[+]	34,000	89.84	1	34	NA	34,000	89.84	486,065	0.031	0.096	NA	NA
4340-PS-LP-09[**]	35,000	93.24	2	35 and 38	2	38,000	101.23	35,096	0.028	0.077	NA	NA

*First-step initiation
**Cracking away from pit
[+]Crack in taper

Table 32. 4340 Steel Laser-Peened Fatigue Test Results for $R = 0.7$

Specimen ID	Initial Test Parameters					Final Test Parameters			Measurements			
									Pit Measurement		Pit + Crack Initiation Measurement	
	P_{max} (lb)	S_{max} (ksi)	No. of Load Steps	Maximum Loads (kip) $R = 0.7$	Cycles Per Step 10^6	Final P_{max} (lb)	Final S_{max} (ksi)	Cycles in Final Step	a (inch)	2c (inch)	a (inch)	2c (inch)
4340-PS-LP-04	30,000	76.7	6	30, 33, 36, 39, 42, and 45	2	45,000	115.06	1,689,372	0.047	0.1	0.092	0.165
4340-PS-LP-05	40,000	102.5	2	40 and 44	2	44,000	112.75	2,000,000	0.05	0.1	0.085	0.102
4340-PS-LP-06*	40,000	102.27	5	40, 44, 48, 52, and 56	2	56,000	143.18	492,732	0.048	0.101	NA	NA
4340-PS-LP-07	40,000	101.93	7	40, 42, 44, 46, 48, 50, and 52	3	52,000	132.51	80,495	0.025	0.072	0.076	0.113
4340-PS-LP-10	40,000	102.27	7	40, 44, 48, 52, 24, 62, and 68	3	68,000	173.87	110,879	0.023	0.053	0.042	0.041
4340-PS-LP-11	48,000	127.87	3	48, 53, and 58	3	58,000	154.5	211,197	0.02	0.051	0.042	0.083

*Spot weld initiation

All test nuances were documented but the most common problems included first-step cracking, spot weld cracking, and cracking away from the pit. A total of seven specimens initiated cracks either at the tack weld or away from the corrosion pit, and five of these specimens had pit sizes that were smaller than 0.030″. Only two of the five laser-peening specimens with a load ratio of $R = 0.1$ initiated cracks in the pits. The remaining three specimens initiated cracks outside the pits.

The results are also shown in raw data form in figures 19 and 20 for load ratios $R = 0.1$ and $R = 0.7$, respectively. The test results are compared to the MMPDS S-N data of 4340 steel with a fatigue notch factor of $K_f = 2.9$. This notch factor is more conservative than the test data, which had fatigue notch factors in the range of $K_f = 2.1$-2.8. The test results demonstrate that the MMPDS curve was conservative compared to all the test data for both load ratios. This result is expected because of the higher fatigue notch factor in the MMPDS data compared to the corrosion pit specimens. The figures also demonstrate the threshold stress corresponding to a semicircular surface crack based on an initial flaw size and threshold SIF range. Again, the surface crack-based threshold appears to be conservative compared to the test results.

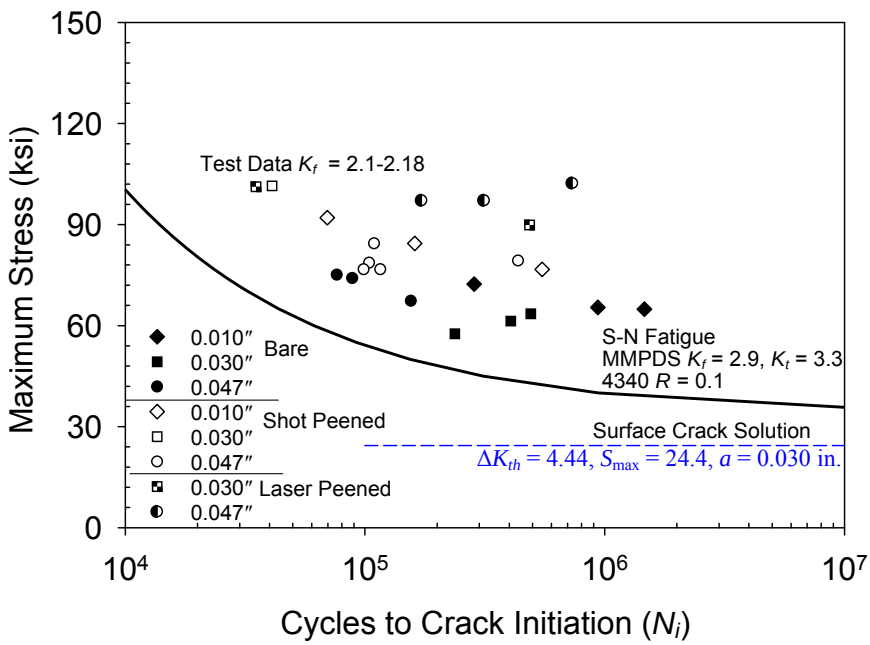

Figure 19. 4340 Steel Fatigue Test Results for all Surface Conditions, $R = 0.1$

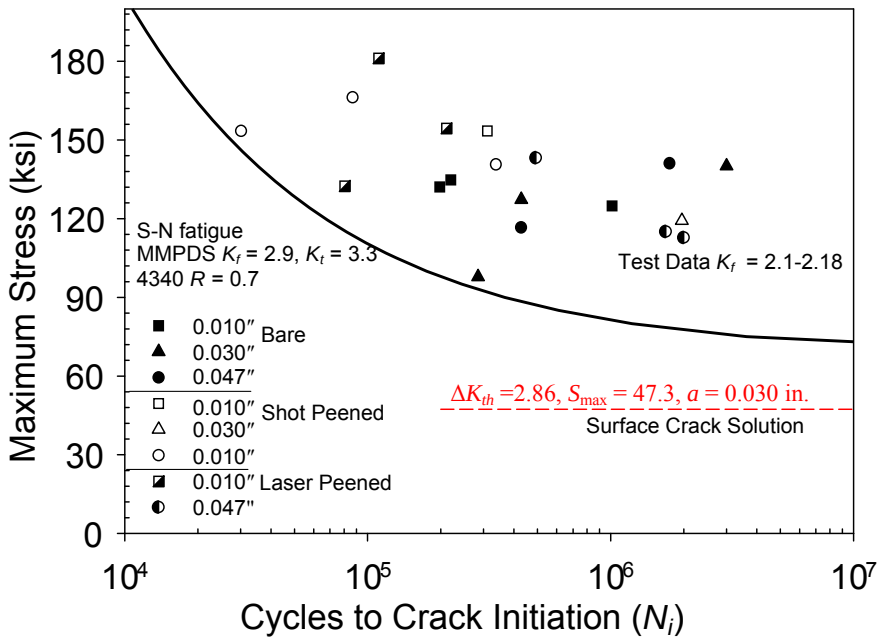

Figure 20. 4340 Steel Fatigue Test Results for all Surface Conditions, $R = 0.7$

Upon initial observation, it is apparent that the shot- and laser-peened specimens provide benefit toward the fatigue initiation stress. This is very evident with the $R = 0.1$ test results. The laser-peened specimens exhibited the most improvement followed by the shot-peened specimens. None of these results were postprocessed to account for residual stresses, but it is believed that the benefit is due to the residual stress effects from the surface enhancements.

A summary of the initial observations from the test results are listed below for reference.

- The notch fatigue (S-N) data from MMPDS is a conservative estimate of the corrosion pit test results for the 4340 steel. This result is expected because the notch fatigue factor is slightly more conservative for the MMPDS data than the corrosion pit data.

- There is an apparent residual stress effect for both the laser- and shot-peened test specimens. The surface treatments result in an increased initiation stress that is evident in both the $R = 0.1$ and $R = 0.7$ test results.

- The surface crack threshold estimate is an overly conservative estimate of the 4340 steel corrosion pit test results.

4.4 4340 STEEL PROPAGATION TEST RESULTS.

Like the Al specimens, the surface cracks in the 4340 steel specimens were propagated to a crack depth of 0.15″ after the initiation phase of the test was complete. The propagation data were recorded, and a sample of test results from three specimens are shown in figure 21. For reference, the Al 7075-T7351 fatigue crack growth data are shown next to the 4340 steel data within figure 21.

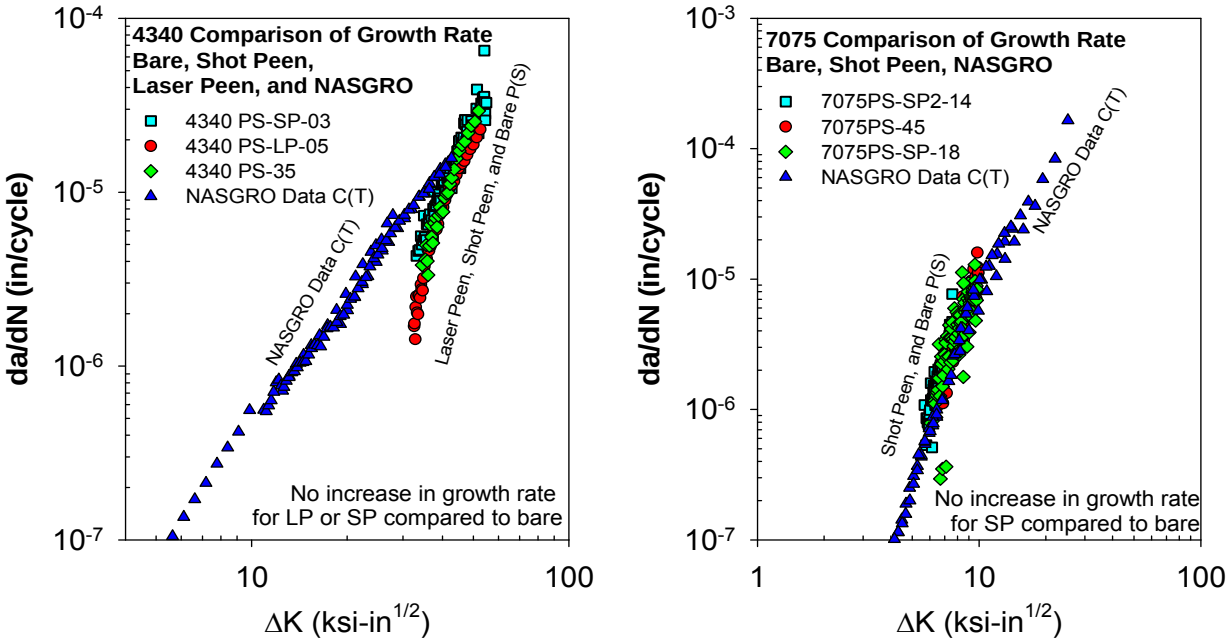

Figure 21. 4340 Steel Fatigue Crack Growth Rate Data Compared to Corrosion Pit Data With Supporting Fracture Surface Images (Al data shown on right for reference.)

Unlike the Al specimens, the 4340 steel propagation data did not correlate well with the NASGRO data. The fatigue crack growth response from the 4340 steel test specimens was nonconservative compared to the NASGRO data at low growth rates and converged to the NASGRO data at higher growth rates. This is not believed to be a surface enhancement or residual stress effect because the bare specimen exhibited the same trend and responded very similar to the laser- and shot-peened specimens. The results suggest that there is a geometry effect that influences the propagation of the crack. The geometry effects are discussed further in section 5.10.

A few summary points that should be highlighted for this section are listed below.

- The fatigue crack growth response of the corrosion pit specimens was nonconservative compared to the NASGRO fatigue crack growth data. This means that the test data will exhibit longer life than a NASGRO-based life prediction.

- As the growth rate increases, the response converges to the NASGRO data. This implies that the geometric differences are negligible at higher growth rates.

- There does not appear to be a significant residual stress effect due to the laser- or shot-peened specimens during the crack propagation phase. This is supported by the fatigue crack propagation results, which all correspond well regardless of surface enhancement.

4.5 D6AC STEEL INITIATION TEST RESULTS.

The test results for the bare and shot-peened D6AC steel with corresponding load ratios are included in tables 33 through 36. In general, the D6AC steel tests were successful with a few first-step crack initiation tests. There were no problems associated with cracking in the taper or weld on the D6AC steel specimens, and there were only four first-step failures within these tests.

The results from the table are also displayed in their raw form in figures 22 and 23 for load ratios R = 0.1 and R = 0.7, respectively. None of the test results were postprocessed to account for propagation or residual stress. The test results are also shown with the S-N data of D6AC steel with a fatigue notch factor of K_f = 2.0, which is nonconservative compared to the test data with a fatigue notch factor of K_f = 2.09-2.16. Two caveats regarding the S-N data that should be discussed are the strength of the S-N material was not the same as the corrosion pit material and the load ratios were similar but not the same (R = 0.0 versus R = 0.1 and R = 0.5 versus R = 0.7) [6]. The material tensile strength associated with the S-N data was 270 ksi, whereas the corrosion pit material strength was 160 ksi. It is not clear how the strength influences the fatigue data for this material, but the most dramatic effects would occur at stresses near or above 80 ksi, which is the yield stress for the D6AC steel tested in this program.

The figures also demonstrate the threshold stress corresponding to a semicircular surface crack based on an initial flaw size and threshold SIF range. Again, the surface crack-based threshold appears to be overly conservative compared to the test results. The threshold effects will be discussed in more detail in section 5.9.

Upon initial observation, it is apparent that shot peening provides some fatigue benefit for the R = 0.1 tests with the larger pit diameters. The initiation stresses of the smaller pit diameter specimens did not exhibit the same improvement and corresponded better with the bare test results.

It was difficult to discern any benefit in the R = 0.7 test results for all pit sizes. These results were processed to account for residual stress. Section 5 provides more information regarding the observations.

A summary of the important observations from the test results are listed below.

- The notch fatigue data used to compare the test results was for different strength D6AC steel and different load ratios. Keeping those differences in context, the notch fatigue data provides a reasonable characterization of the test results.

- The surface crack-based threshold stress estimation is an overly conservative estimate to characterize the D6AC steel test results.

- The test results reveal that the D6AC steel corrosion pit specimens appear to be sensitive to residual stress at R = 0.1 and the effects are more pronounced for larger pit diameters. The effect of residual stress is negligible at R = 0.7.

Table 33. D6AC Steel Bare Fatigue Test Results for $R = 0.1$

Specimen ID	Initial Test Parameters					Final Test Parameters			Measurements			
									Pit Measurement		Pit + Crack Initiation Measurement	
	P_{max} (lb)	S_{max} (ksi)	No. of Load Steps	Maximum Loads (kip) $R = 0.1$	Cycles Per Step 10^6	Final P_{max} (lb)	Final S_{max} (ksi)	Cycles in Final Step	a (inch)	2c (inch)	a (inch)	2c (inch)
D6AC-PS2-7	18,000	51.37	5	18, 19, 20, 22, and 24	2.5	24,000	68.49	255,223	0.024	0.068	0.045	0.104
D6AC-PS2-8*	18,000	66.28	1	18		18,000	66.28	175,540	0.023	0.065	0.05	0.102
D6AC-PS2-9	17,000	54.98	4	17, 18, 19, and 21	2.5	21,000	67.91	337,176	0.025	0.078	0.049	0.100
D6AC-PS2-10	11,000	31.91	4	11, 13, 15, 17, and 19	3	19,000	55.11	345,037	0.046	0.100	0.141	0.243
D6AC-PS2-11	16,000	45.61	4	16, 17, 18, and 19.5	3	19,500	55.59	152,714	0.045	0.099	0.055	0.133
D6AC-PS2-12	16,000	46.83	4	16, 17, 18, and 19	3	19,000	55.61	521,214	0.041	0.115	0.081	0.189
D6AC-PS2-13	16,000	46.95	5	16, 17, 18, 19.2, and 23	3	23,000	67.5	114,099	0.046	0.104	0.063	0.133
D6AC-PS2-14	18,000	54.36	2	18 and 20	3	20,000	60.4	220,434	0.046	0.110	0.068	0.160
D6AC-PS2-17*	20,000	57.36	1	20		20,000	57.36	441,687	0.046	0.104	0.085	0.150

*First-step initiation

Table 34. D6AC Steel Bare Fatigue Test Results for $R = 0.7$

Specimen ID	Initial Test Parameters					Final Test Parameters			Measurements			
									Pit Measurement		Pit + Crack Initiation Measurement	
	P_{max} (lb)	S_{max} (ksi)	No. of Load Steps	Maximum Loads (kip) $R = 0.7$	Cycles Per Step 10^6	Final P_{max} (lb)	Final S_{max} (ksi)	Cycles in Final Step	a (inch)	2c (inch)	a (inch)	2c (inch)
D6AC-PS2-1	20,000	60.1	9	20, 22, 24, 27, 30, 33, 36, 40, and 44	3	44,000	132.23	293,769	0.023	0.058	0.048	0.089
D6AC-PS2-2	33,000	93.14	5	33, 36, 39, 43, and 47	3	47,000	132.8	501,709	0.022	0.067	0.059	0.116
D6AC-PS2-3	36,000	103.92	4	36, 39, 43, and 47	3	47,000	135.83	334,648	0.026	0.066	0.054	0.094
D6AC-PS2-4	40,000	116.65	2	40 and 44	3	44,000	128.31	442,707	0.025	0.062	0.051	0.1
D6AC-PS2-5	40,000	115.47	3	40, 44, and 48	3	48,000	138.56	644,712	0.024	0.064	0.039	0.094
D6AC-PS2-6	40,000	117.55	2	40 and 44	3	44,000	129.31	515,419	0.025	0.062	0.042	0.098
D6AC-PS2-15	30,000	85.62	5	30, 33, 36, 40, and 44	3	44,000	125.57	1,197,348	0.052	0.114	NA	NA
D6AC-PS2-16	36,000	101.97	4	36, 40, 44, and 48	3	48,000	136.99	172,600	0.048	0.111	0.065	0.129
D6AC-PS2-18	40,000	112.47	4	40, 44, and 48	3	48,000	134.96	277,400	0.047	0.104	0.08	0.087

Table 35. D6AC Steel Shot-Peened Fatigue Test Results for $R = 0.1$

Specimen ID	Initial Test Parameters					Final Test Parameters			Measurements			
									Pit Measurement		Pit + Crack Initiation Measurement	
	P_{max} (lb)	S_{max} (ksi)	No. of Load Steps	Maximum Loads (kip) $R = 0.1$	Cycles Per Step 10^6	Final P_{max} (lb)	Final S_{max} (ksi)	Cycles in Final Step	a (inch)	2c (inch)	a (inch)	2c (inch)
D6AC-PS-SP-16	20,000	50.96	4	20, 23, 26, and 29	2	29,000	73.9	117,366	0.046	0.094	0.076	0.128
D6AC-PS-SP-17	24,000	65.16	3	24, 27, and 30	3	30,000	81.45	117,146	0.047	0.096	0.077	0.148
D6AC-PS-SP-18*	24,000	62.62	1	24	NA	24	62.62	200,547	0.045	0.095	0.064	0.147
D6AC-PS-SP-32	21,000	54.42	2	21 and 24	3	24	62.2	199,610	0.05	0.103	0.059	0.065
D6AC-PS-SP-33	18,000	50.3	4	18, 20, 22, and 24	3	24,000	67.07	135,610	0.048	0.113	0.072	0.216
D6AC-PS-SP-34	20,000	50.79	10	20, 22, 24, 26, 28, 30, 32, 34, 36, and 39	3	39,000	99.04	79,233	0.046	0.095	0.06	0.136
D6AC-PS-SP-38	22,000	56.19	2	22 and 25	2	25,000	63.85	210,390	0.028	0.091	0.069	0.114
D6AC-PS-SP-42*	20,000	50.84	1	20	NA	20,000	50.84	231,400	0.024	0.055	0.052	0.11

*First-step initiation

Table 36. D6AC Steel Shot-Peened Fatigue Test Results for $R = 0.7$

Specimen ID	Initial Test Parameters					Final Test Parameters			Measurements			
									Pit Measurement		Pit + Crack Initiation Measurement	
	P_{max} (lb)	S_{max} (ksi)	No. of Load Steps	Maximum Loads (kip) $R = 0.7$	Cycles Per Step 10^6	Final P_{max} (lb)	Final S_{max} (ksi)	Cycles in Final Step	a (inch)	2c (inch)	a (inch)	2c (inch)
D6AC-PS-SP-14*	36,000	94.04	6	36, 39, 42, 45, 48, and 49.9	3	49,900	130.35	4,000,000	0.049	0.094	NA	NA
D6AC-PS-SP-15	36,000	94.26	6	36, 39, 42, 46, 49.5, and 55	2	55,000	144	200,793	0.045	0.089	0.063	0.138
D6AC-PS-SP-35	36,000	91.22	2	36 and 38	2	38,000	96.29	913,680	0.047	0.098	0.075	0.141
D6AC-PS-SP-36	36,000	91.43	6	36, 39, 42, 46, 50, and 54	2	54,000	137.14	114,308	0.048	0.094	0.064	0.13
D6AC-PS-SP-37	40,000	102.16	4	40, 44, 48, and 53	2	53,000	135.36	2,000,000	0.024	0.089	0.038	0.116
D6AC-PS-SP-39	46,000	115.66	2	46 and 50	2	50,000	125.71	258,696	0.025	0.052	0.054	0.064
D6AC-PS-SP-40	36,000	91.74	1	36		36,000	91.74	661,961	0.023	0.048	0.054	0.106
D6AC-PS-SP-41	40,000	104.85	6	40, 44, 48, 52, 54, and 60	3	60,000	157.27	1,699	0.023	0.048	0.037	0.09

*Aborted test

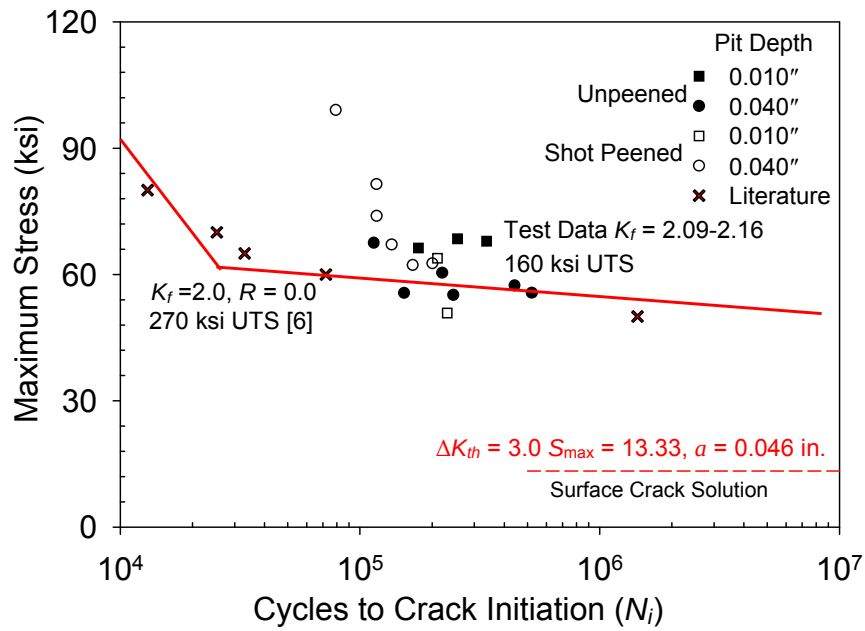

Figure 22. D6AC Steel Bare and Shot-Peened Test Results for R = 0.1

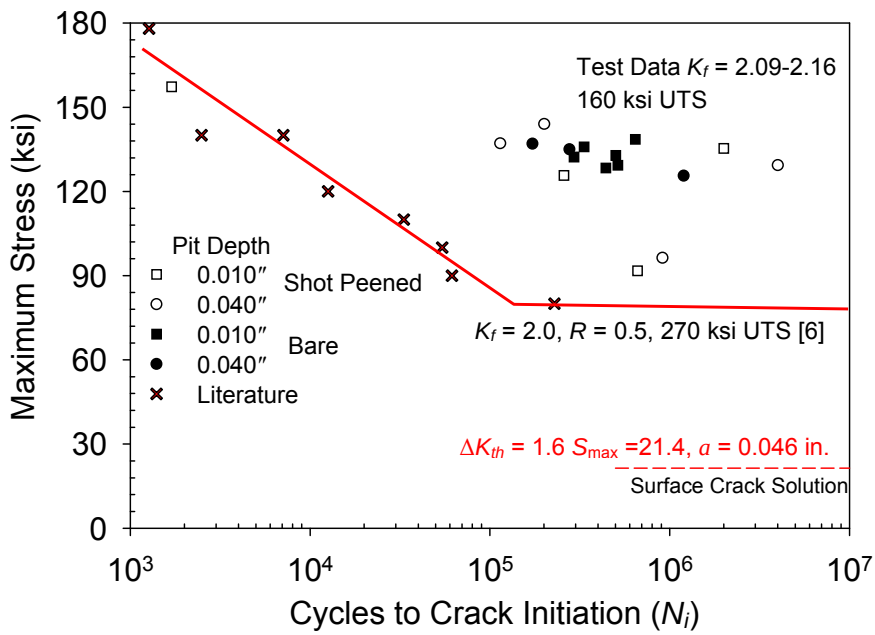

Figure 23. D6AC Steel Bare and Shot-Peened Test Results for R = 0.7

4.6 D6AC STEEL PROPAGATION TEST RESULTS.

The D6AC steel crack propagation after the initiation phase was also recorded for each specimen. For reference, the growth rate for two D6AC steel specimens are displayed in figure 24 and compared to the NASGRO data. For reference, the Al 7075-T7351 fatigue crack growth test results are shown next to the D6AC steel results. Like the 4340 steel results, the growth

rates in the D6AC steel corrosion pit specimens did not align well with the NASGRO data like the Al 7075-T7351 test results. The corrosion pit fatigue test results are nonconservative at lower growth rates compared to the NASGRO fatigue crack growth data. The results converge to the NASGRO data as the growth rates increase. This effect is discussed in the analysis, but it is believed to be geometry-dependent. By the fact that the shot peen and bare fatigue crack growth results exhibit the same trend implies that the difference is not due to the surface enhancement or shot-peening residual stresses.

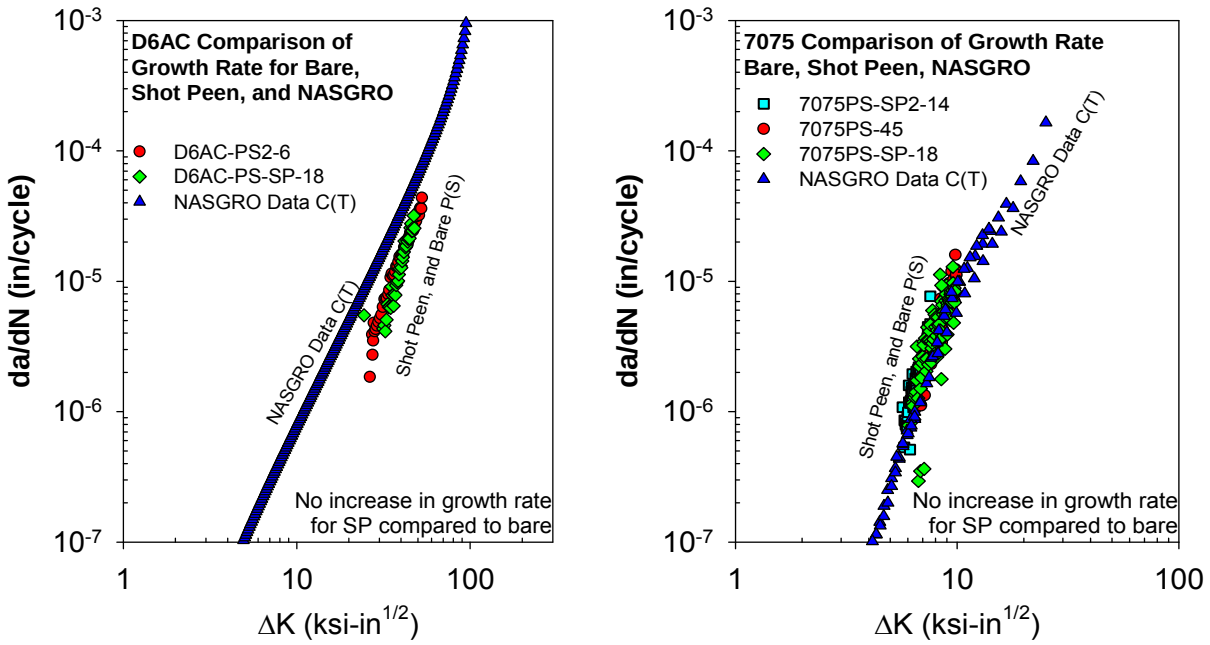

Figure 24. D6AC Steel Fatigue Crack Growth Comparisons of a Corrosion Pit (Al data shown on right for reference.)

A summary of the important observations are listed below:

- The D6AC steel fatigue crack growth from the corrosion pit is nonconservative compared to the NASGRO fatigue crack growth data. This result is consistent for the shot-peened and bare specimens. It is also consistent with the 4340 steel test results.

- The fatigue crack propagation rates appear to be insensitive to residual stress because the shot-peened and bare results have the same behavior.

5. ANALYSIS AND DISCUSSION.

After the test results were processed, an analysis effort was established to characterize and eventually predict the corrosion pit crack initiation and propagation from a variety of materials. The initial analysis effort developed the tools for NASGRO and is discussed in more detail in section 5.1. After the development of the tools, the new NASGRO model was used to perform

postprocessing and predictions of the test results. The approaches to analysis are discussed and compared to the test results.

5.1 NASGRO CORROSION PIT MODEL.

During the tests, the initial results were not characterized well by the surface crack solutions in NASGRO. This is evident in the test results shown in section 4 for the Al and steel specimens. The general trend was that the surface crack solution was very conservative compared to the test results. From this observation, a study was performed to generate a surface crack SIF solution emanating from a hemispherical notch.

The initial study, performed by Jacobs Engineering Sciences Contract Group, compared the SIF solutions for a surface crack and a crack from a hemispherical notch of the same size. The results, as shown in figure 25, demonstrate that the SIF values near the notch root are less than the SIF values from a surface crack of the same size. This result suggests that the remote stress required to propagate a surface crack is less than the remote stress in a component with a crack emanating from a hemispherical notch. It does not imply anything with respect to the crack initiation from the corrosion pit. The results also demonstrate that the hemispherical notch crack solution converges to the surface crack solution when the crack is approximately 75% of the pit diameter. Based on these differences, a new NASGRO solution called SC-31 was developed.

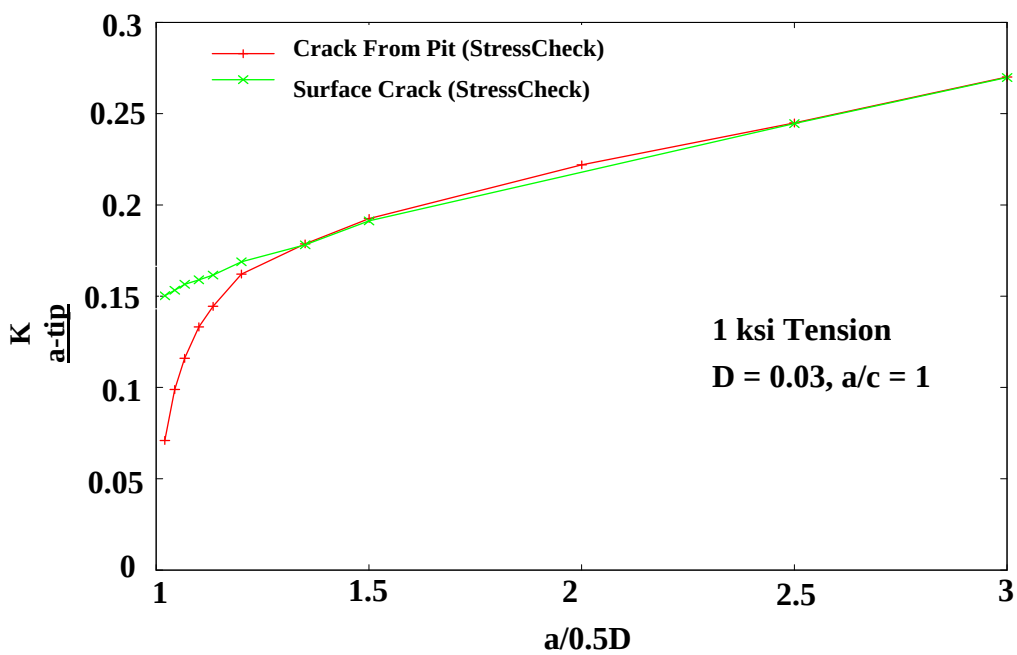

Figure 25. A Comparison of Surface Crack and Corrosion Pit Crack Solutions

The new SC-31 solution is an empirical NASGRO model based on finite element results obtained from a study performed using the StressCheck™ program by Engineering Software Research and Development, Inc. As an experimental solution, it is not yet available for public use, but was installed for this evaluation in an experimental NASGRO release. A depiction of

the SC-31 model is shown in figure 26 and operates within the fatigue crack growth module of NASGRO in the surface crack solutions. The model allows for tension and/or bending cases for a variety of corrosion pit sizes.

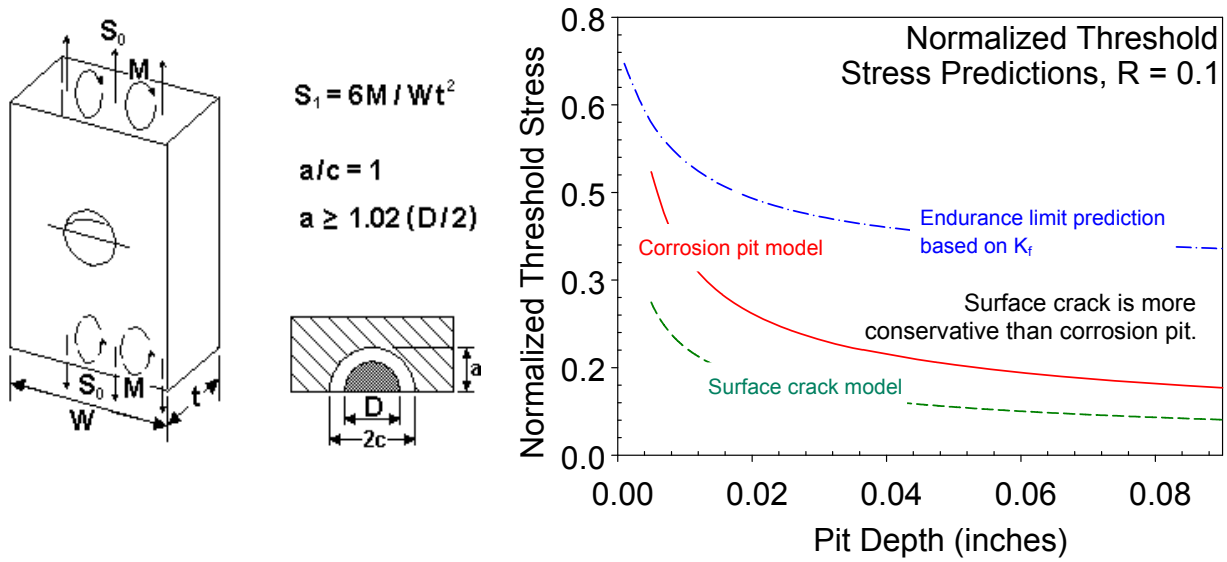

Figure 26. NASGRO SC-31 Solution and Generalized Threshold Stress Predictions

An advantage of having this model is that the efficiency of analyzing the test results with the NASGRO software was fully utilized. A variety of pit sizes are allowed, and the model can be used seamlessly with the material database and load cases. A major limitation of the model is that the crack aspect ratio is limited to a/c = 1, which implies that the crack will always propagate as a semicircular crack and cannot transition to a semi-elliptical surface crack. Another limitation is that the initial crack size is limited to $a \geq 1.02\ (D/2)$. In general, this is not a significant limitation, but it did prove to be a minor problem during the equivalent initial flaw evaluation. The final limitation is that the residual stress field cannot be superimposed on the solution to account for surface enhancements. Although there were significant limitations with the software, the analytical results will show that the addition of the SC-31 solution to NASGRO is a necessary addition.

For reference, the NASGRO geometry labels "a" as the crack depth, which includes the pit radius plus any additional cracking. In this section, reference is made to an equivalent initial flaw size (EIFS). This EIFS only pertains to the crack size beyond the pit depth. For input into NASGRO, the pit depth would have to be added.

To exercise the new NASGRO solution, a normalized threshold assessment is displayed for a range of corrosion pit sizes in figure 26. This assessment compares an endurance limit prediction based on K_f, the NASGRO SC-17 surface crack solution, and the new NASGRO SC-31 corrosion pit crack solution. It was immediately apparent that the surface crack threshold predictions were conservative compared to the new NASGRO SC-31 corrosion pit solution. The new NASGRO capability allows for unnecessary conservatism to be removed from damage tolerance predictions.

In summary, a few key points regarding the new NASGRO corrosion pit model are listed below.

- A new crack solution was developed for NASGRO that characterizes a crack emanating from a corrosion pit.

- The new NASGRO SC-31 solution removes the conservatism from surface crack solutions and provides a new approach for characterizing fatigue cracking from a corrosion pit.

5.2 CORROSION PIT EIFS FATIGUE ANALYSIS.

With the new capability of the SC-31 solution in NASGRO, the first method of evaluating the test results from a predictive capacity was to perform an EIFS investigation. The EIFS method incorporates an initial flaw size that is small enough so that the fatigue life can be accurately predicted. It should also be noted that the initial flaw size does not need to be relevant with respect to a nondestructive evaluation capability, it is purely an analytical technique. The approach mentioned here is used for the new corrosion pit NASGRO solution and was not intended for use with a surface crack model.

To use the EIFS approach, a literature-based EIFS can be incorporated or the test results can be posttest-predicted. For this evaluation, EIFS sizes from the literature were used [11 and 12]. The Al 7075-T7351 implemented a 0.001″ EIFS and the steel alloys attempted to implement a 0.0004″ EIFS. It should be noted again that the limitations of SC-31 require that the initial flaw size must satisfy the following relationship, $a \geq 1.02 * (D/2)$. This limitation sometimes required that the EIFS had to be set to the lower crack size limit of NASGRO.

Instead of performing the EIFS study from an initial size to failure, the NASGRO solution allows for the propagation to end at a specified crack length. To mimic the tests, the NASGRO predictions were allowed to propagate from the EIFS to the EIFS +0.010″. This means that the EIFS study only accounts for 0.010″ of growth that represented the tests.

Because the NASGRO predictions were limited to 0.010″ growth, it was necessary to postprocess the test results so that the comparisons were equivalent. This signifies the test results were postprocessed to subtract any growth beyond 0.010″ of growth. The test results in section 4 show the initial pit size, the crack initiation size, and the final crack size. The test program was designed to limit initial growth to 0.010″, but that was not always possible, so the actual growth was measured. To account for the propagation from the designated 0.010″, a NASGRO analysis was performed for each specimen to posttest correct the test data. This means that an analysis was performed for each specimen to account for the crack propagation beyond the initial 0.010″ of growth.

As an example, specimen 7075-PS-SP2-14 had an initial pit depth of 0.068″. The initiation crack size should have stopped at 0.078″, but the posttest crack measurement revealed a crack depth of 0.192″, which corresponded to an initiation life of 1,044,904 cycles. To be able to compare this result with the NASGRO prediction of 0.010″ growth, the test was corrected posttest to account for the propagation from 0.078″ to 0.192″, which resulted in 444,484 cycles beyond the 0.010″ of growth. The modified initiation life was then computed to be equal to the

test result of 1,044,904 cycles minus the predicted 444,484 cycles, which equaled 600,420 cycles. The majority of specimens, with the exception of the heavy-peened Al, only had a few hundredths of an inch of growth, so the modified lives were not as pronounced as the example.

In summary, an approach to predict the fatigue initiation phase from a corrosion pit was developed and a few key points are reiterated below.

- An EIFS approach was developed to predict initiation life out of corrosion pits. Specifically, the approach used for this project was a crack that emanated out of a corrosion pit and not from a surface crack-based EIFS.

- The EIFS approach used for this study was based on values obtained from the literature (0.001″ for Al and 0.0004″ for steels). It was not a value obtained from postpredicting the test results.

- The study only accounts for the fatigue initiation phase, which is approximately 0.010″ of fatigue crack growth. For the test specimens, the cycles corresponding to fatigue crack growth beyond 0.010″ were subtracted from the initiation life.

5.3 Al 7075-T7351 CORROSION PIT EIFS PREDICTIONS.

The test results for the Al 7075-T7351 specimens had pit diameters that ranged from 0.010″ to 0.080″, with the heavy-peened specimens generally, having the larger pit sizes. The NASGRO EIFS predictions were based on an initial pit size such as 0.010″, 0.030″, and 0.050″ for the smaller pits, and the results are shown in figures 27 and 28 for $R = 0.1$ and $R = 0.7$, respectively. A schematic of the pit geometry and corresponding crack sizes is shown at the bottom of figure 27.

The results demonstrate that the EIFS method is generally a good prediction for these results, which appears to work equally well for both the shot-peened and bare specimens. It should be noted that the shot-peened specimen test results were not processed to account for residual stress. This means that the Al test results appear to be insensitive to residual stress for a corrosion pit crack initiation, with the exception of the larger (>0.047″) shot-peened specimens. Referring back to the residual stress measurements in figure 1 for Al 7075-T7351, it is apparent that the roots of the larger pits either do not benefit from the compressive stress or cross into the tensile residual stress region. This observation is consistent with the results shown in figure 27 for the larger pit sizes, but it does not explain the results of the heavy-peened specimens discussed below. Another more likely explanation is that the postprocessed propagation life was nonconservative and too much life was subtracted from the initiation phase of the test results. This means that postprocessing the initiation results was too conservative for the larger shot-peened specimens.

The heavy-peened test results are shown in figures 29 and 30 and the corrosion pit EIFS prediction method characterizes the data accurately. The EIFS for Al is 0.001″ but the limitation in NASGRO requires that the 0.080″ pit diameter used a 0.0016″ initial flaw size. This limitation does not appear to have a great influence on the life prediction. Again, the residual

stress field was not included in the analysis, so the observation is that residual stress is not a factor in the initiation for this alloy.

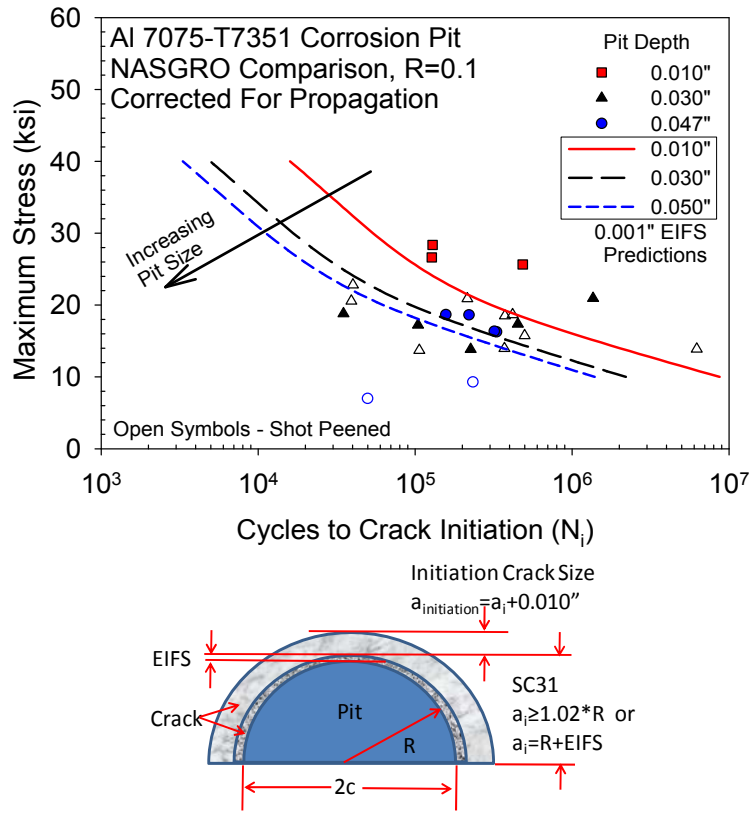

Figure 27. The EIFS Predictions for Al 7075-T7351, $R = 0.1$ (top) and Reference Geometry (bottom)

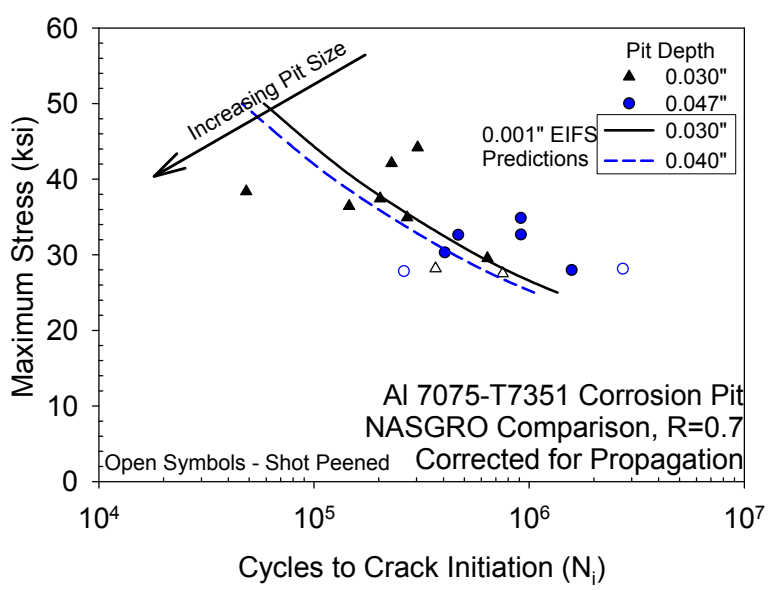

Figure 28. The EIFS Predictions for Al 7075-T7351, $R = 0.7$

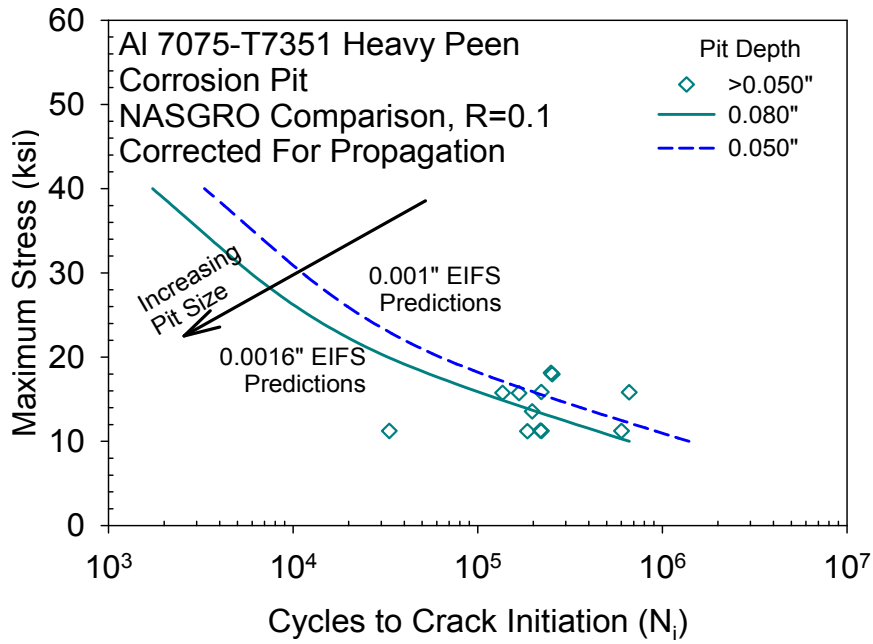

Figure 29. The EIFS Predictions for Al 7075-T7351 Heavy Peen, $R = 0.1$

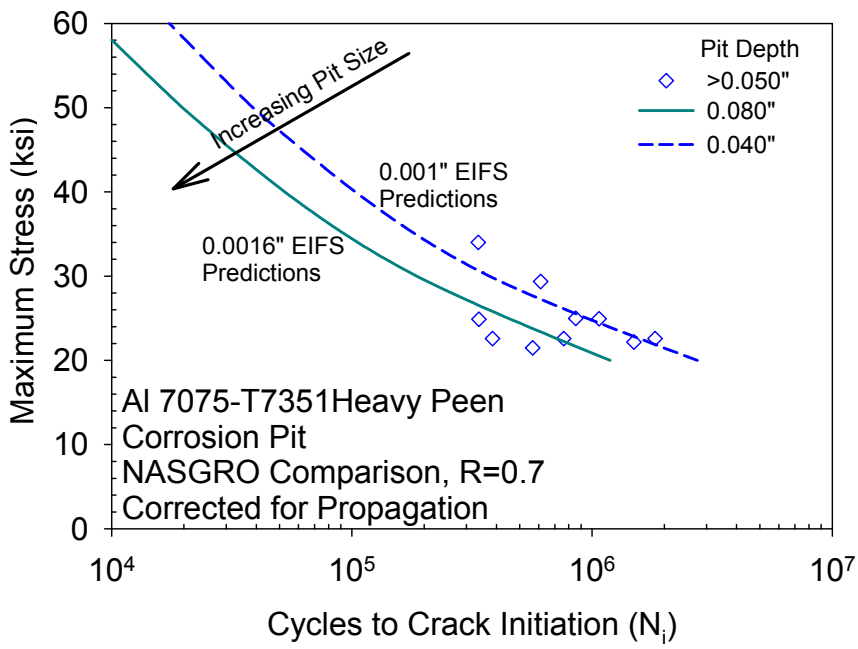

Figure 30. The EIFS Predictions for Al 7075-T7351 Heavy Peen, $R = 0.7$

Based on the analysis and observations of the results, a few key points are reiterated below.

- The NASGRO corrosion pit EIFS predictions appear to capture the test results accurately for both load ratios and all surface-treated conditions.

- The fatigue crack initiation of the specimens with the nominal shot peening appear to be insensitive to the residual compressive stress, and the EIFS predictions capture these test results as well. The only exception is larger pits with nominal shot peen. The predictions are nonconservative compared to these two test results, and it is believed that the postprocessing of the test results was too conservative for these two specimens.

- The heavy peen test results are accurately characterized by the NASGRO EIFS predictions. This suggests that the fatigue crack initiation process for larger pit sizes is not sensitive to the residual stress field.

5.4 4340 STEEL CORROSION PIT EIFS PREDICTIONS.

Unlike the Al EIFS predictions, the 4340 steel predictions were all conservative compared to the test results regardless of surface enhancement method or applied load ratio. The results are shown in figures 31 and 32 for $R = 0.1$ and $R = 0.7$, respectively. From an initial observation, the NASGRO predictions are approximately one order of magnitude too conservative. One possible explanation is that the initial flaw size used for the evaluation was intended to be 0.0004″, but the larger pit diameters were limited by NASGRO input requirements. This implies the 0.0004″ initial flaw size was too small for the NASGRO model. To accommodate the NASGRO limitations, the 0.030″ pit used a 0.0006″ initial flaw and the 0.050″ pit used a 0.001″ initial flaw. Another possible explanation for the difference in predictions is the crack geometry. The NASGRO solution propagates as a semicircular crack, but the corrosion pit cracks initiated out of the pit root and propagated more like a subsurface or embedded flaw.

Closer observation of the test results show that the 4340 steel specimens were sensitive to the residual stress effects, so the true comparison of the prediction is for the bare specimens only. This result is consistent with the residual stress measurements shown previously in figure 2 for the 4340 steel. The laser-peened compressive residual stress field completely encompasses the entire set of corrosion pit sizes tested. The shot-peened compressive residual stress field did not encompass the notch root of the specimens; therefore, the benefit was not as pronounced as with the laser-peened specimens.

In summary, the primary observations for this analysis are discussed below.

- The NASGRO corrosion pit EIFS predictions for 4340 steel were conservative by approximately one order of magnitude for both load ratios tested. The difference is believed to be based on the geometric differences between the idealized NASGRO crack and actual crack. It should also be noted that the NASGRO initial crack size limitations did prohibit the use of the 0.0004″ EIFS for some of the corrosion pit sizes, which only added to the conservatism.

- Shot peening and laser peening provide a fatigue benefit compared to the bare specimens. The laser-peening benefit is more pronounced than the shot peening.

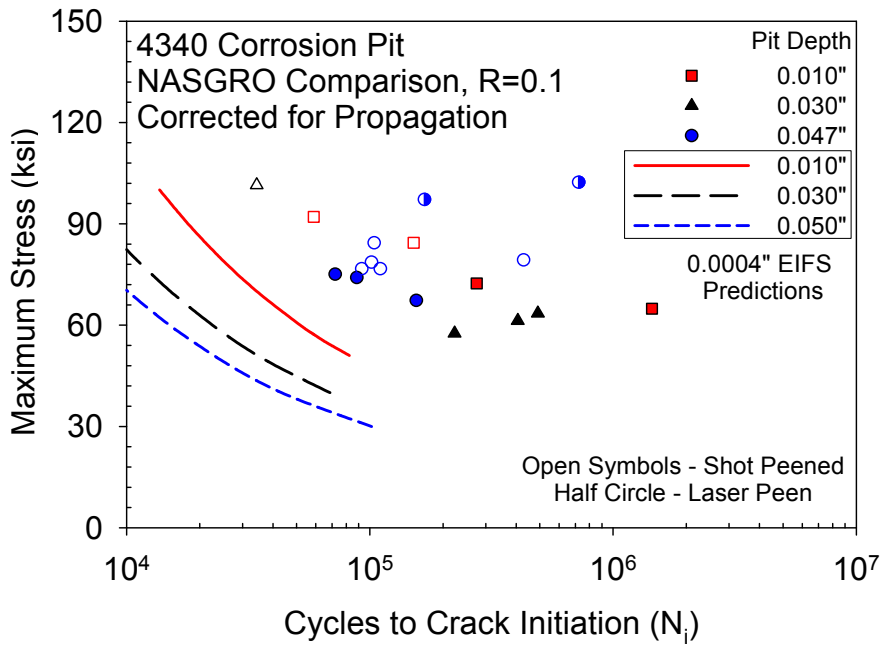

Figure 31. The EIFS Predictions for 4340 Steel, $R = 0.1$

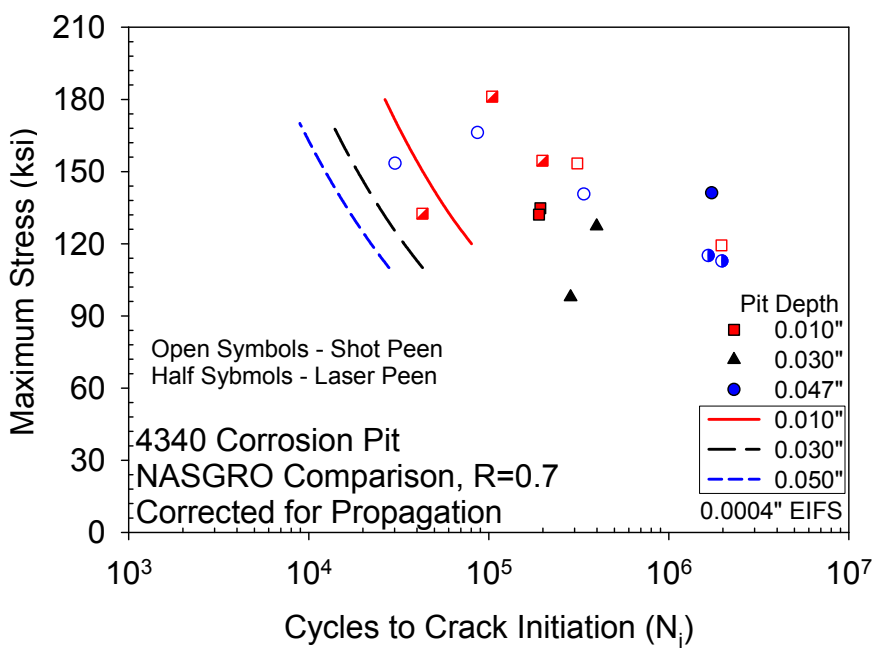

Figure 32. The EIFS Predictions for 4340 Steel, $R = 0.7$

5.5 D6AC STEEL CORROSION PIT EIFS PREDICTIONS.

Like the 4340 steel specimens, the D6AC steel EIFS predictions were conservative, and the results are shown in figures 33 and 34. These predictions represent a 0.030″ pit and an initial flaw size of 0.0006″. Based on the literature, the 0.0004″ EIFS was not possible due to the

NASGRO initial flaw size limitation, it is not believed that this would have had a significant influence on the predictions, but it would have reduced some of the conservatism. In general, postprocessing the test results to remove the propagation cycles beyond 0.010″ compressed the data and removed the scatter with the exception of a few tests.

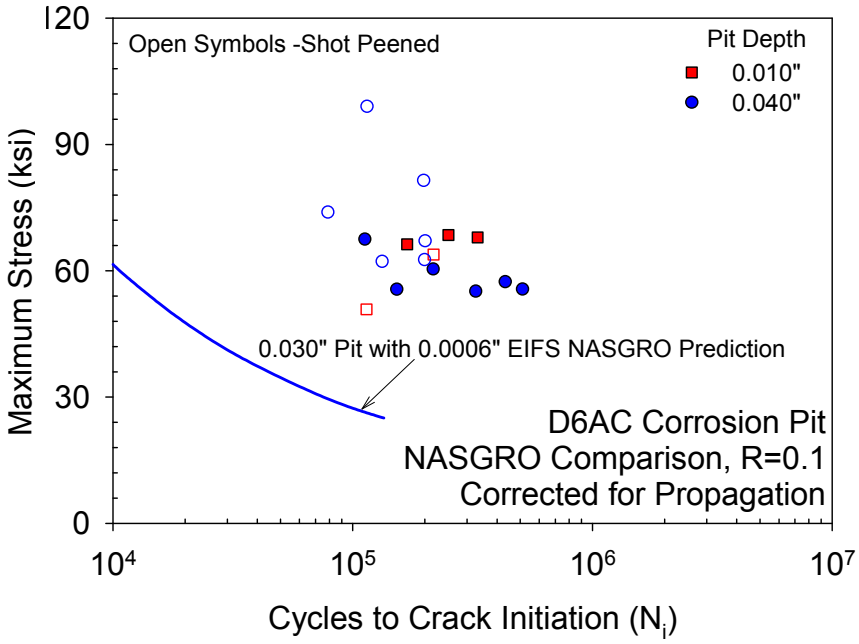

Figure 33. The EIFS Predictions for D6AC Steel, $R = 0.1$

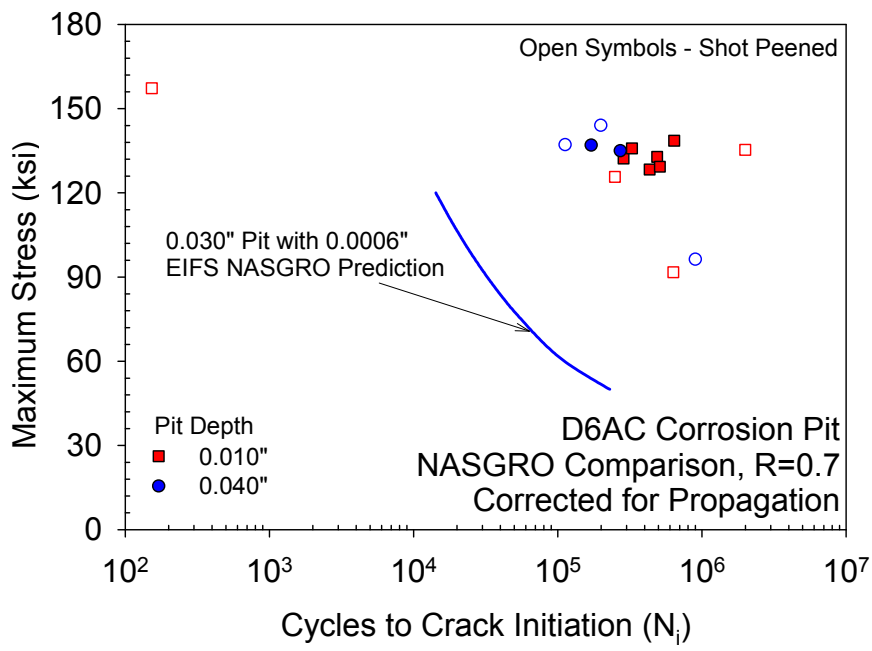

Figure 34. The EIFS Predictions for D6AC Steel, $R = 0.7$

The postprocessed test results show that there was some sensitivity to residual stress for the larger pit depths. This suggests that the resulting threshold stress was increased due to shot peening. Referring back to the residual stress measurements in figure 3, it is apparent that the notch root for all D6AC steel corrosion pits crossed into the residual tensile stress field. The results show that the residual stress effects are more pronounced at the larger pit sizes and for the lower load ratio. Because the yield stress for this material is at 80 ksi, it is not clear how the notch effects combined with the localized yielding affect the fatigue results.

To summarize the observations from this analysis, a few points are reiterated below.

- The D6AC steel specimens are susceptible to residual stress effects from shot peening. This observation is more apparent for larger pit sizes and lower load ratios.

- The NASGRO corrosion pit EIFS predictions were conservative compared to the test results. Some conservatism would have been removed if the NASGRO initial flaw size limitations had not been imposed.

5.6 FATIGUE THRESHOLD ASSESSMENT.

The results discussed in the previous section provide a method of assessing the threshold stress as a function of applied cycles. One problem associated with this method of displaying the results is that the initiation cycles from a previous step are not included. A different approach to displaying these results is to plot the applied stress versus the pit depth, but this approach does not account for the load associated with the previous runout step. This section discusses an approach that used the test results to establish the threshold stress.

The step-test approach used to determine threshold implies that the true initiation and/or propagation threshold occurs somewhere between the previous load step and the current load step. To account for this, an equation can be used that interpolates the threshold load based on the applied loads and applied cycles. The interpolation equation is given in equation 3, where P_{th} is the threshold load, P_{ps} is the previous load from the previous step, P_f is the current load step, N_f is the number of cycles in the current step, and N_{step} is the number of cycles per step. The threshold load can then easily be converted to stress, and the results can be shown as threshold stress as a function of pit depth.

$$P_{th} = P_{ps} + \frac{(P_f - P_{ps})N_f}{N_{step}} \tag{3}$$

Another advantage of this approach is that these results can be compared to an analytic threshold prediction based on either the endurance limit or fracture mechanics. This analytical approach is very similar to the Kitagawa diagram, but it has been modified to account for the pit diameter rather than the crack size [13].

The NASGRO model can provide the geometry factor and SIF for a variety of pit depths. For this study, several pit depths were chosen to predict the threshold stress so the analytic trend could be observed. Because the K_{th} is known for R = 0.1 and R = 0.7, the stress associated with

threshold for a variety of pit diameters was determined by solving for the maximum stress in the SIF relationship.

The other method used in assessing the threshold stress was to use the S-N endurance limit and adjust it to account for the notch. For most cases, the S-N data in MMPDS was used to determine the endurance limit associated with 2 million cycles. This endurance stress was then reduced to account for the K_f and respective pit diameter. This is not the same as using notched fatigue properties. It is a method of adjusting the unnotched parameters to assess the effect of a notch.

To summarize the method, a few key points are reiterated below.

- The threshold stress can be predicted using the threshold SIF, crack geometry, and applied load ratio.
- The endurance stress for a corrosion pit specimen can be predicted using the fatigue notch factor and basic fatigue (stress-life) properties for the given material.

5.7 Al 7075-T7351 THRESHOLD AND ENDURANCE STRESS PREDICTIONS.

The threshold stress predictions and test results for the Al 7075-T7351 are shown in figures 35 through 38. The results are separated to show the bare and nominal shot peen in figure 35, the heavy peen results in figure 36, and the combined data in figure 37. Then, the endurance limit prediction and NASGRO surface crack predictions are shown in figure 38 compared to the NASGRO corrosion pit crack solution.

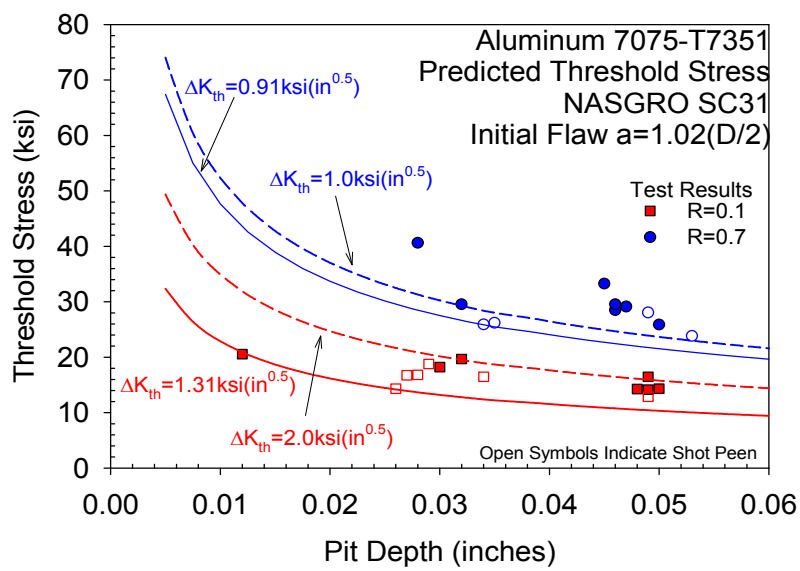

Figure 35. Predicted Threshold Stress for Al 7075-T7351

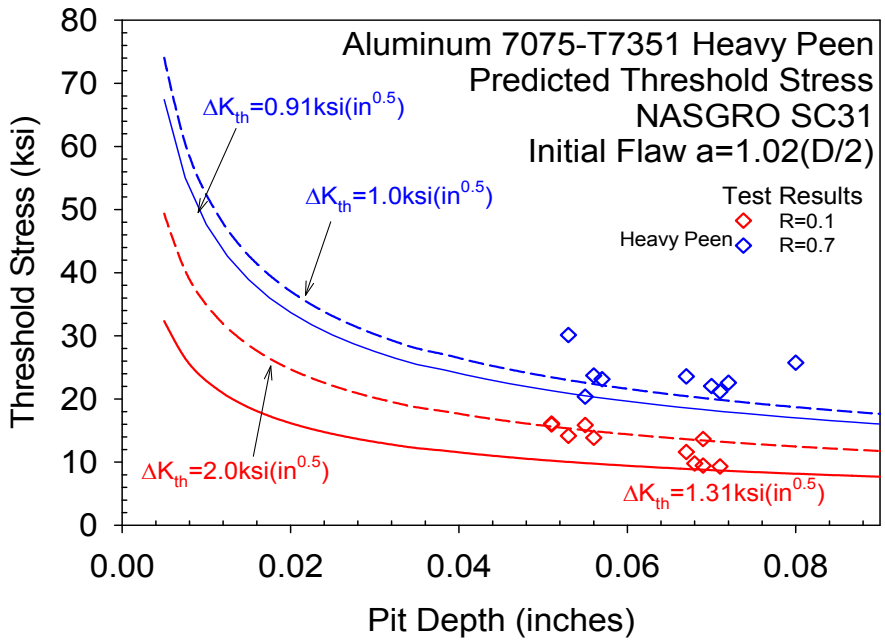

Figure 36. Predicted Threshold Stress for Al 7075-T7351 Heavy Peen

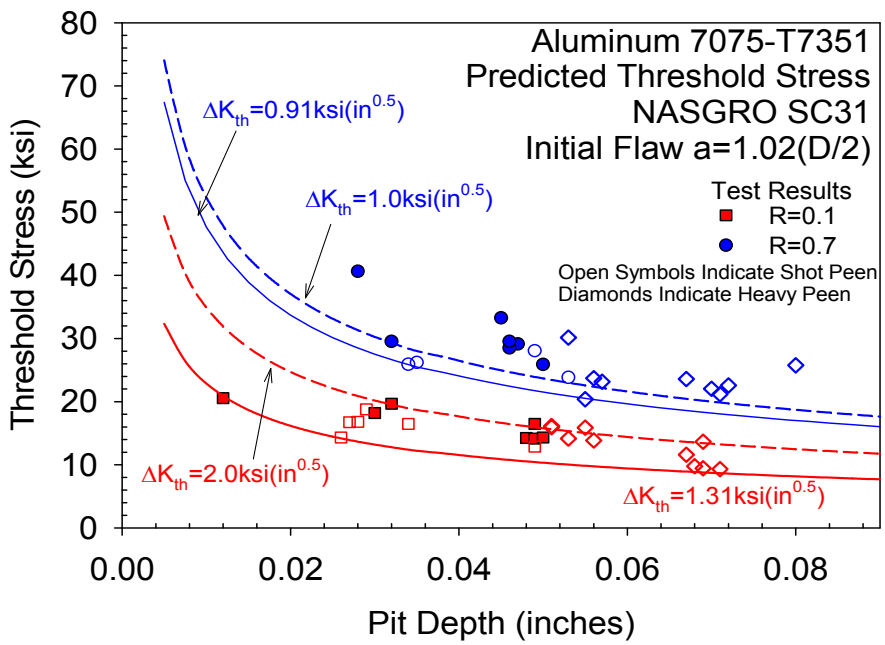

Figure 37. Predicted Threshold Stress for all Al 7075-T7351 Test Results

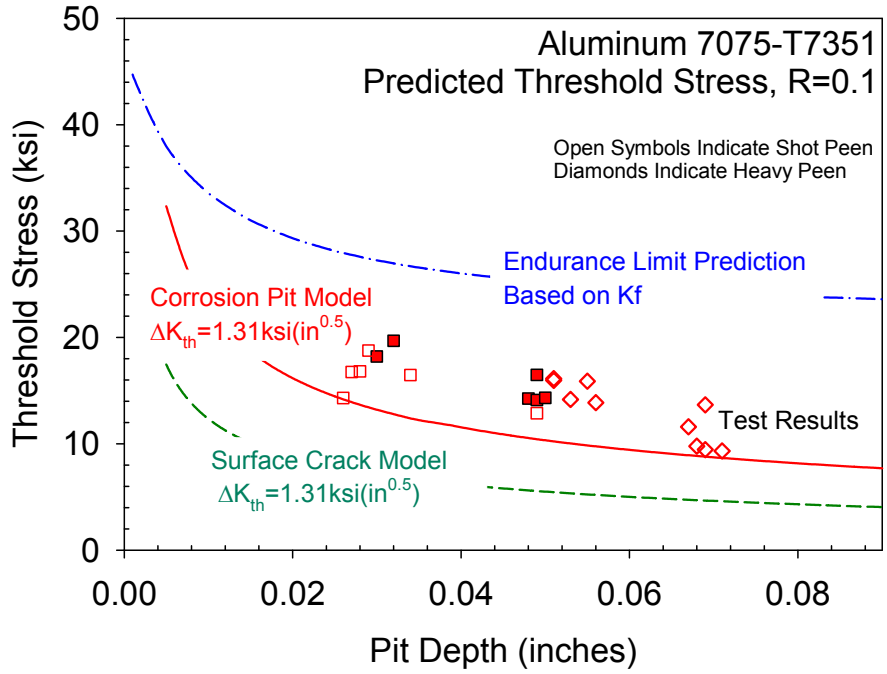

Figure 38. Predicted Threshold Stresses at $R = 0.1$ Showing Endurance Limit Predictions

Initial observation suggests that the threshold stress prediction method is very effective in characterizing the test results. The $R = 0.1$ data are better characterized by the predictions than the $R = 0.7$, but both predictions are conservative. In an attempt to bound the prediction, the threshold SIF ranges were taken from the experimental data and the NASGRO predicted threshold. For example, the $R = 0.1$ conservative prediction uses a ΔK_{th} of 1.31 ksi √in where the upper bound used a ΔK_{th} of 2.0 ksi √in. The more conservative prediction is based on the NASGRO equation, whereas the upper bound is based on the threshold from the fatigue crack growth test data. Both values come from the NASGRO database.

The shot-peened test results are also well characterized by the predictions; this suggests that the threshold or initiation properties are insensitive to the residual stresses. For all pit sizes and load ratios tested, the results also suggest that the threshold behaves according to fracture mechanics predictions. It should be noted that the smallest pit size tested in the heavy-peened condition was 0.050″ and that smaller pits might have demonstrated a dependence on residual stress in the heavy-peened condition.

To further support the use of the NASGRO corrosion pit crack solution, the endurance limit prediction and surface crack prediction are compared to the corrosion pit crack solution in figure 38. The results demonstrate that an endurance limit prediction is nonconservative and not appropriate for this Al alloy and that the fracture mechanics-based approach is much more effective for this range of pit sizes. The results also reveal that the surface crack-based threshold solution is overly conservative compared to the new NASGRO SC-31 solution. The new NASGRO SC-31 solution effectively removes the conservatism from the surface crack solution.

In summary, the threshold predictions based on the NASGRO SC-31 solution accurately characterized the test results. Several points that were made in this section are reiterated for reference.

- The NASGRO corrosion pit fracture mechanics-based threshold assessments conservatively, but accurately, predict the threshold stress for the entire set of Al 7075-T7351 corrosion pit specimens. The predictions are effective for both load ratios and both surface treatment methods tested.

- The surface crack-based predictions are overly conservative approximations of the test results, and the endurance limit-based predictions are nonconservative.

- The results suggest that the residual stress effects from either the nominal shot-peened or heavy-peened surface treatments do not influence the threshold stresses. This is only applicable to the 0.029″ to 0.053″ pits with nominal shot peen and 0.050″ to 0.080″ pits with heavy peen.

5.8 4340 STEEL THRESHOLD AND ENDURANCE STRESS PREDICTIONS.

The 4340 steel threshold stress predictions are shown in figure 39 for $R = 0.1$ compared to the test results. It is apparent for the $R = 0.1$ case that the NASGRO threshold predictions are overly conservative compared to the test results. Although the NASGRO SC-31 predictions are conservative, they are less conservative than the surface crack threshold predictions would have been. Closer examination reveals that the bare threshold stress response for $R = 0.1$ appears to be constant with respect to the pit diameter, which implies that the initiation process may be controlled by fatigue (i.e., endurance limit) rather than fracture mechanics. This observation is also supported by the fact that the notch fatigue factor, K_f, for steel alloys does not vary much for pit sizes above 0.02″. Likewise, the shot- and laser-peened specimens do not follow the fracture mechanics predictions, but the curve does not account for residual stress. The effect of residual stress is apparent for the $R = 0.1$ threshold results with laser peening, resulting in the most increase in threshold stress.

The predictions for the $R = 0.7$ load case are shown in figure 40 compared to the test results. Unlike the $R = 0.1$ predictions, it is difficult to discern whether the NASGRO predictions or the endurance limit predictions are the better approximations. For pit diameters below 0.04″, the fracture mechanics predictions appear to have the same trend, but at larger pit diameters, the endurance limit appears to capture the results better. The shot- and laser-peened specimens still show some benefit, but it is not as pronounced as in the $R = 0.1$ test results. This may be explained by the fact that the localized stresses are above yield, so the influence of shot peening or laser shock peening may not be as apparent as they are in the $R = 0.1$ results.

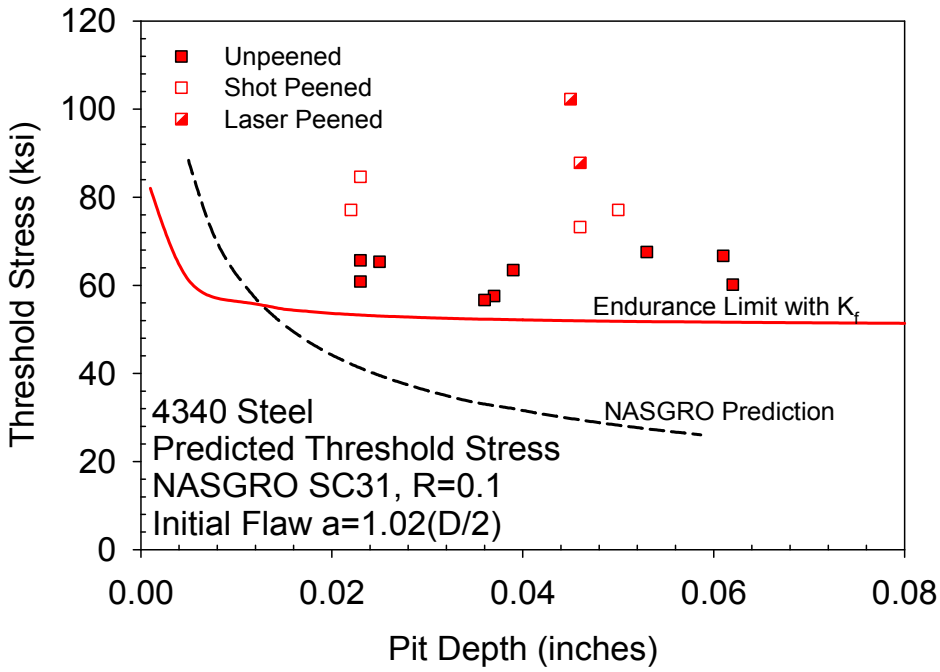

Figure 39. Predicted Threshold Stress for the 4340 Steel $R = 0.1$ Test Results

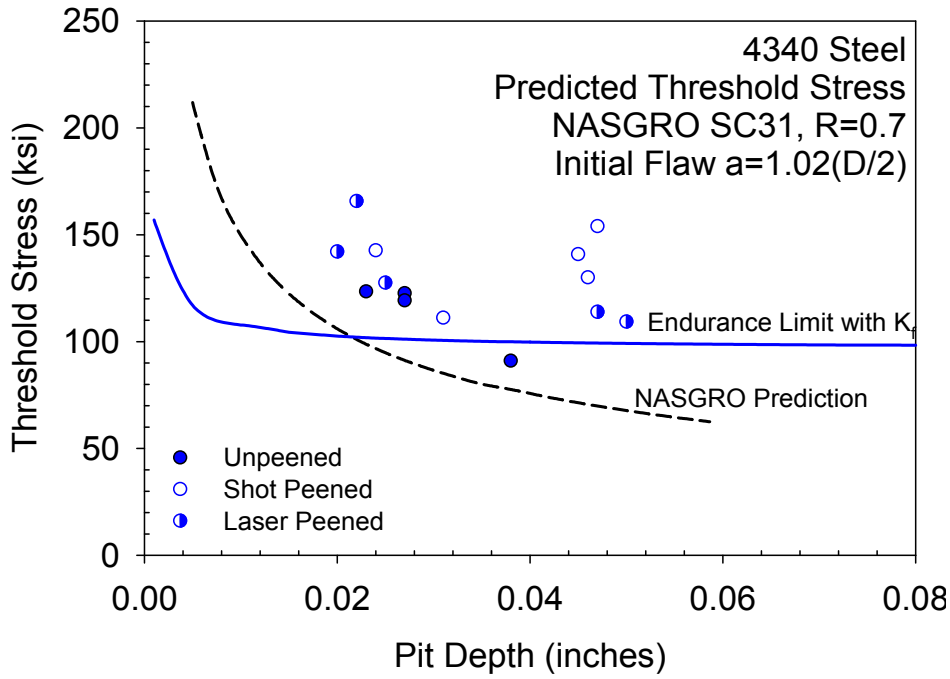

Figure 40. Predicted Threshold Stress for the 4340 Steel $R = 0.7$ Test Results

In summary, the 4340 steel threshold stress predictions were not as accurately characterized by the fracture mechanics predictions. A few key points are summarized below.

- The NASGRO corrosion pit crack solution was generally overly conservative compared to the threshold test results. This solution was still less conservative than surface crack-based threshold predictions.

- The 4340 steel bare and shot-peened corrosion pit test results show little influence with regard to pit size at either $R = 0.1$ or $R = 0.7$ load ratios. There does appear to be a notch size effect for the laser-peened $R = 0.7$ test results.

- The threshold test results were generally well characterized by the endurance limit-based prediction, which accounts for the fatigue notch factor. These predictions were slightly conservative, which implies that they would be effective in modeling corrosion pits.

- Surface treatments like shot peening and laser peening increase the threshold stress, and therefore, the predictions were all overly conservative compared to the specimens with residual stress.

5.9 D6AC STEEL THRESHOLD AND ENDURANCE STRESS PREDICTIONS.

The threshold stress predictions for the D6AC steel specimens are shown in figures 41 and 42 for the $R = 0.1$ and $R = 0.7$ tests, respectively. It is immediately apparent that the NASGRO predictions are overly conservative compared to the test data for both load ratios. Again, the surface crack-based solution is not shown because it is even more conservative than the corrosion pit crack solution. The endurance limit predictions for $R = 0.1$ characterize the larger pits (>0.04″) better than the smaller pits. It should be noted that the $R = 0$ endurance limit for 270 ksi D6AC steel was used for the prediction [6]. The $R = 0.1$ endurance data would most likely fit better, but it is difficult to discern what the effect of reduced strength would have on the endurance limit. For the $R = 0.1$ test results, the residual stress from the shot peening appeared to have the effect of increasing the threshold stress at the larger pit diameters.

The $R = 0.7$ endurance limit predictions are very conservative compared to the test results. These results are for an $R = 0.5$ load ratio instead of $R = 0.7$, so the actual discrepancy may not be as significant if the predictions had been based on $R = 0.7$ data. The tests showed an insensitivity to pit diameter at the higher load ratio. This would imply that the D6AC steel can be better characterized with the endurance limit rather than with the fracture mechanics threshold approach. It is also interesting to note that the high load ratio test data was performed well above the yield stress. Again, the residual stress effects for the $R = 0.7$ test results were not obvious, so the effect of localized yielding may have had an effect on these specimens.

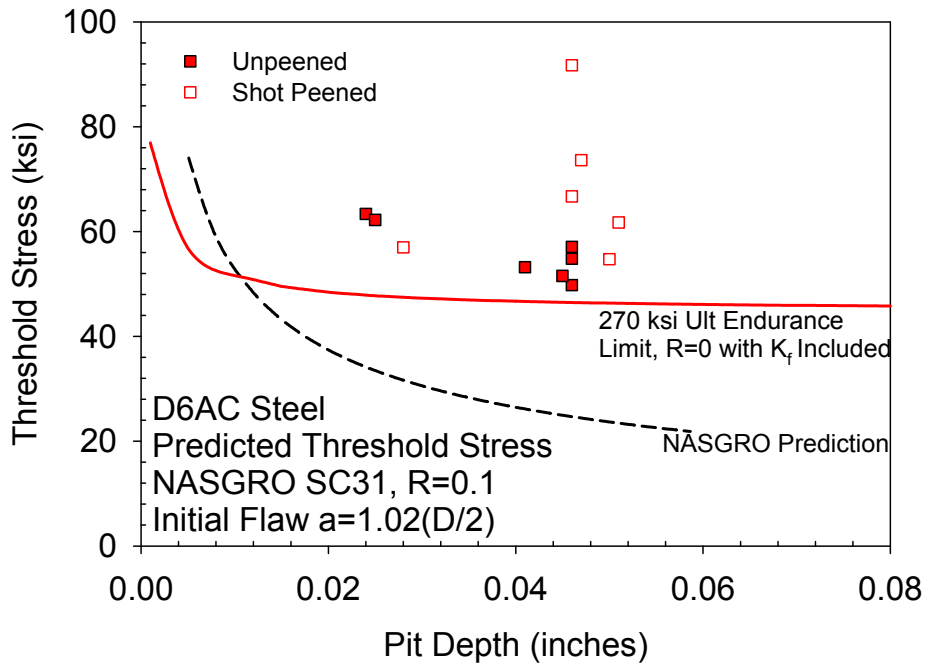

Figure 41. Predicted Threshold Stress for the D6AC Steel R = 0.1 Test Results

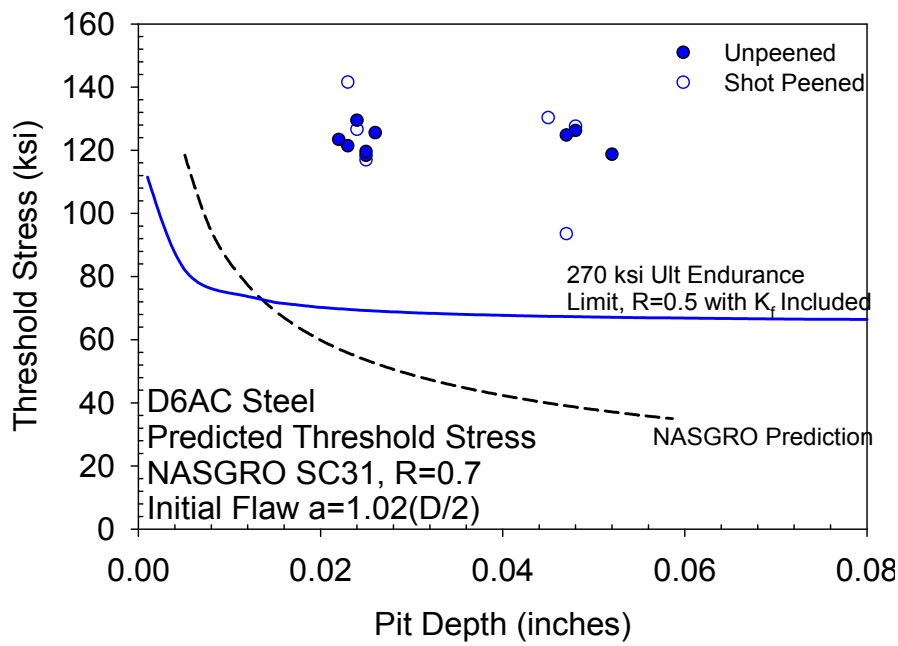

Figure 42. Predicted Threshold Stress for the D6AC Steel R = 0.7 Test Results

To summarize the predictions, a few key points are reiterated below.

- The NASGRO corrosion pit threshold stress predictions were overly conservative compared to the test results.

- Better fatigue (S-N) data would help assess the quality of the endurance limit-based threshold predictions, but it appears that the endurance limit approach is more accurate than the fracture mechanics-based predictions.

- The residual stress effects are more apparent and provide more benefit at the lower load ratio ($R = 0.1$) and higher pit sizes (>0.04″). The benefit of residual stress is not apparent at the higher load ratio ($R = 0.7$).

5.10 FATIGUE CRACK PROPAGATION ASSESSMENT.

In section 4, a comparison of the NASGRO fatigue crack growth rate (FCGR) data for 4340 steel and the postinitiation growth rates for specimens 4340-PS-LP-05 and 4340-PS-35 was performed, shown previously in figure 21. The comparison shows that the laser-peened and bare specimens exhibited essentially the same growth rate; this implies that the residual stresses inherent in the laser-peened specimen may not have a drastic influence in growth rate once the crack has initiated. The fracture surfaces, as discussed in section 6, indicate that the surface residual stress has a role in the evolution of the morphology, but the subsurface tensile stress may negate any of the compression benefit on the surface.

Another interesting aspect of figure 21 was that the test specimen growth rates deviated from the NASGRO FCGR data. It was hypothesized that the difference in growth rates could be explained with the difference in postprocessing by the FTA. The FTA processes the growth rate as if it were a surface crack, but previous work has shown that the SIFs associated with cracks out of a hemispherical pit did not initially behave like a surface crack. An analysis was performed to determine whether the difference in growth rate between the specimens and the NASGRO data was due to the accuracy of the SIF or some other underlying aspect such as load history.

To perform this analysis, the FCGRs from the test data had to be modified or corrected to account for the differences in the SIF solution. The premise behind this approach is that the growth rate (da/dN) and crack size ("a" or "c") remain the same, but that K_{max} and ΔK change because of the modified SIF solution. The correction was established by mapping the test data crack size onto the associated NASGRO pit solution. The following paragraphs provide more detail into the process.

The first step in the procedure was to perform a NASGRO prediction to obtain the K_{max} values in terms of the corrosion pit NASGRO model, SC-31. For reference, the K_{max} predictions for three initial pit size diameters, D, are shown for 4340-PS-35 in figure 43. The initial pit diameter corresponds to geometry measured from the specimen: 2c = 0.102″, 2a = 0.124″, and $\sqrt{ac} = 0.112''$. The initial flaw size used for the assessment was always $a = 1.02(D/2)$, and this size corresponds to the limiting initial flaw size used in NASGRO for SC-31.

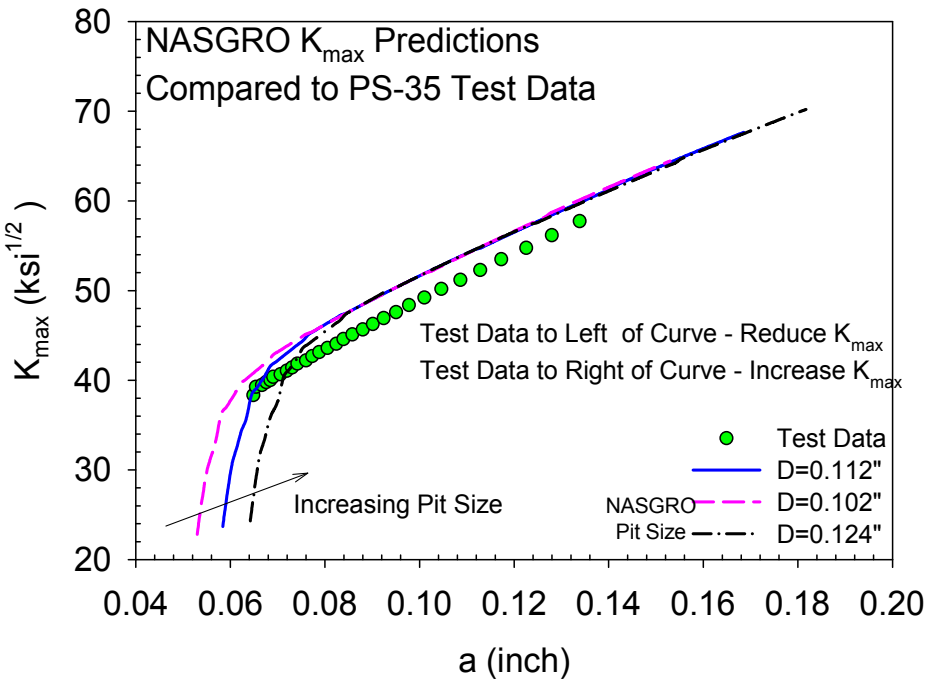

Figure 43. Comparison of NASGRO K_{max} Predictions With Test Data

In addition to the predictions shown in figure 43, the actual test results for 4340-PS-35 are shown. It is shown that the test data intersect the NASGRO prediction curves as the pit size increases. This implies that any test data to the left of the prediction would get a K_{max} reduction to match the NASGRO prediction and any test data to the right of the prediction would get a K_{max} increase to match the prediction. By referring back to figure 21, the lower FCGR test data needed a ΔK reduction to match the NASGRO FCGR data.

To correct the test data to match the NASGRO SIF solutions, a mapping technique was developed. Ideally, the crack sizes could be entered into the NASSIF module, but that feature was not available for SC-31 at the time of this writing. A third-order polynomial was fit to the curved region, and a straight line was fit to the linear region. These curves generated equations that predict K_{max} as a function of crack size. Once the functions were known, the crack sizes from the test data were input to get mapped on the NASGRO K_{max} solution, as shown in figure 44. With the test data mapped to K_{max}, ΔK could easily be determined.

Another approach used during the assessment was to first posttest correct the test data with the visual measurements and then map the crack size to the NASGRO SIF solution. Following the logic that the FTA results should be calibrated to match the actual results, this approach was performed by linearly shifting the test data to match the visual measurements for the initiation and final fracture crack sizes. For reference, this approach is shown schematically in figure 45, where the original test data for 4340-PS-LP-05 (orange triangles) shifts to the left (cyan triangles), and then the corrected data are mapped to the NASGRO prediction. The original test data for 4340-PS-LP-05 did not intersect the NASGRO prediction, so this implies that these data points will get an increase in K_{max} if mapped to the NASGRO solution. This approach was

performed for a, c, and √(ac). The crack size adjustment approach was developed because increasing K_{max} is not the appropriate correction for these test results.

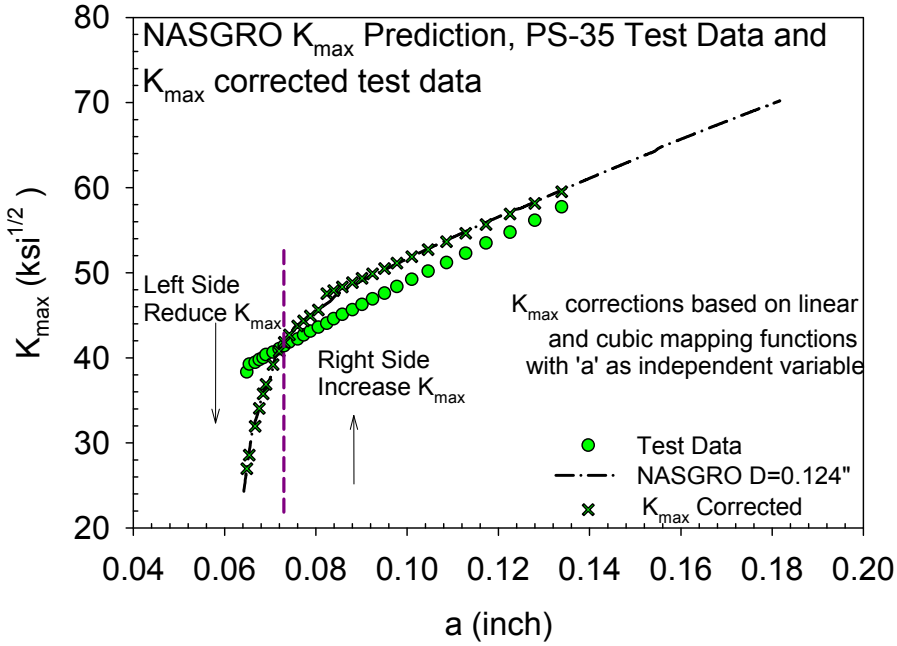

Figure 44. Mapping Procedure for 4340-PS-35 to Determine the Corrected K_{max}

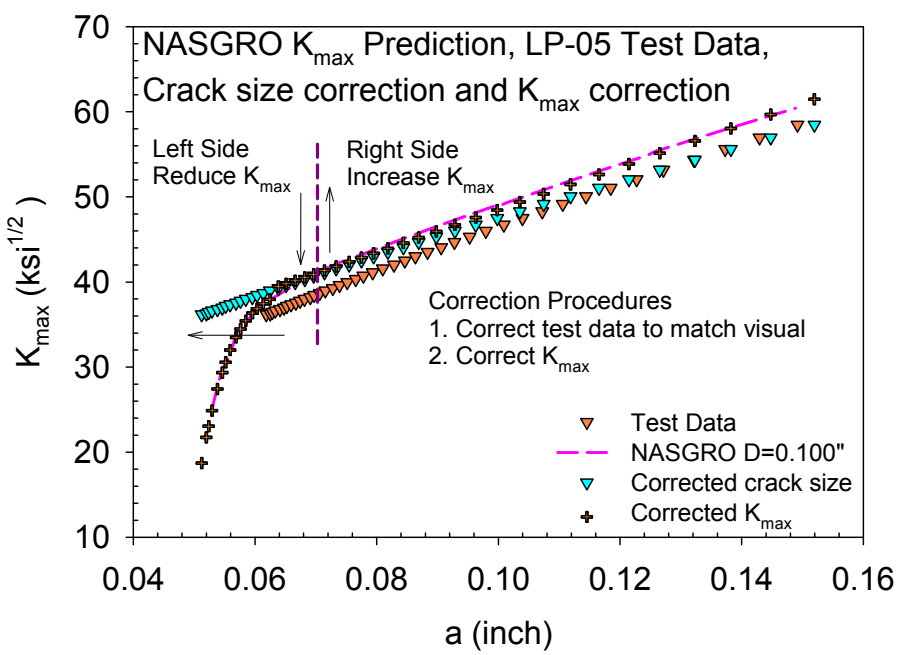

Figure 45. Procedure to Correct for Crack Size and K_{max} for 4340-PS-LP-05

Once the test data were corrected to the NASGRO SIF solutions, they were compared to the existing test data and NASGRO FCGR data for the 4340 steel. The results for 4340-PS-35 are shown in figure 46, which indicate that the K_{max} adjustment corrected the lower portion of the test data, but the entire curve was not corrected. The other three approaches did not work as well because the posttest-corrected crack measurements shifted the data in the wrong direction for the final crack size.

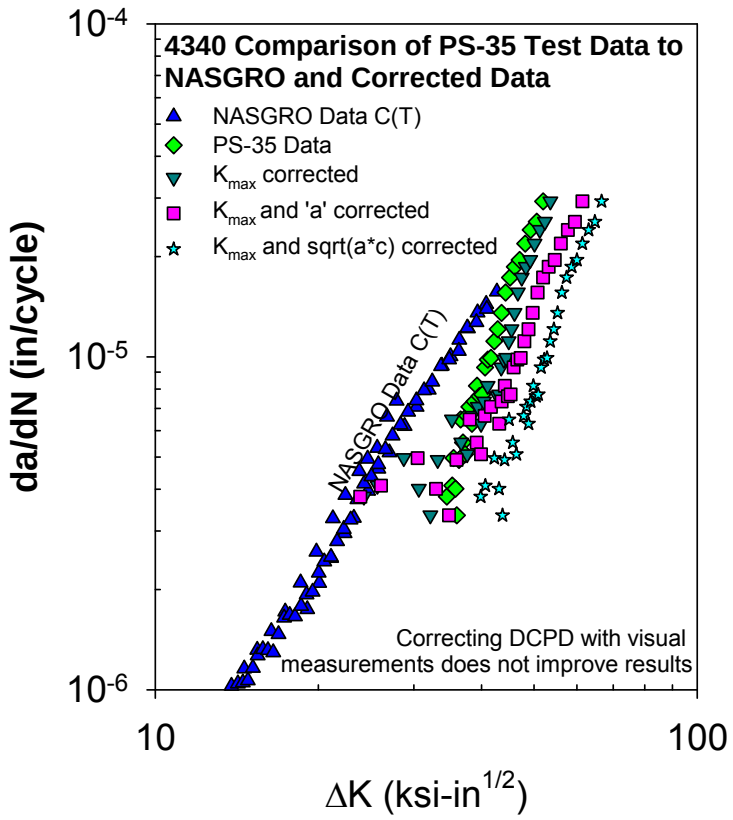

Figure 46. The K_{max} Corrected Test Results for 4340-PS-35 Compared to Original and NASGRO Data Sets

The results for 4340-PS-LP-05 are shown in figure 47, which indicate that the only prediction method that adjusted the data in the correct direction was the posttest-corrected data based on the c measurement. The other models did not adjust the test data in the correct direction. Although this approach appears to have some promising aspects, better understanding of the crack geometry, and updated SIF solutions based on the actual geometry may yield better results. The NASGRO SC-31 solution always assumes a crack ratio of a/c = 1, but the geometry associated with these specimens does not usually reflect that shape until the crack size is beyond the influence of the pit.

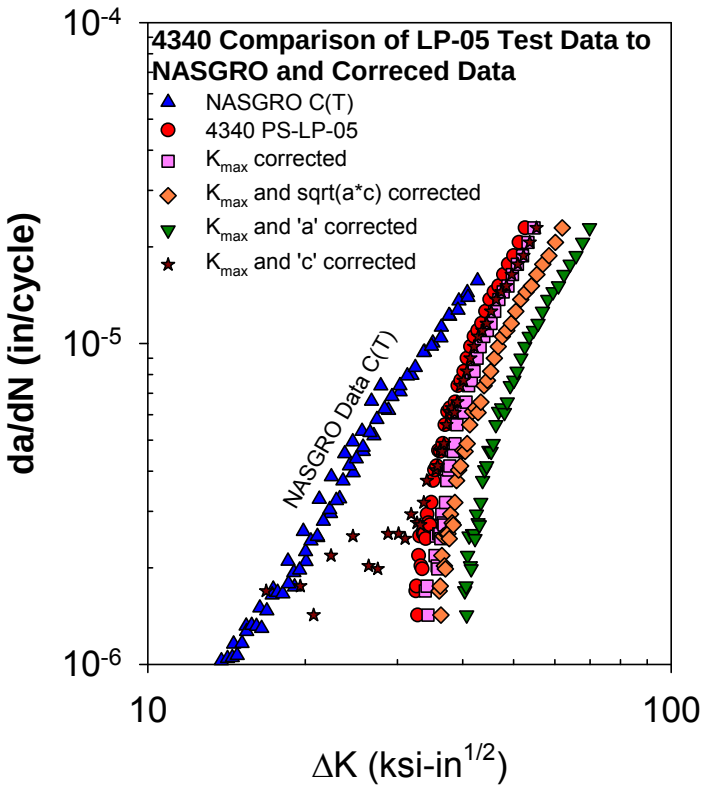

Figure 47. The K_{max} Corrected Test Results for 4340-PS-LP-05 Compared to Original and NASGRO Data Sets

Because this SIF modification approach was not completely successful in explaining the discrepancies in FCGR, other aspects of fracture mechanics might aid in the explanation. For instance, none of the crack closure variables have been accounted for in the assessment. The most likely explanation is the geometry of the crack. NASGRO cannot currently model the variety of crack geometries that emanate from a corrosion pit. It should be noted that the Al specimens did not exhibit these differences as pronounced as the steels, and they also compared better to the NASGRO data. This aspect needs to be considered while developing an explanation.

To summarize the section, a few key points are reiterated below.

- The fatigue crack growth data from the FTA uses surface crack geometry to process the data, but the actual geometry is dependent upon the corrosion pit.

- The test results can be postprocessed to modify the SIFs so that a more representative geometry is used. The NASGRO SC-31 solution is more representative of the actual crack propagation, but does not capture all of the geometrical nuances.

- By posttest correcting the data to account for the geometry effects, the test results begin to trend in the correct direction.

6. FRACTOGRAPHIC OBSERVATIONS.

After the mechanical testing of each specimen was complete, the specimens were fractured to expose the surfaces, and the pit and crack dimension measurements were taken using a digital microscope. A photograph of each specimen was taken and is shown in appendix A. For most cases, the specimens that were tested at a load ratio of $R = 0.7$ and then propagated at a load ratio of $R = 0.1$ had cracks that were much easier to see compared to the specimens that were tested at $R = 0.1$. This is a result of marking the fracture surface because the different load ratios exhibit different fracture morphology.

During this test program, observations of the fracture surfaces revealed interesting trends regarding the crack initiation and propagation out of corrosion pits that required further investigation. Each material is discussed in the following sections with respect to some similar characteristics that were observed in the fracture surfaces. Although each fracture surface had distinctive characteristics, there were some trends, which are discussed in sections 6.1 through 6.4.

6.1 Al 7075-T7351 FRACTOGRAPHIC OBSERVATIONS.

As discussed, the Al specimens were tested in bare, shot-peened, and heavy-peened configurations. Initial observations of all three fracture surfaces show that the cracks initiated at the root of the pit and propagated into the depth while also propagating around the circumference of the pit to the surface. Another general observation for all Al specimens was that the widest region of the crack was subsurface. This was a consistent finding regardless of surface condition and is indicative of an embedded semicircular crack that intersects with the free surface.

The fracture surface from the bare specimen Al 7075-PS-34 is shown in figure 48, and the general trend was consistent with a semicircular surface crack once the propagation reached a sufficient depth. This evidence supports the success of the fracture mechanics predictions for the Al 7075-T7351 specimens. All the bare specimens exhibited the same feature of having the widest part of the crack located subsurface. Some specimens exhibited a preferential side for propagation, so the resulting crack was not symmetrical about the corrosion pit.

The nominally shot-peened and heavy-peened representative specimens are shown in figures 49 and 50. The general trend of all the shot-peened specimens included a deeper crack depth than surface dimension with constrained growth at the surface. This is referred to as a dumbbell shape because it looks like a dumbbell when the two fractured halves are placed front to front. The nominally shot-peened specimens did not have a drastic reduction in surface propagation like the heavy-peened specimens. This observation is consistent with the residual stress fields associated with the different types of surface enhancement. The growth into the depth might have been aided by the subsurface residual tensile stresses. Observation of these flaws and geometry suggest that a NASGRO propagation analysis might also be well characterized by a subsurface elliptical flaw.

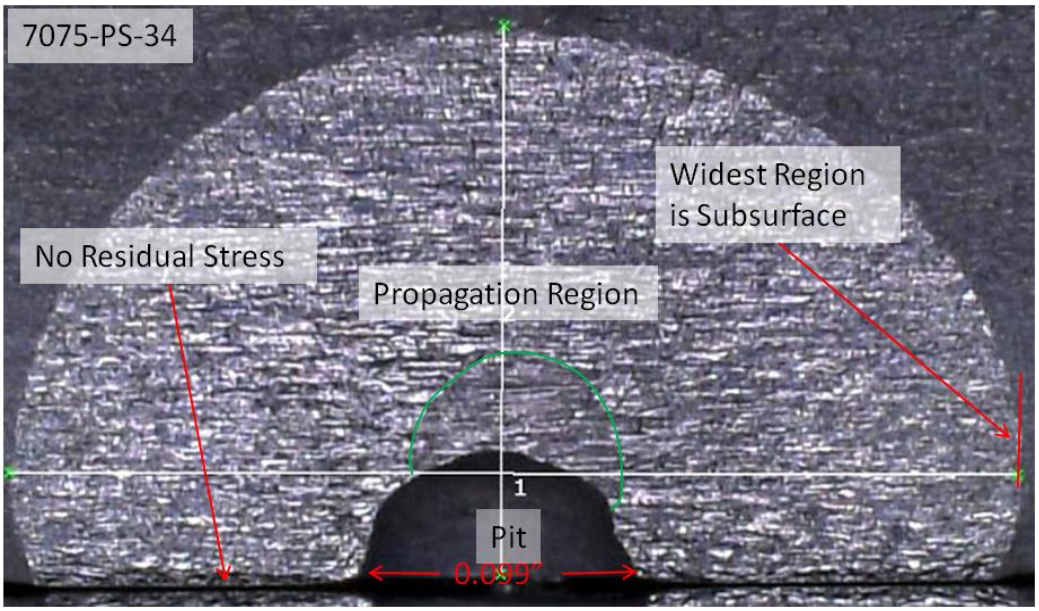

Figure 48. Fracture Surface of 7075-PS-34

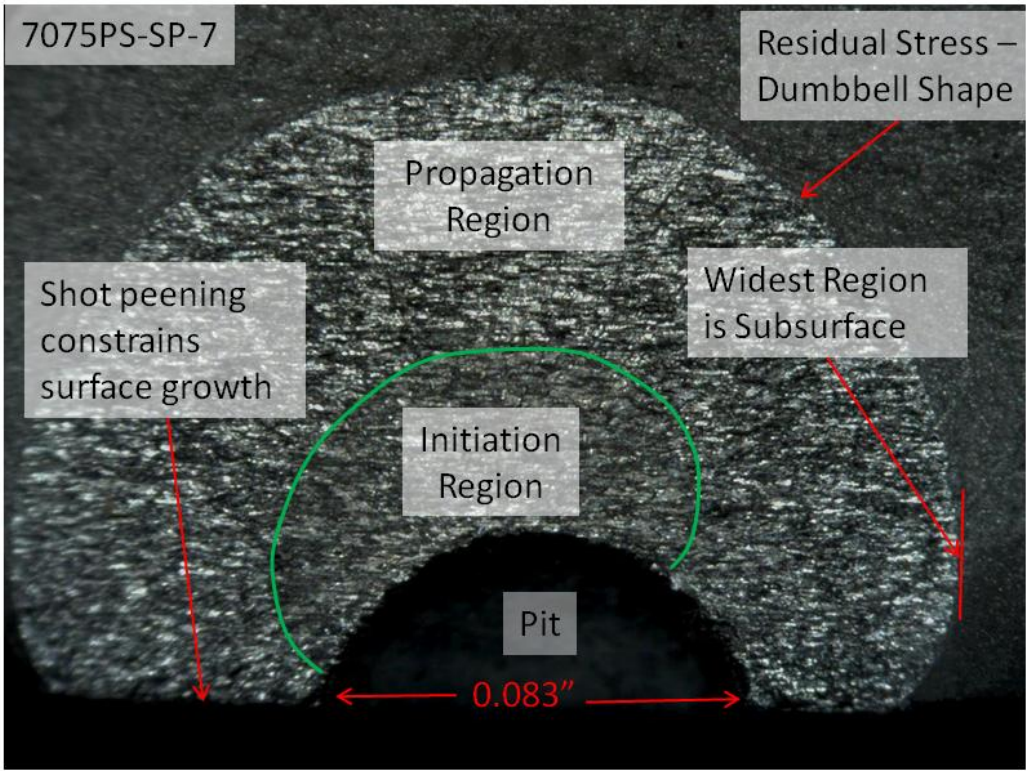

Figure 49. Fracture Surface of 7075-PS-SP-7

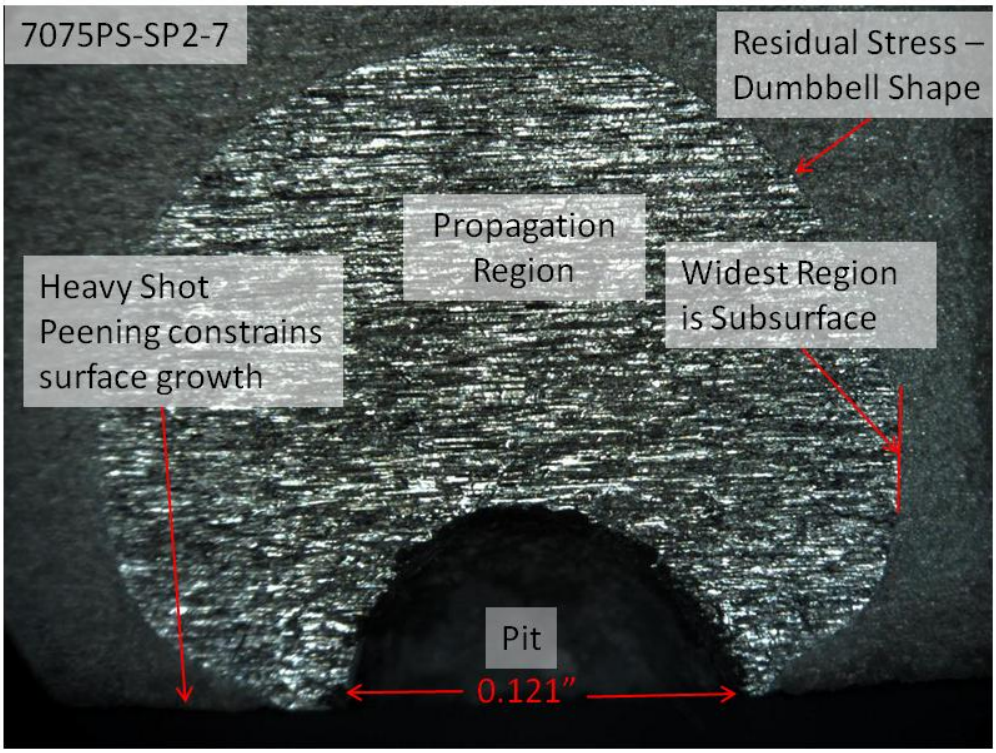

Figure 50. Fracture Surface of 7075-PS-SP2-7

6.2 4340 STEEL FRACTOGRAPHIC OBSERVATIONS.

The 4340 steel specimens were tested in three different surface-enhanced conditions that included bare, shot peened, and laser peened. Each condition exhibited different trends. The specific features of each surface condition are discussed separately.

The bare or unpeened specimens initiated cracks at the root of the notch, which then propagated into the depth and around the circumference of the pit until it intersected with the free surface of the specimen. A bare specimen example is shown in figure 51 for 4340-PS-34. The crack propagated as a semicircular crack until the test was stopped. Unlike the bare Al specimens, the 4340 steel specimens did not exhibit much delayed surface crack growth, if any. This means that the propagation in the steel specimens was very similar to the idealized semicircular crack used in NASGRO SC-31. This observation suggests that the 4340 steel bare specimens should have been predicted with more accuracy, and the propagation data should have correlated better to the NASGRO data. However, some specimens exhibited a preferential propagation direction that favored either the right or left side of the pit.

The laser-peened specimens initiated cracks at the root of the notch like the other specimens, but the propagation around the circumference of the pit was very constrained. The laser-peened example is shown in figure 52 for 4340-PS-LP-05. This resulted in the dumbbell-shaped fracture surface that resembled a semicircular embedded flaw that intersected with the surface. Even the specimen that initiated a crack at a spot weld (4340-PS-LP-06) exhibited the constrained surface propagation.

The shot-peened specimens exhibited fracture surface features more consistent with the bare specimens than the laser-peened specimens. The crack propagation was slightly constrained at the surface, so the largest width of the crack was subsurface, but the cracks still resembled semicircular cracks. The fracture surface for the shot-peened specimens is shown in figure 53 for 4340-PS-SP-11.

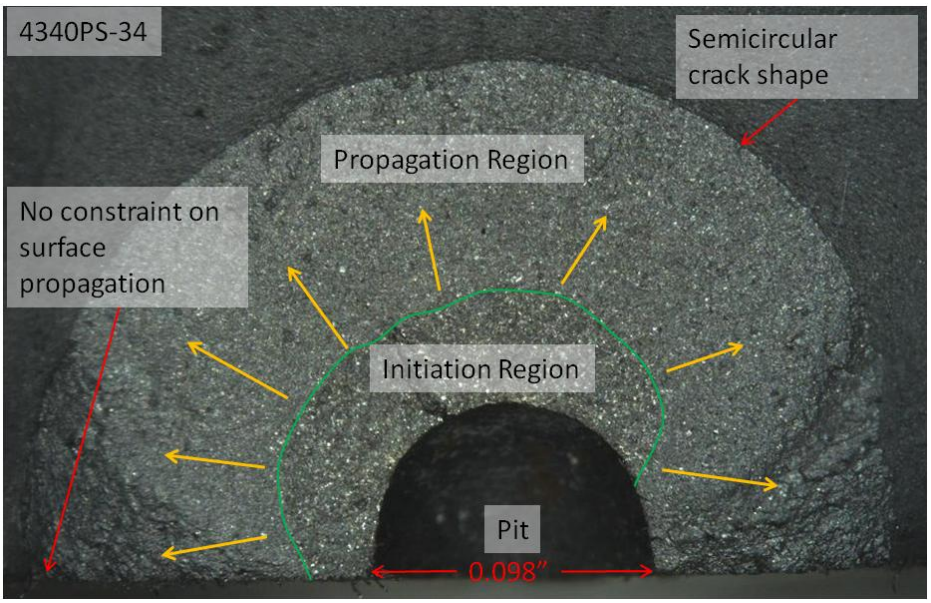

Figure 51. Fracture Surface of 4340-PS-34

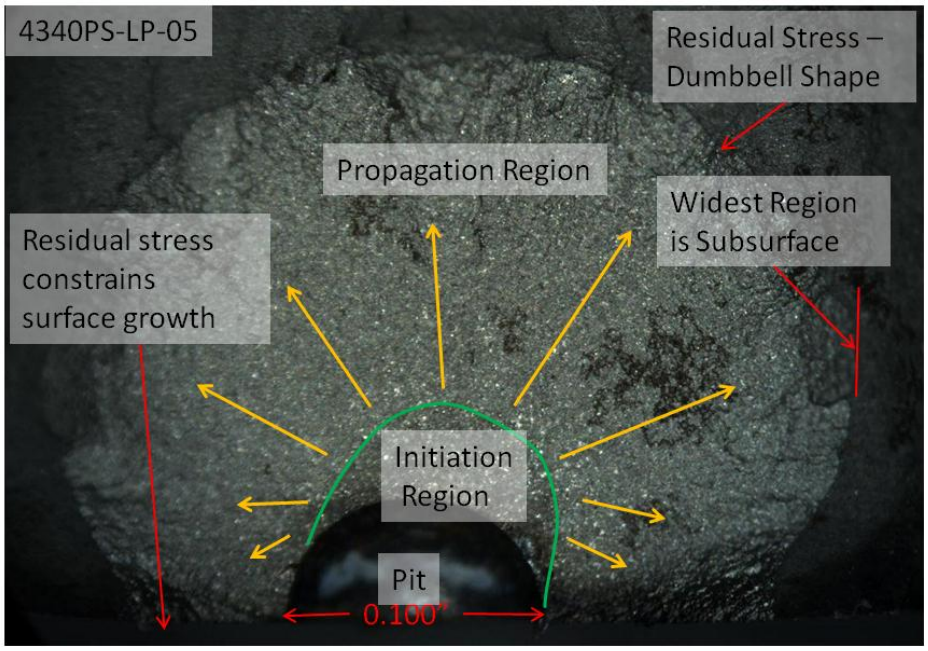

Figure 52. Fracture Surface of 4340-PS-LP-05

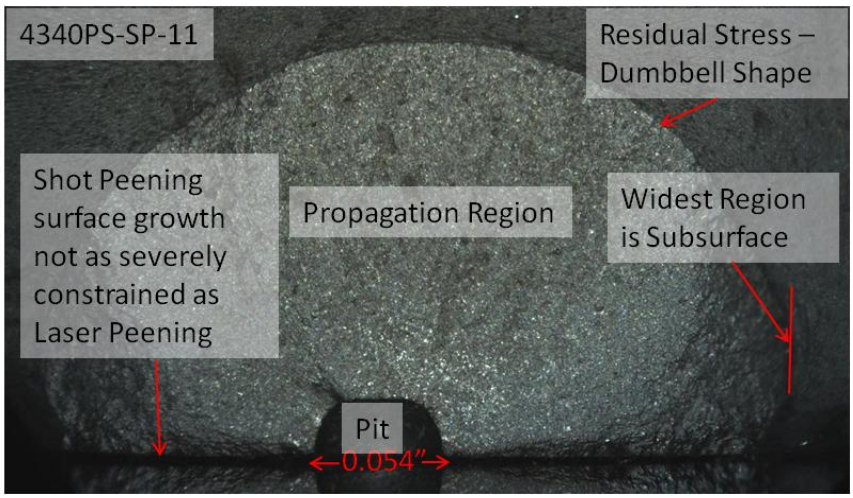

Figure 53. Fracture Surface of 4340-PS-SP-11

6.3 D6AC STEEL FRACTOGRAPHIC OBSERVATIONS.

The D6AC steel specimens were tested in the bare and shot-peened conditions. In general, the cracks initiated from the notch root or offset from the notch root and propagated along the pit until intersecting the free surface. The width measurements of the cracks at the end of the tests were generally greatest just below the surface. This observation was slightly more pronounced for the shot-peened specimens but was also apparent for the bare specimens. The two examples of the fracture surfaces are shown in figures 54 and 55 for D6AC-PS2-18 and D6AC-PS-SP-18, respectively.

The initiation region for the D6AC steel specimens varied from the notch root, as shown in figure 54, to being offset from the notch, as shown in figure 55. It is not clear how the offset initiation affected the test results, but the resulting crack shapes generally trended the same to eventually become a semicircular surface crack with some constrained growth at the surface.

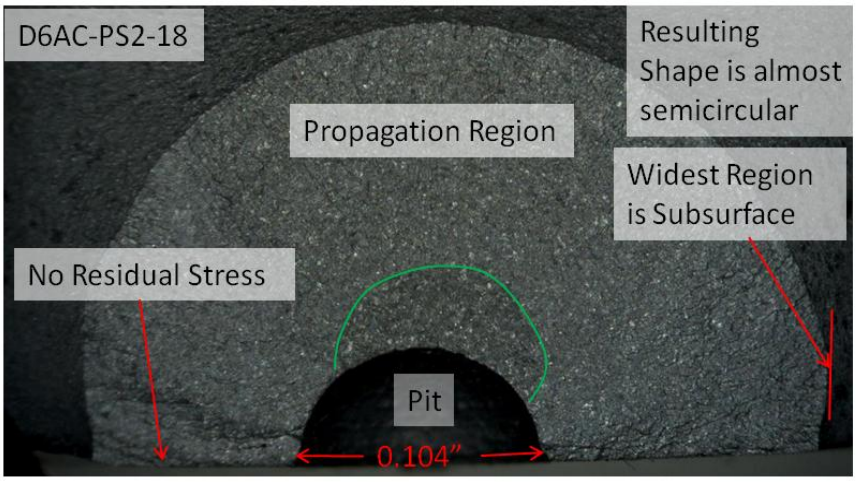

Figure 54. Fracture Surface of D6AC-PS2-18

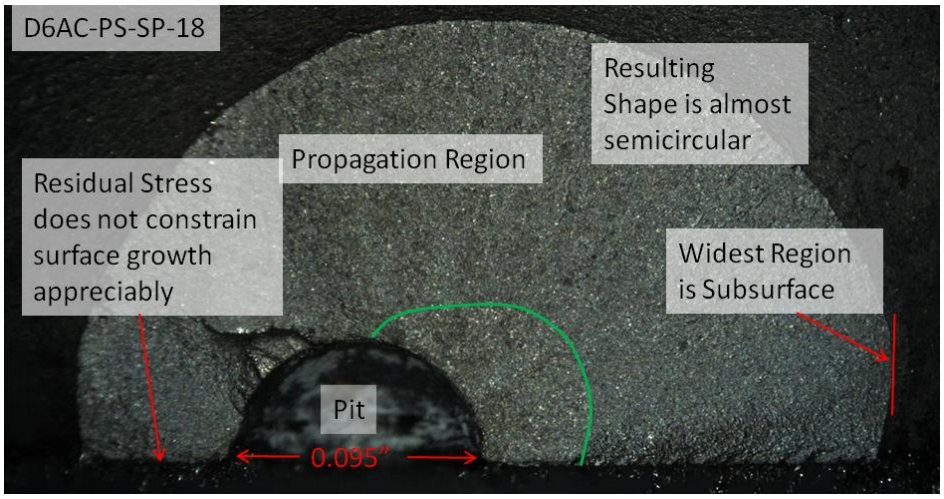

Figure 55. Fracture Surface of D6AC-PS-SP-18

6.4 DISCUSSION OF FRACTOGRAPHIC OBSERVATIONS.

The fractographic observations provide a method to physically characterize the crack initiation and propagation test results so the implications of the features can be discussed in the context of the analysis. In all specimens observed, the cracks initiated in preferential locations that were either at the root of the pit or offset from the root. The crack then propagated into the depth of the material and then around the circumference of the pit until it reached the free surface. This type of crack initiation and propagation was not captured by the analytical NASGRO SC-31 solution until the crack propagated around the notch. This observation can help to explain the differences in propagation rates from the corrosion pit specimens and the NASGRO database. Once the crack intersects the free surface, the NASGRO model appears to be a good approximation for the geometry, except for the cases of residual stress. When the aspect ratio of the crack deviates from a/c = 1, then the NASGRO approximation and the actual geometry also begin to deviate.

In the cases where the surface residual stress constrained the crack growth, a different NASGRO model might be more appropriate. For instance, an embedded flaw may capture the geometry better than a semicircular crack. These results will also motivate future modifications to the NASGRO SC-31 solution to be more representative of the observations.

7. SUMMARY AND CONCLUSIONS.

In summary, a test program was developed and executed to evaluate the influence of hemispherical corrosion pits on crack initiation and propagation in aluminum (Al) and steel alloys. In addition to the general corrosion pit influences, the effects of surface enhancements, such as shot peening and laser shock peening, were also evaluated. The test program used the fatigue testing capabilities available at the National Aeronautic and Space Administration Johnson Space Center (NASA-JSC). Once the fatigue test program was completed, the analysis effort was established to characterize the results. The NASA-JSC team developed a new

NASGRO solution called SC-31 that is empirically based on a crack emanating from a hemispherical corrosion pit. This model was then used in the analysis to predict the test results.

All test results and analytical predictions were presented and the fractographic results were discussed to support the analytical predictions. The specific conclusions for the test program and analysis are provided below.

- A general surface crack fatigue crack growth model is much too conservative to capture the real behavior of a crack initiating and propagating out of a corrosion pit. A new corrosion pit crack growth model was developed for NASGRO that idealizes the corrosion pit crack geometry and reduces the conservatism from the surface crack model to reasonably predict crack initiation and propagation behavior.

- A corrosion pit-based equivalent initial flaw size (EIFS) life prediction method was developed to capture the initiation behavior of cracks initiating and propagating from corrosion pits.

- A threshold stress prediction model was developed to capture the step-test approach and predict the applied stresses at which cracks will initiate from corrosion pits.

- Al 7075-T7351 fatigue initiation from a hemispherical corrosion pit appeared to be insensitive with respect to nominal and/or heavy shot-peened surface enhancements. This observation is independent of corrosion pit size (pit depth = 0.01″ to 0.08″) and applied load ratio ($R = 0.1$ or $R = 0.7$).

- The Al specimens were well characterized by the 0.001″ corrosion pit-based EIFS predictions. This observation is true for the bare, shot-peened, and heavy-peened specimens and supports the previous conclusion that this alloy is insensitive to shot peening with respect to fatigue crack initiation from a corrosion pit.

- The Al threshold test results were also well characterized by the fracture mechanics-based threshold predictions for both the $R = 0.1$ and $R = 0.7$ test cases. The results were not well characterized by an endurance limit knockdown based on the fatigue notch factor, K_f.

- The fatigue initiation from a hemispherical corrosion pit in 4340 steel is sensitive to both shot-peened and laser-peened surface enhancements. Shot peening provides benefit over the bare condition and the laser peening provides benefit over both the bare and shot-peened conditions. This observation is more pronounced at a load ratio of $R = 0.1$ with pit depths ranging from 0.02″ to 0.04″.

- The 4340 steel 0.0004″ corrosion pit-based EIFS NASGRO predictions were conservative compared to the corrosion pit test results for either the $R = 0.1$ or $R = 0.7$ cases. It should be noted that a surface crack-based prediction would only add to the conservatism.

- The threshold stress predictions based on an endurance limit adjusted for the fatigue notch factor appear to reasonably characterize the 4340 steel corrosion pit threshold stresses for both the $R = 0.1$ and $R = 0.7$ cases.

- The fatigue crack propagation rates in the 4340 and D6AC steels were nonconservative compared to the NASGRO database materials. Further testing and/or analysis are required, but the difference is believed to be dependent upon the crack geometry. This observation is supported by the fracture surface observations. This is in contrast to the Al 7075-T7351 propagation data that agreed with the NASGRO database.

- D6AC steel fatigue initiation from a hemispherical corrosion pit appears to be sensitive to shot peening at a load ratio of $R = 0.1$, but insensitive to shot peening at $R = 0.7$. This observation includes all pit depths tested from 0.02″ to 0.06″.

- The D6AC steel 0.0004″ EIFS NASGRO predictions were conservative at characterizing the corrosion pit test results for either the $R = 0.1$ or $R = 0.7$ test cases.

- The NASGRO-based D6AC steel threshold predictions were also conservative compared to the test results for both the $R = 0.1$ and $R = 0.7$ cases. Although the endurance limit prediction characterizes the data better, the actual fatigue properties that match this version of D6AC steel are required to confirm the conclusion. The fractographic evidence supports the use of the NASGRO model to generically capture the fatigue crack growth from a corrosion pit once the crack has propagated around the pit and intersected the free surface. Any subsequent semicircular growth is well captured by the NASGRO model.

- The NASGRO SC-31 model cannot capture the high aspect ratio cracking or constrained surface cracking as apparent in some of the shot-peened and laser-peened specimens. This effect on the predictions is not clear. Further geometric modeling is warranted to capture the initial growth from the notch root.

8. REFERENCES.

1. NASGRO® 6.0, NASA Johnson Space Center and Southwest Research Institute®, March 2006, www.nasgro.swri.org.

2. AFGROW (release 4.0012.05), U.S. Air Force Research Laboratory, VASM, October 2008, www.afgrow.net

3. Rankin, J.E., Hill, M.R., and Hackel, L.A., "The Effects of Process Variations on the Residual Stress in Laser Peened 7049-T73 Aluminum Alloy," *Materials Science and Engineering A*, Vol. 349, 2003, pp. 279-291.

4. Prime, M.B., "Residual Stress Measurement by Successive Extension of a Slot: The Crack Compliance Method," *Applied Mechanics Review*, Vol. 52, No. 2, 1999, pp. 75-96.

5. Metallic Materials Properties Development and Standardization, MMPDS-04, April 2008, Federal Aviation Administration.

6. Davis, S.O., "Elevated Temperature Fatigue Properties of D6AC High Strength Steel," ASD-TDR-63-645, U.S. Air Force Materials Laboratory, Wright Patterson Air Force Base, Ohio, October 1963.

7. Cerit, M., Genel, K., and Eksi, S., "Numerical Investigation on Stress Concentration of Corrosion Pit," *Engineering Failure Analysis*, Vol. 16, 2009, pp. 2476-2472.

8. Eubanks, R.A., "Stress Concentration due to a Hemispherical Pit at a Free Surface," Department of Mechanics, Illinois Institute of Technology, Chicago, Illinois, January 1, 1953, Submitted to Office of Naval Research.

9. Dowling, N.E., *Mechanical Behavior of Materials*, 2nd ed., Prentice Hall, Inc., Upper Saddle River, New Jersey, 1999.

10. Schijve, J., *Fatigue of Structures and Materials*, Kluwer Academic Publishers, Dordrecht, The Netherlands, 1999.

11. Newman, Jr., J.C., Phillips, E.P., and Swain, M.H., "Fatigue-Life Prediction Methodology Using Small-Crack Theory," *International Journal of Fatigue*. Vol. 21, 1999, pp. 109-119.

12. Liu, Y. and Mahadevan, S., "Probabilistic Fatigue Life Prediction Using an Equivalent Initial Flaw Size Distribution," *International Journal of Fatigue*, Vol. 31, 2009, pp. 476-487.

13. Kitagawa, H. and Takahashi, S., "Applicability of Fracture Mechanics to Very Small Cracks or Cracks in the Early Stage," *Proceedings of the Second International Conference on Mechanical Behaviour of Materials*, American Society for Metals, 1976, pp. 627-31.

APPENDIX A—FATIGUE SPECIMEN FRACTURE SURFACES

No Photographs 7075-PS-1, -2, -3, -4, -5, -36	
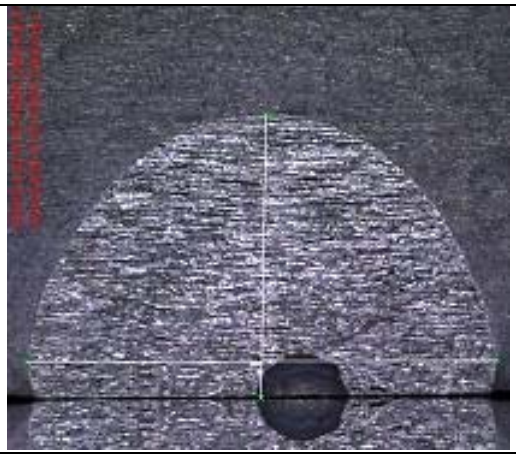	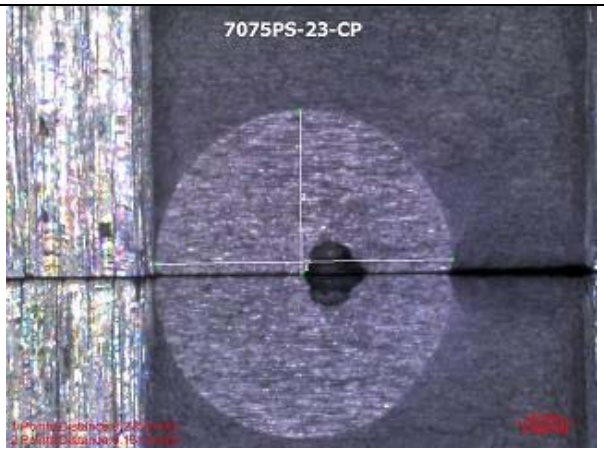
7075-PS-20	7075-PS-23
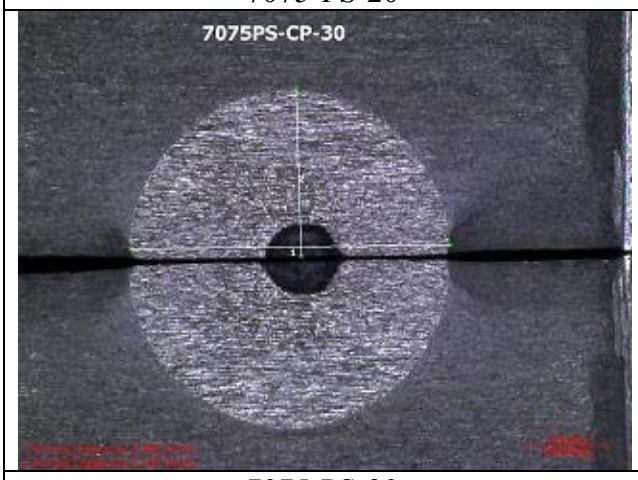	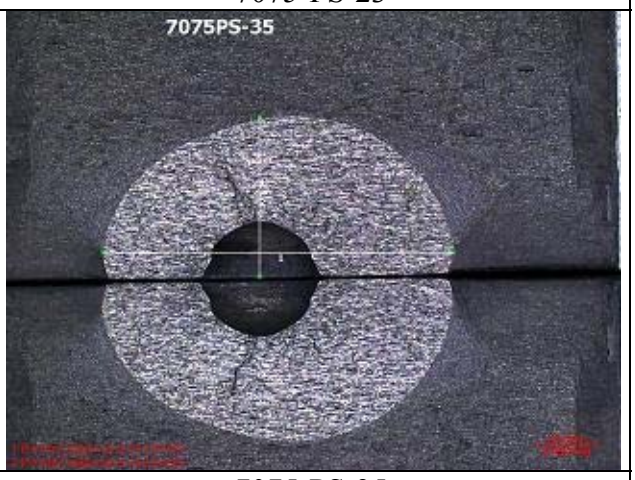
7075-PS-30	7075-PS-35
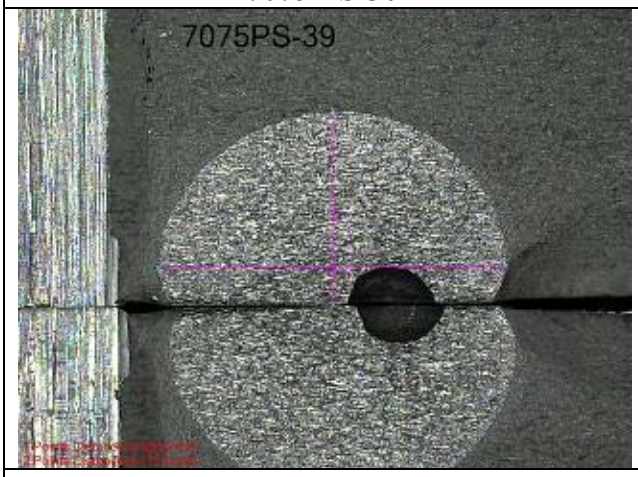	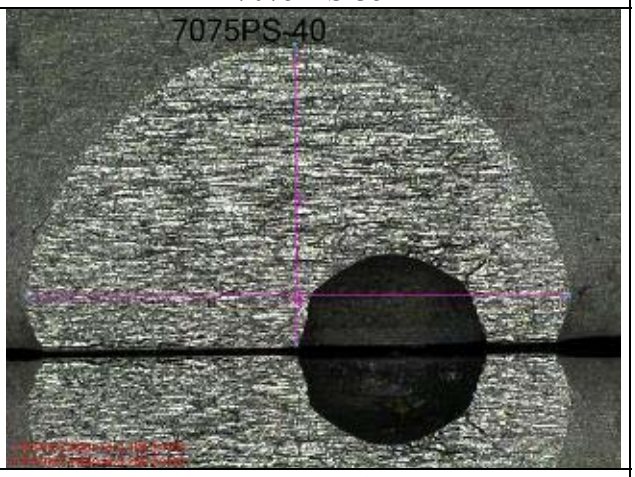
7075-PS-39	7075-PS-40

Figure A-1. Photographs of 7075 PS, $R = 0.1$

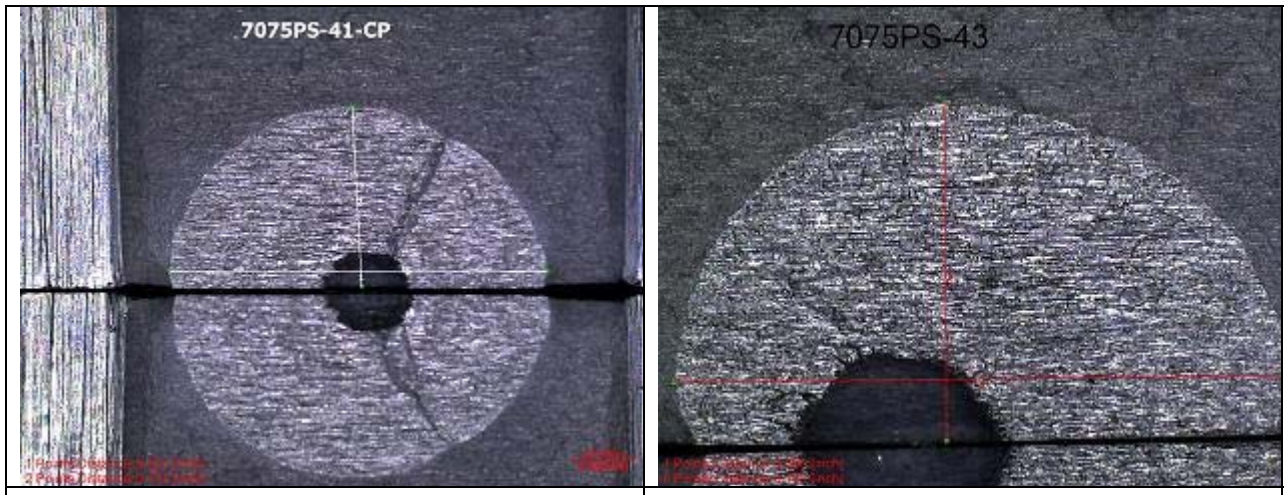

7075-PS-41	7075-PS-43

Figure A-1. Photographs of 7075 PS $R = 0.1$ (Continued)

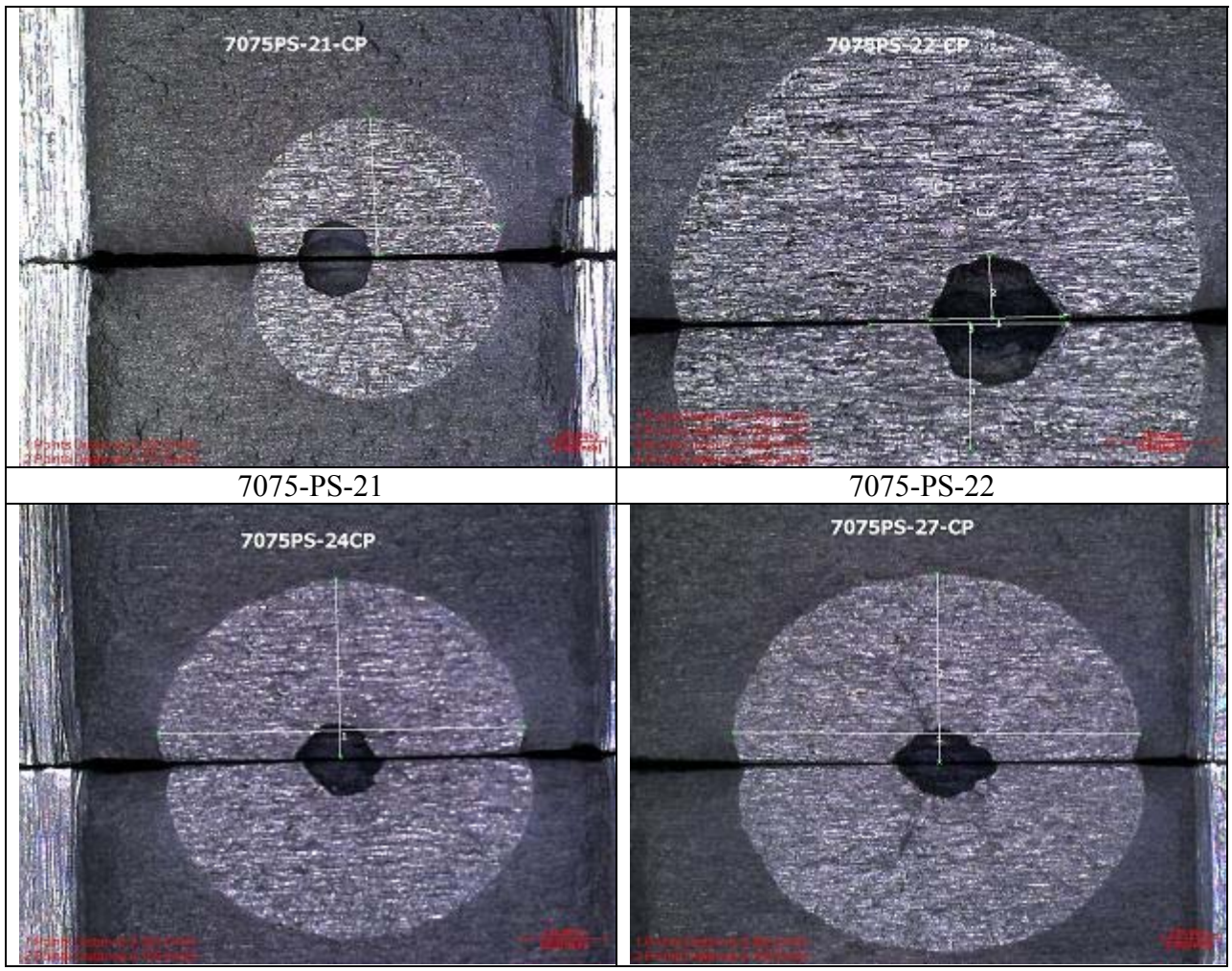

7075-PS-21	7075-PS-22

Figure A-2. Photographs of 7075 Unpeened, $R = 0.7$

7075-PS-24	7075-PS-27
	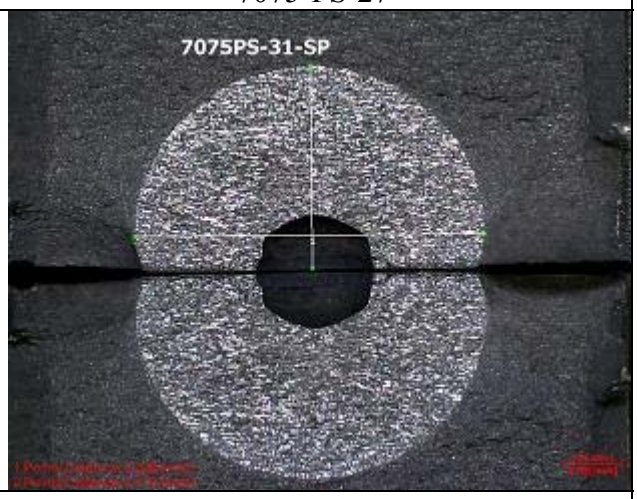
7075-PS-28	7075-PS-31
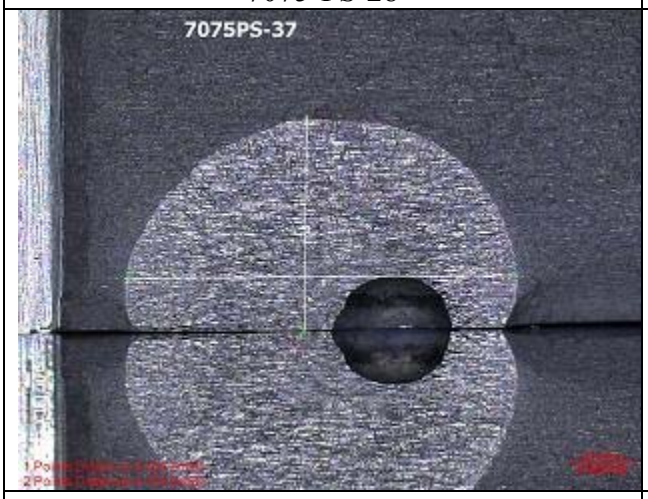	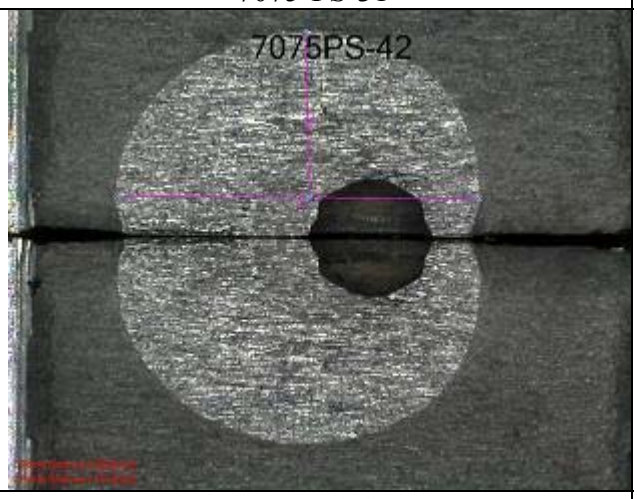
7075-PS-37	7075-PS-42
	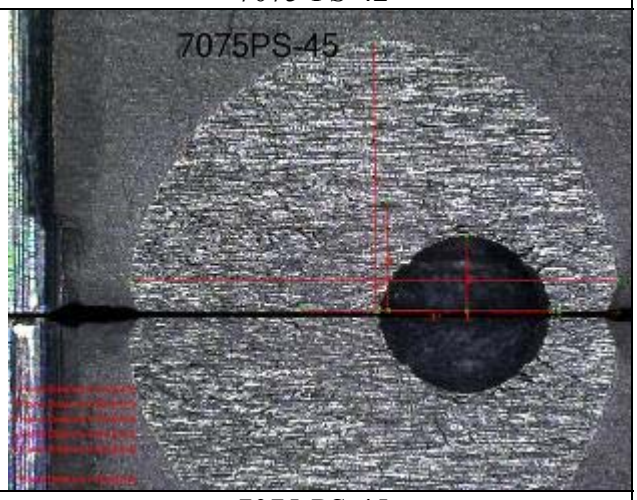
7075-PS-44	7075-PS-45

Figure A-2. Photographs of 7075 Unpeened, $R = 0.7$ (Continued)

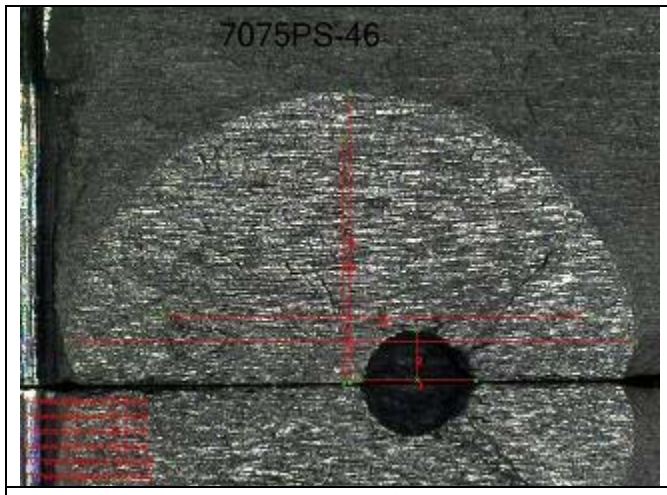	
7075-PS-46	

Figure A-2. Photographs of 7075 Unpeened, $R = 0.7$ (Continued)

7075-PS-SP-5	7075-PS-SP-6
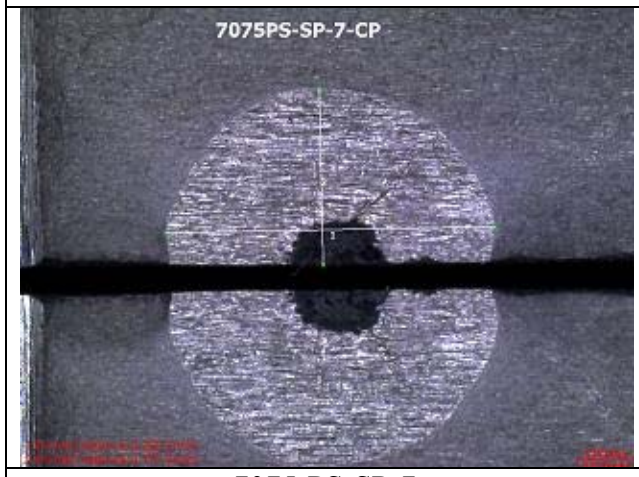	
7075-PS-SP-7	7075-PS-SP-10

Figure A-3. Photographs of 7075 Shot Peened, $R = 0.1$

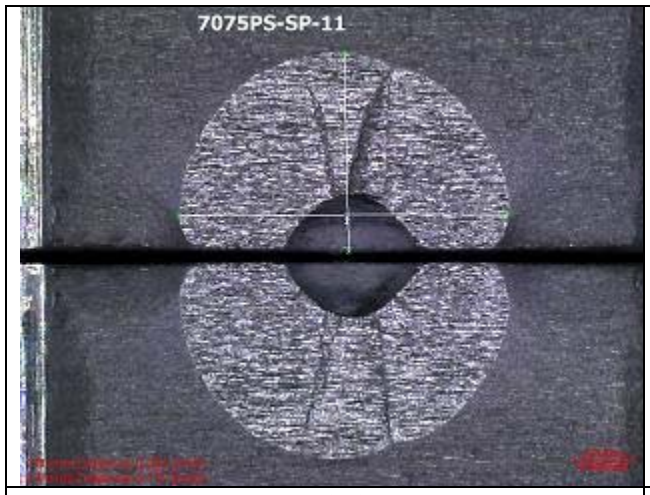	
7075-PS-SP-11	7075-PS-SP-12
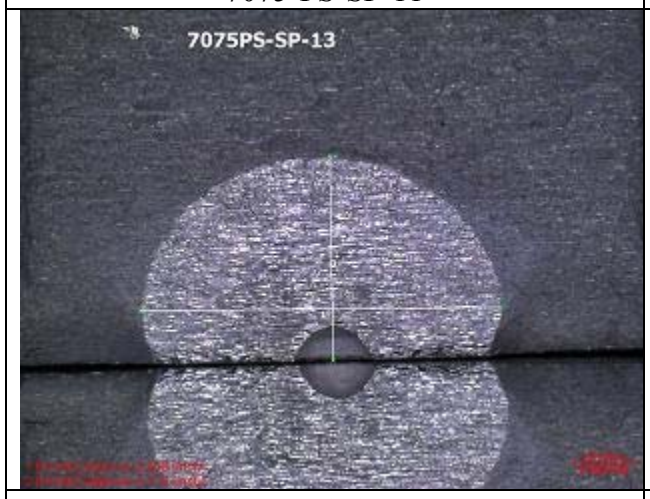	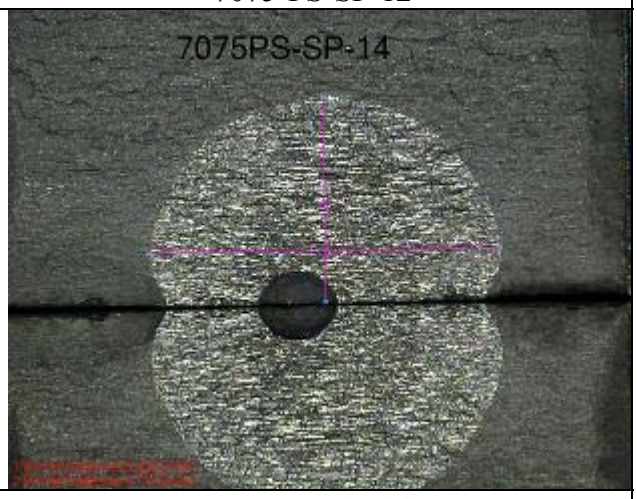
7075-PS-SP-13	7075-PS-SP-14
No Photograph 7075-PS-SP-15, -16	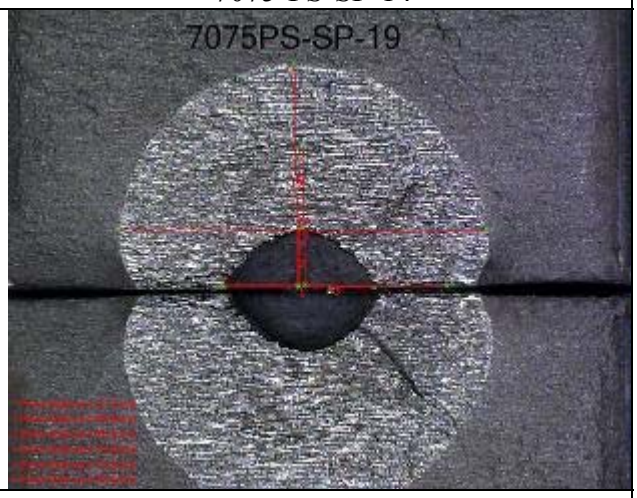
	7075-PS-SP-19

Figure A-3. Photographs of 7075 Shot Peened, $R = 0.1$ (Continued)

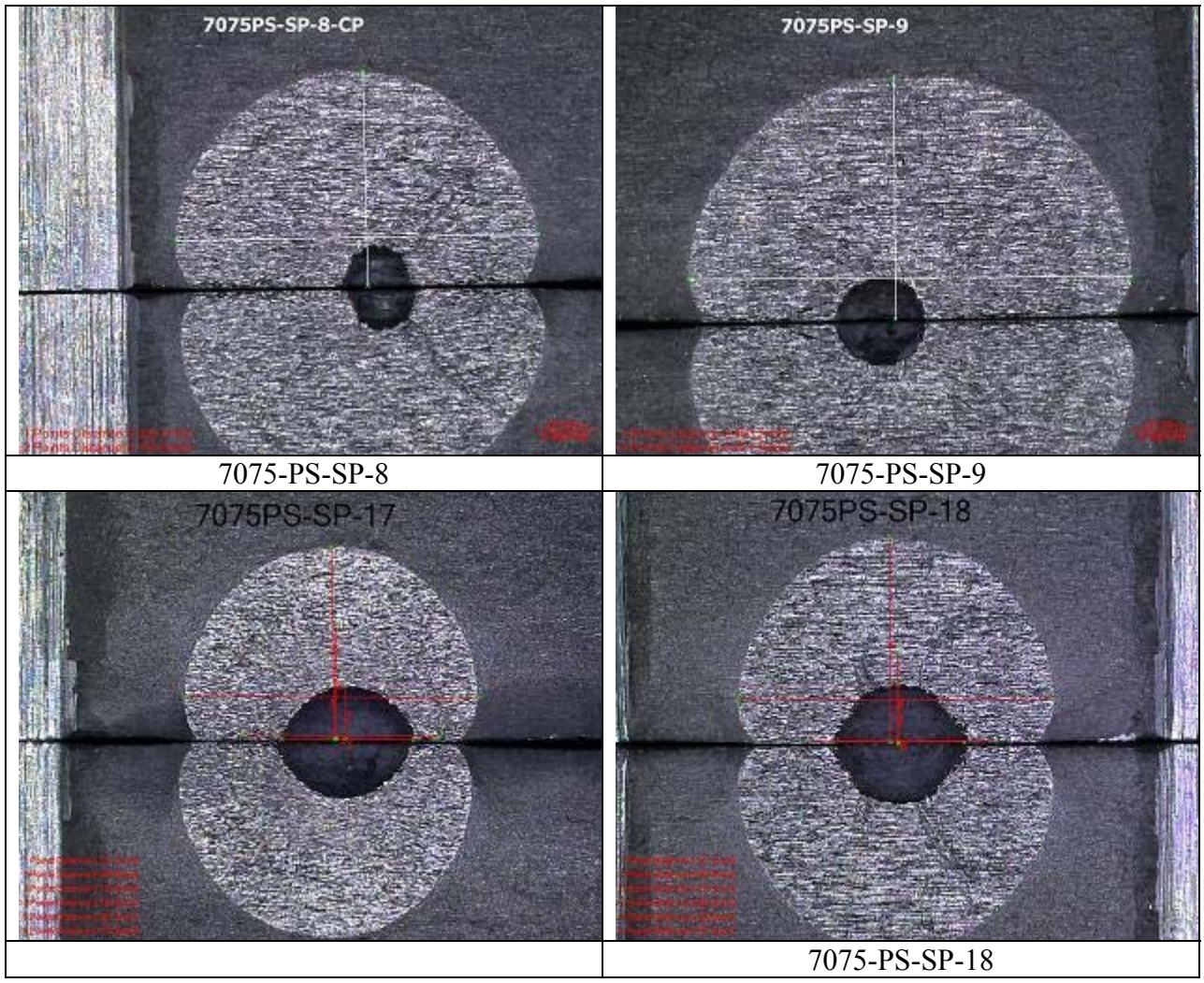

Figure A-4. Photographs of 7075 Shot Peened, $R = 0.7$

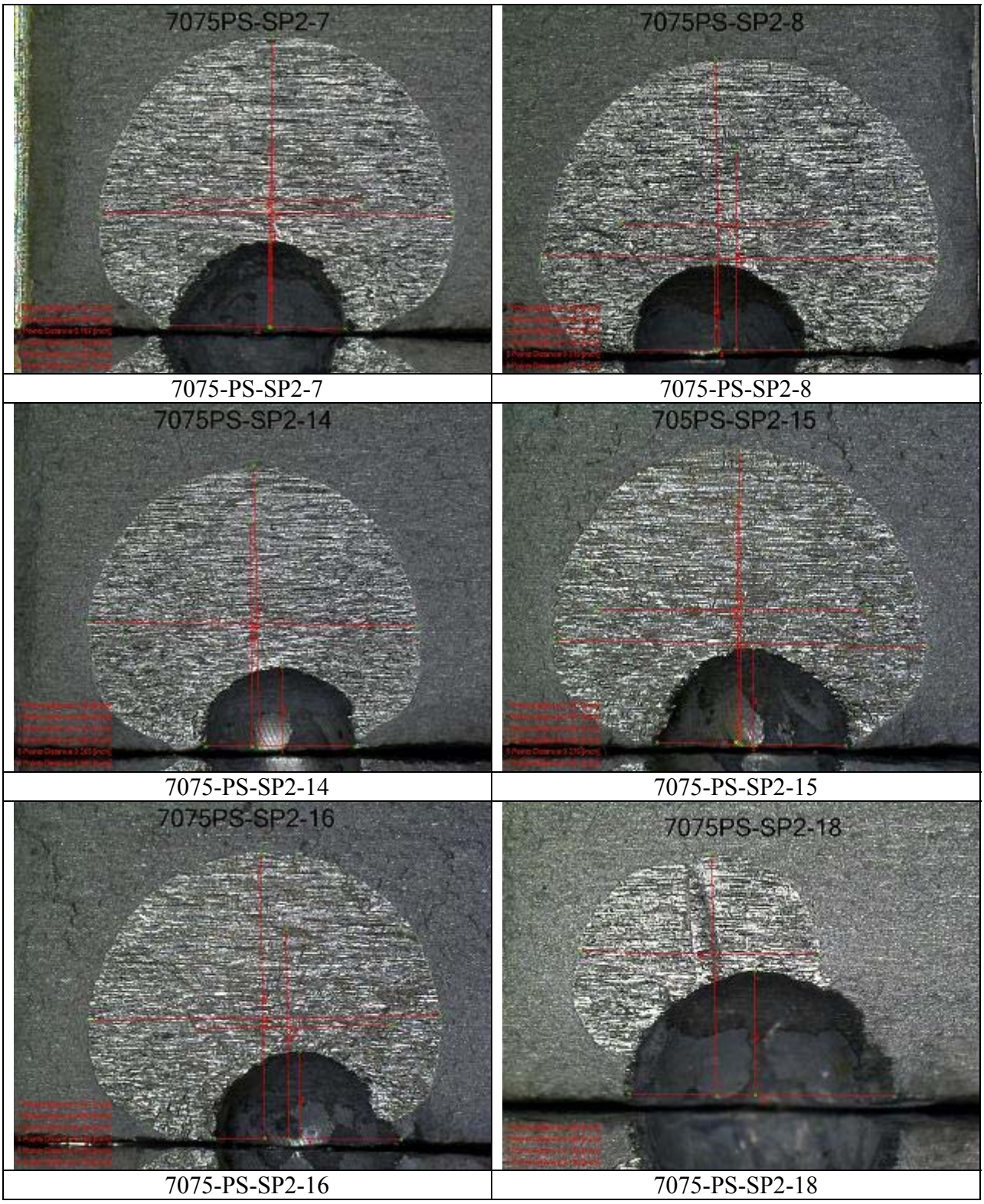

Figure A-5. Photographs of 7075 Heavy Peened, $R = 0.1$

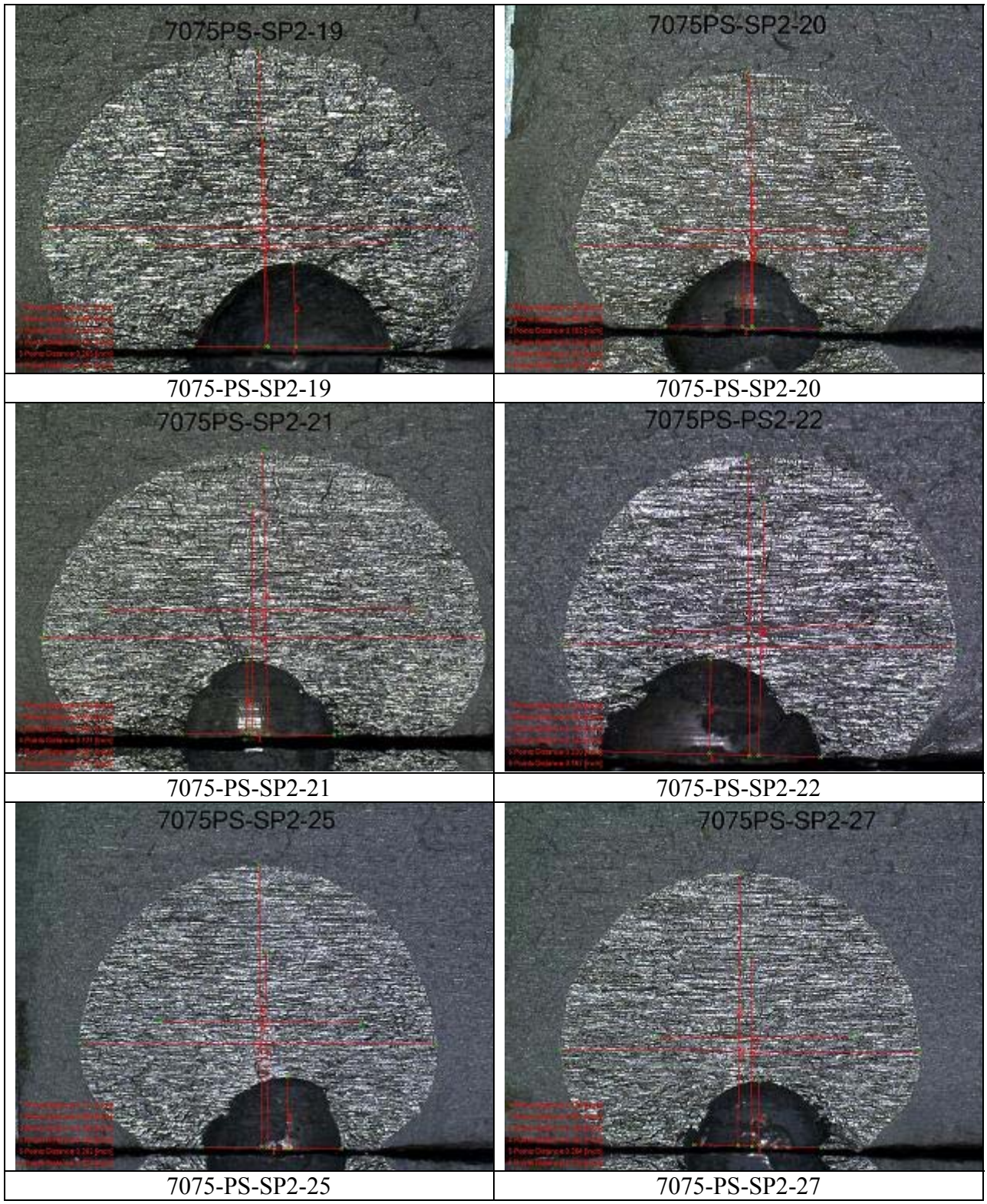

Figure A-5. Photographs of 7075 Heavy Peened, $R = 0.1$ (Continued)

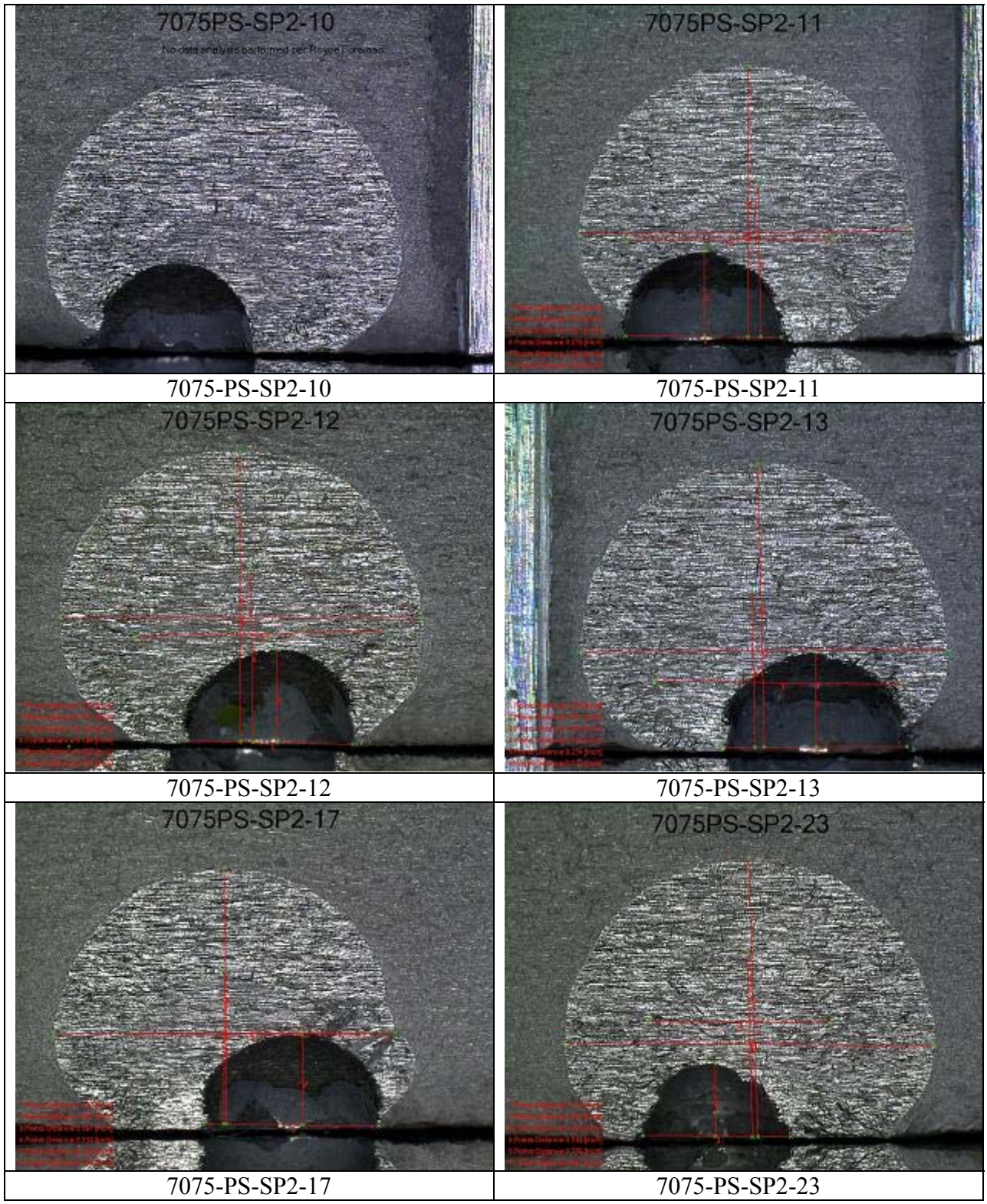

Figure A-6. Photographs of 7075 Heavy Peened, $R = 0.7$

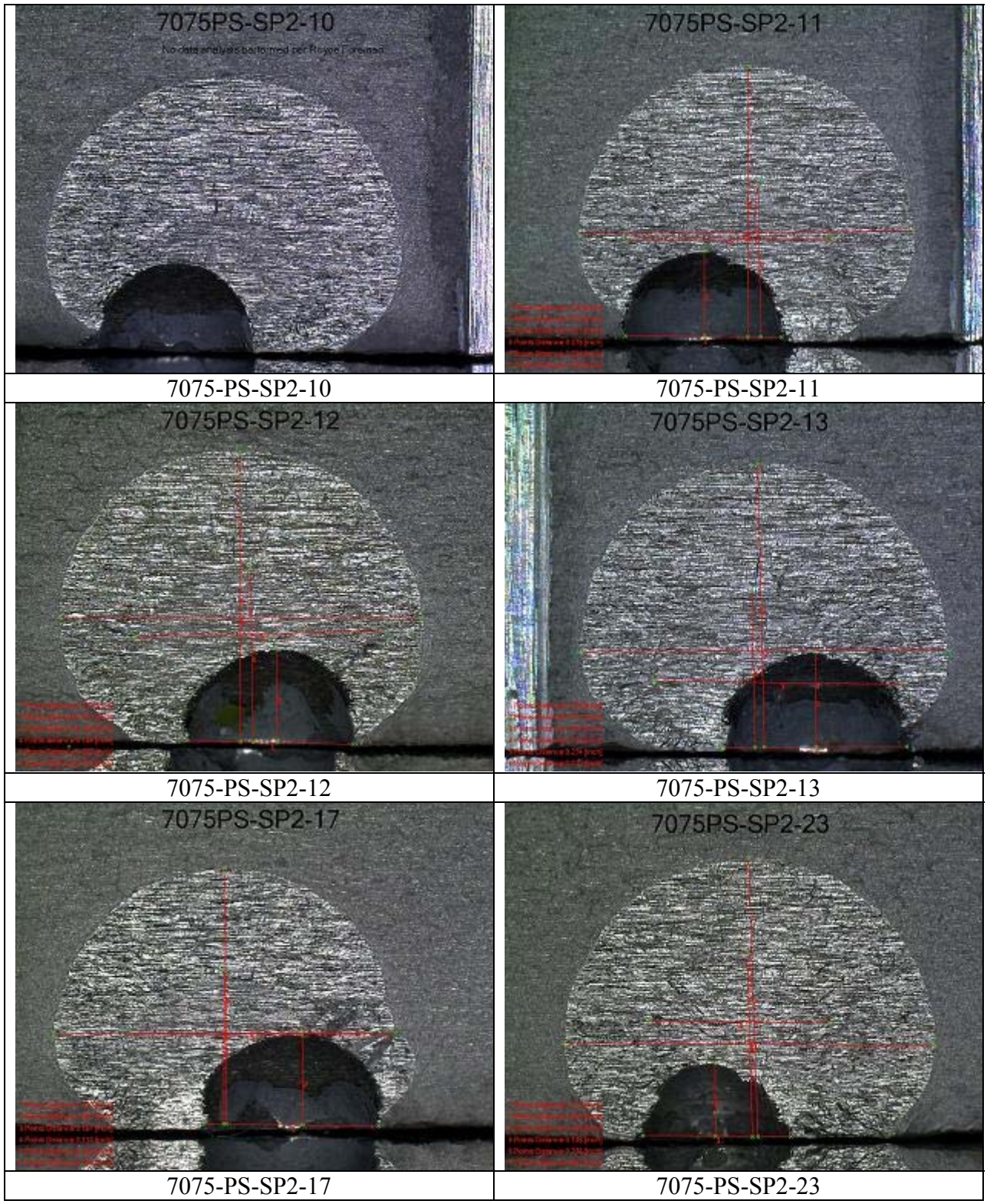

7075-PS-SP2-10	7075-PS-SP2-11
7075-PS-SP2-12	7075-PS-SP2-13
7075-PS-SP2-17	7075-PS-SP2-23

Figure A-6. Photographs of 7075 Heavy Peened, $R = 0.7$ (Continued)

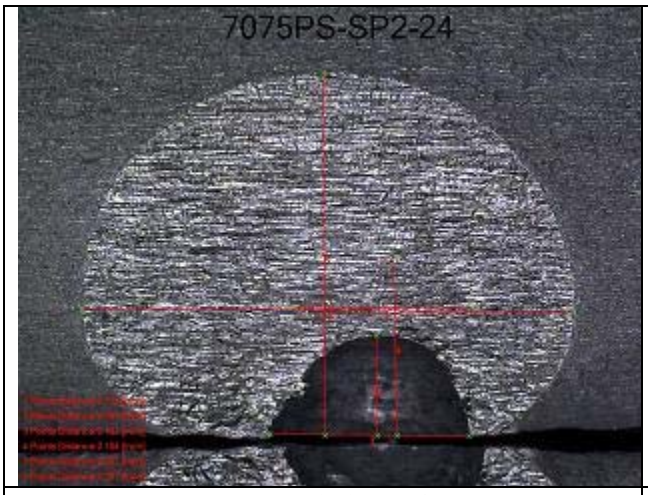

7075-PS-SP2-24

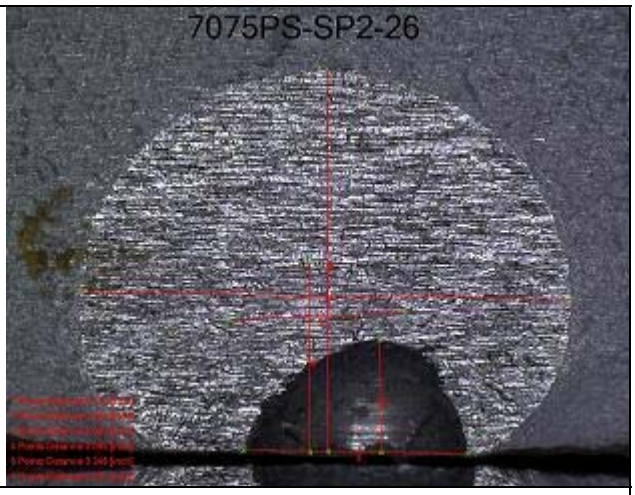

7075-PS-SP2-26

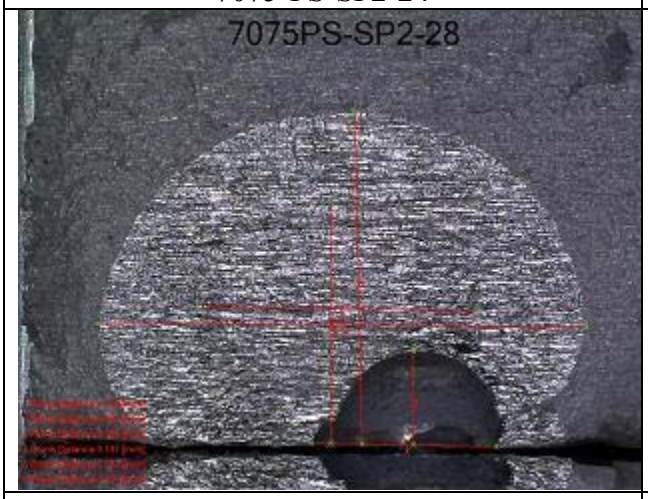

7075-PS-SP2-28

Figure A-6. Photographs of 7075 Heavy Peened, $R = 0.7$ (Continued)

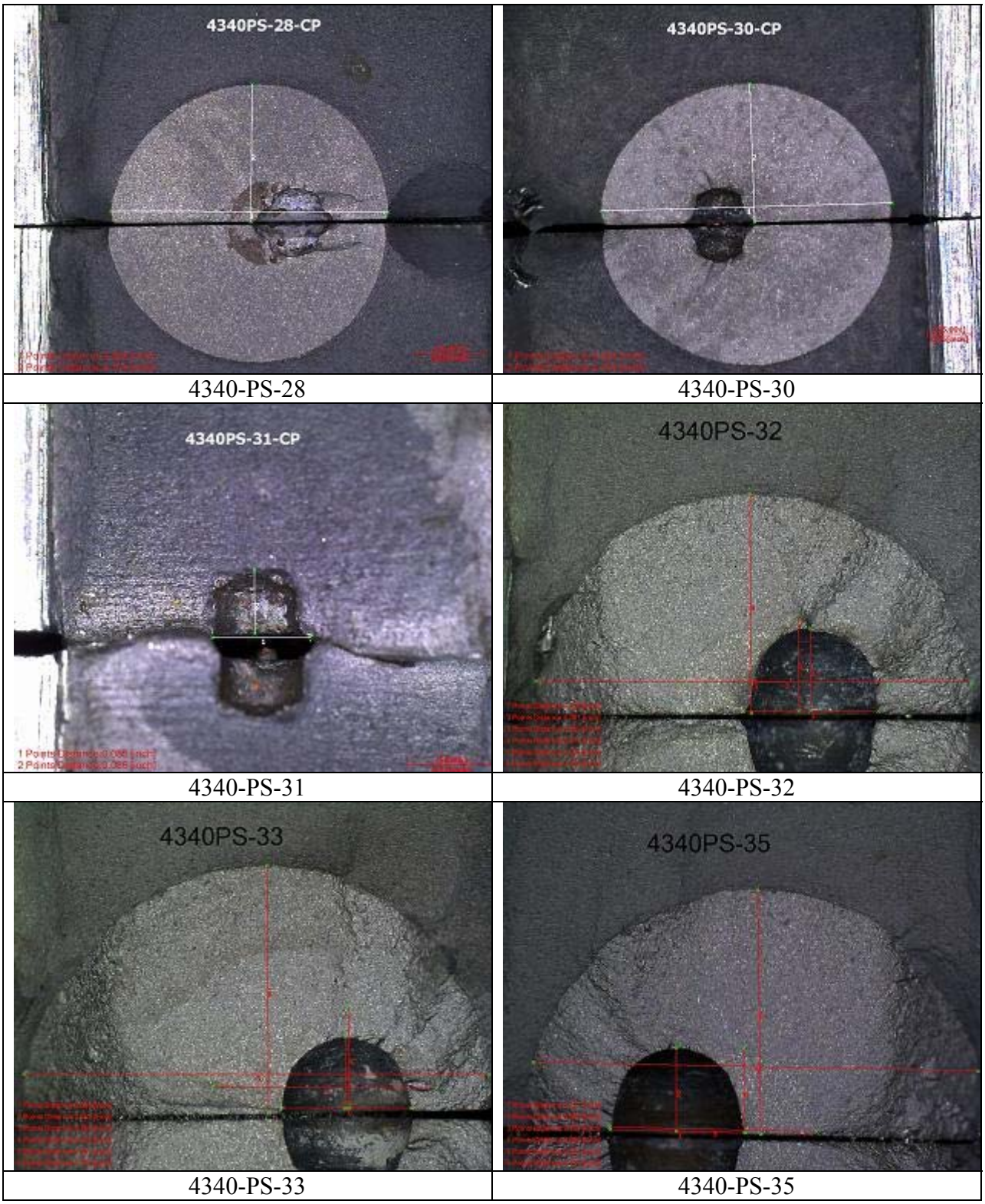

4340-PS-28	4340-PS-30
4340-PS-31	4340-PS-32
4340-PS-33	4340-PS-35

Figure A-7. Photographs of Bare 4340 Steel, $R = 0.1$

4340-PS-37

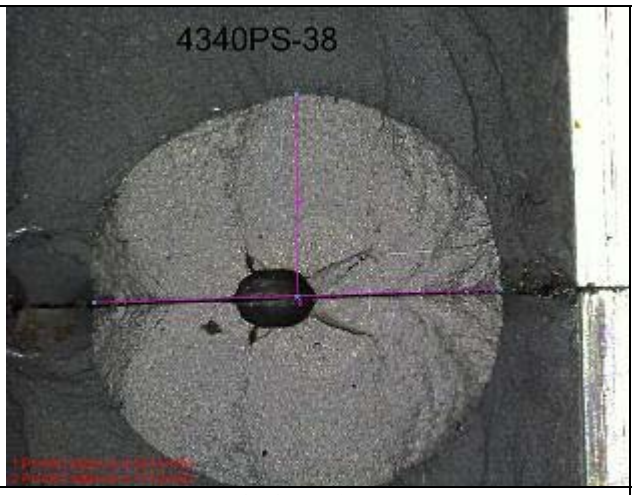

4340-PS-38

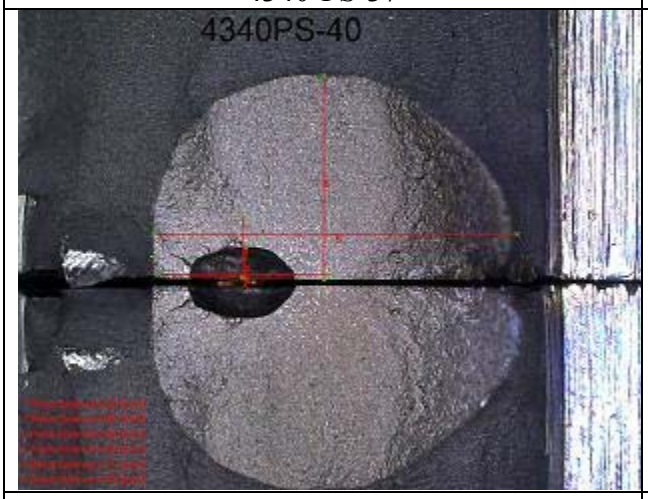

4340-PS-40

Figure A-7. Photographs of Bare 4340 Steel, $R = 0.1$ (Continued)

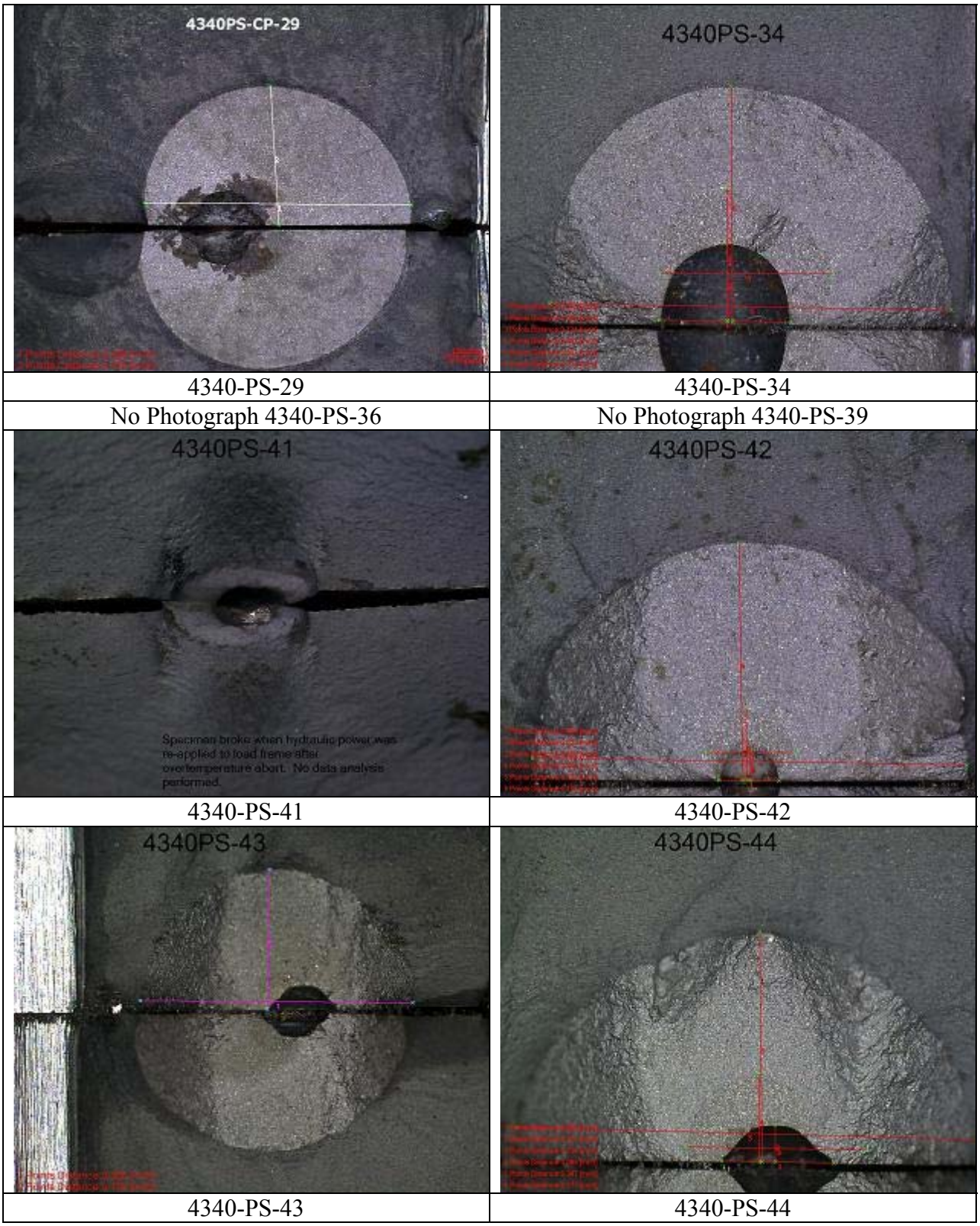

4340-PS-29	4340-PS-34
No Photograph 4340-PS-36	No Photograph 4340-PS-39
4340-PS-41	4340-PS-42
4340-PS-43	4340-PS-44

Figure A-8. Photographs of Bare 4340 Steel, $R = 0.7$

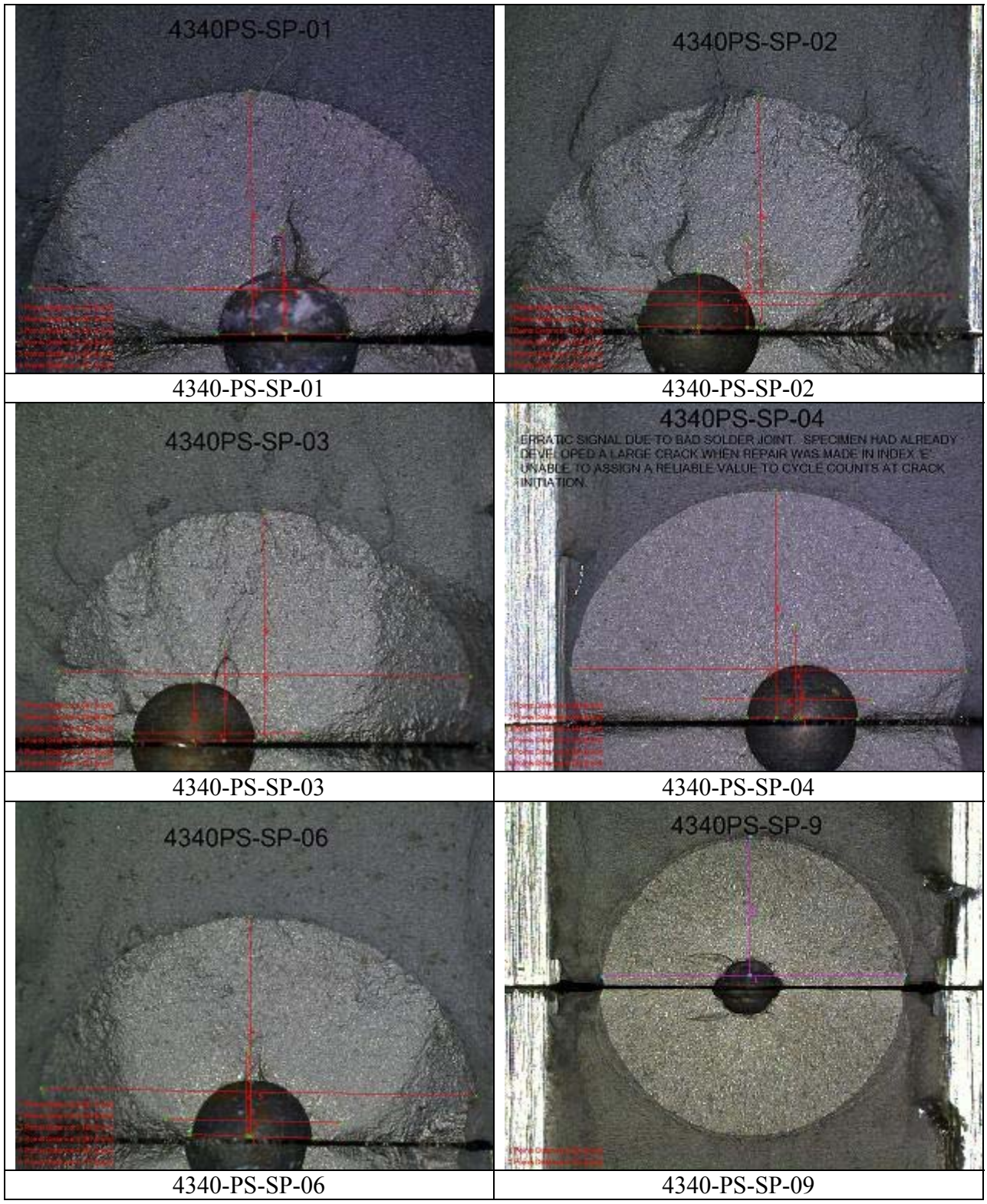

4340-PS-SP-01	4340-PS-SP-02
4340-PS-SP-03	4340-PS-SP-04
4340-PS-SP-06	4340-PS-SP-09

Figure A-9. Photographs of Shot-Peened 4340 Steel, $R = 0.1$

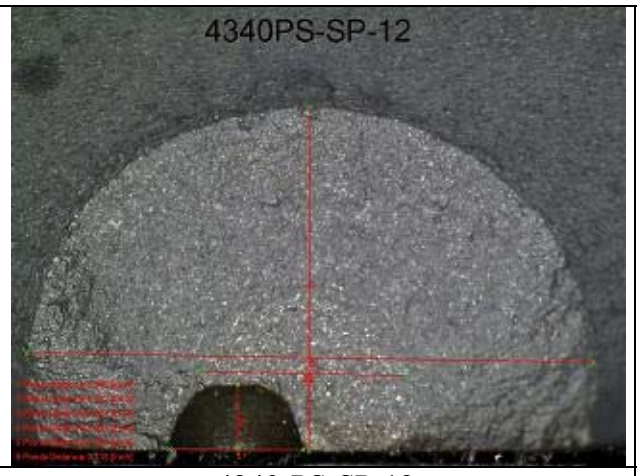

4340-PS-SP-11	4340-PS-SP-12
No Photograph 4340-PS-SP-13	

Figure A-9. Photographs of Shot-Peened 4340 Steel, $R = 0.1$ (Continued)

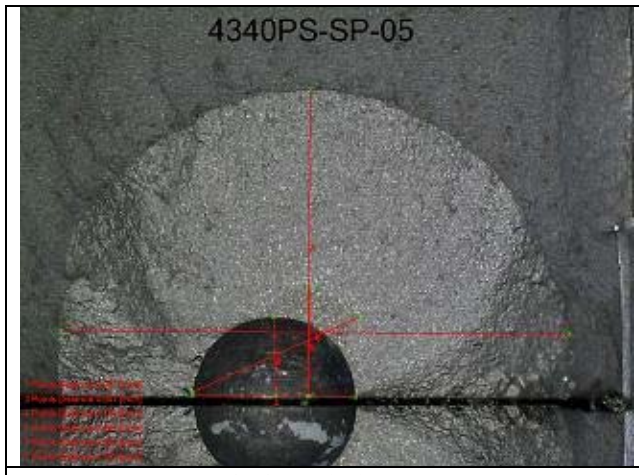

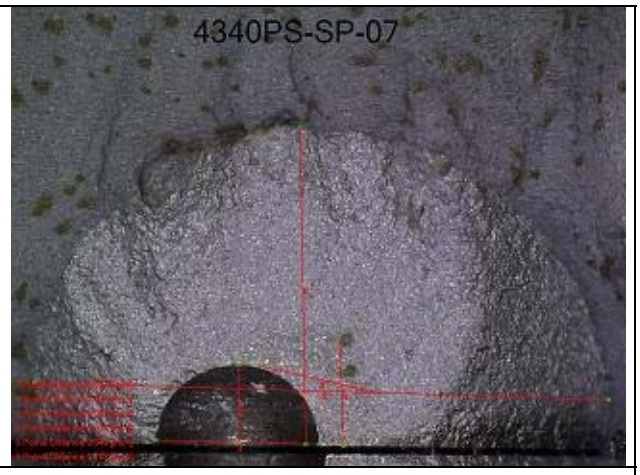

4340-PS-SP-05	4340-PS-SP-07

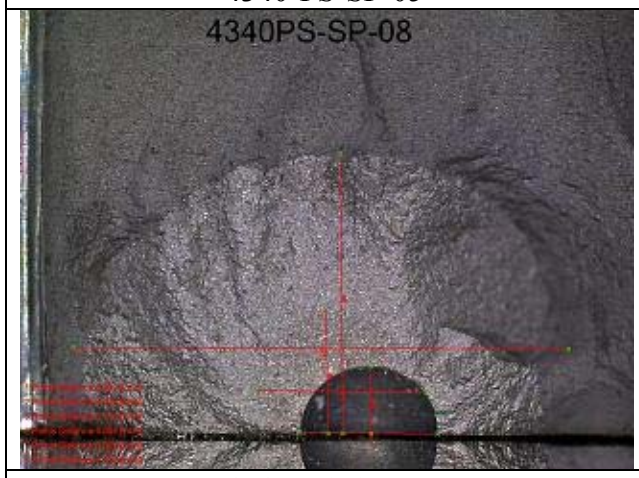

4340-PS-SP-08	4340-PS-SP-10

Figure A-10. Photographs of Shot-Peened 4340 Steel, $R = 0.7$

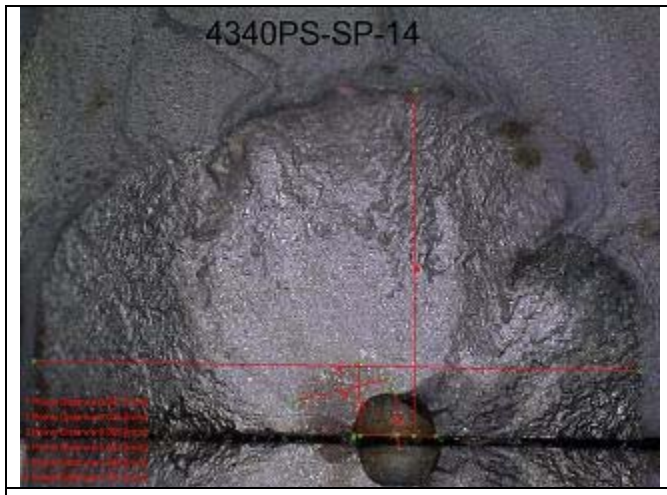	
4340-PS-SP-14	

Figure A-10. Photographs of Shot-Peened 4340 Steel, $R = 0.7$ (Continued)

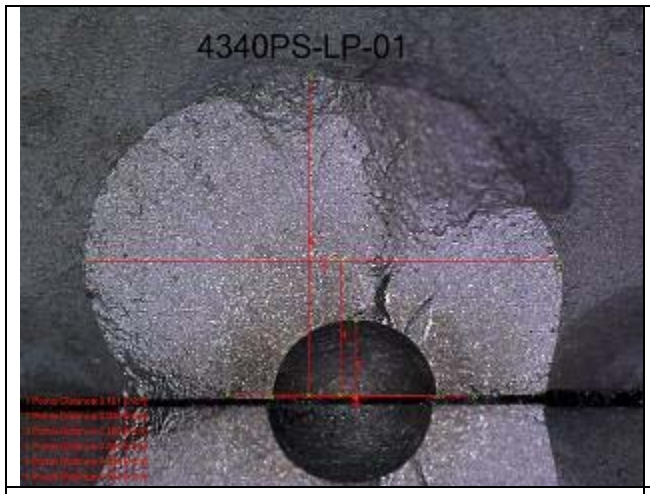	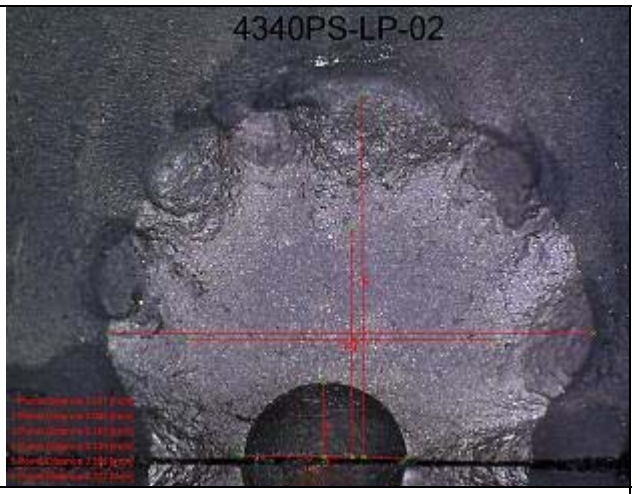
4340-PS-LP-01	4340-PS-LP-02
No Photograph 4340-PS-LP-03	No Photograph 4340-PS-LP-08
No Photograph 4340-PS-LP-09	

Figure A-11. Photographs of Laser-Peened 4340 Steel, $R = 0.1$

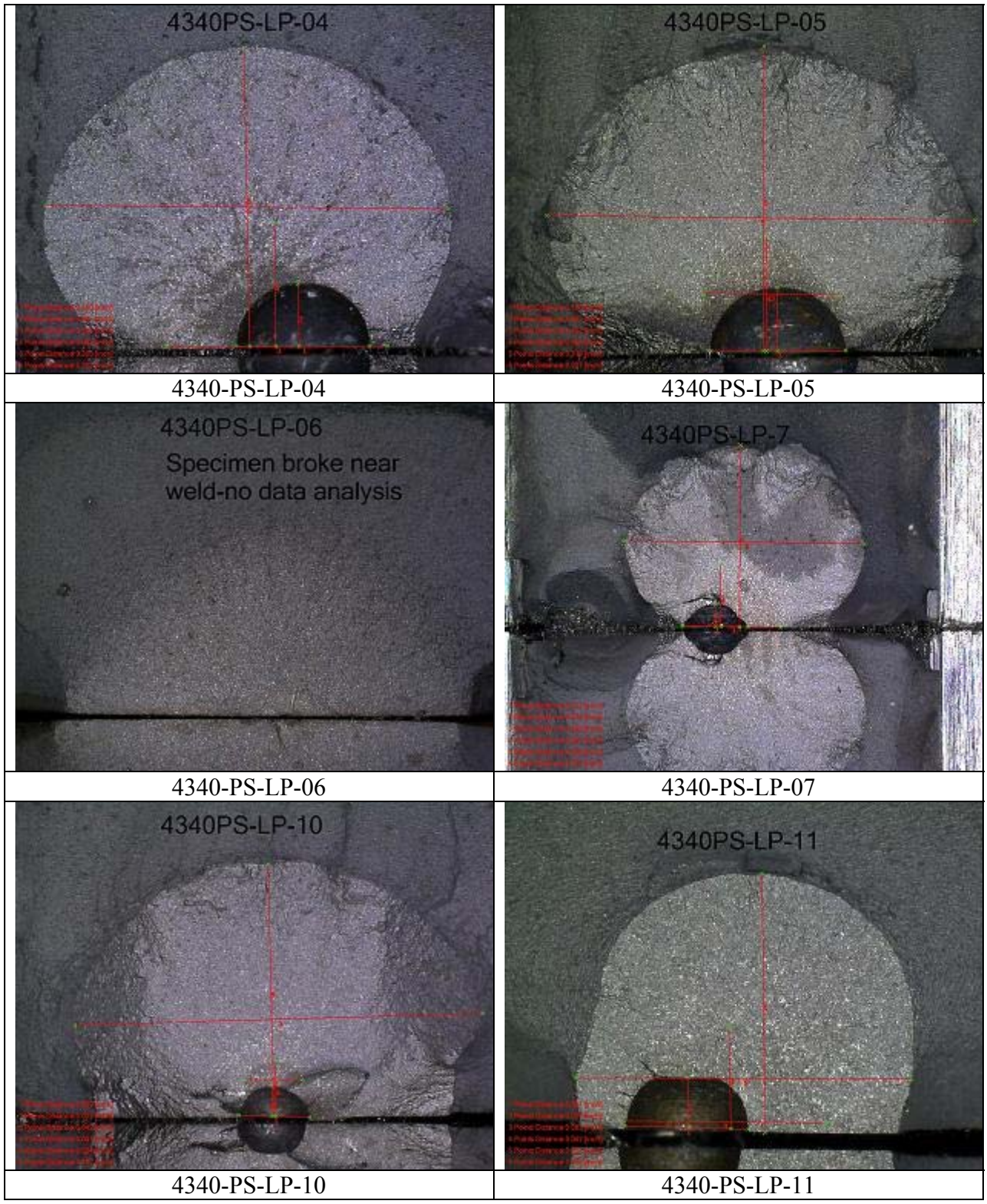

Figure A-12. Photographs of Laser-Peened 4340 Steel, $R = 0.7$

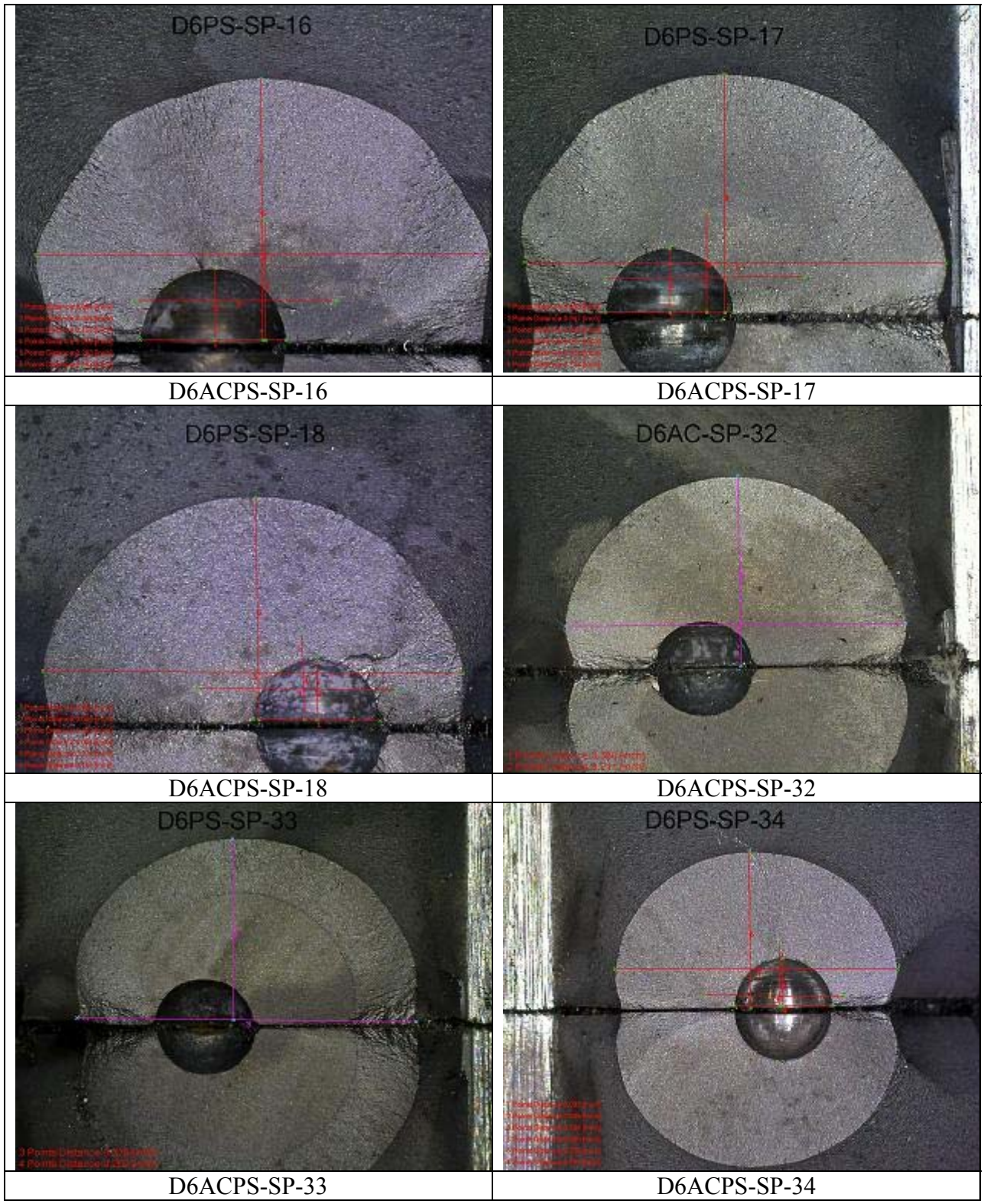

Figure A-13. Photographs of Shot-Peened D6AC Steel, $R = 0.1$

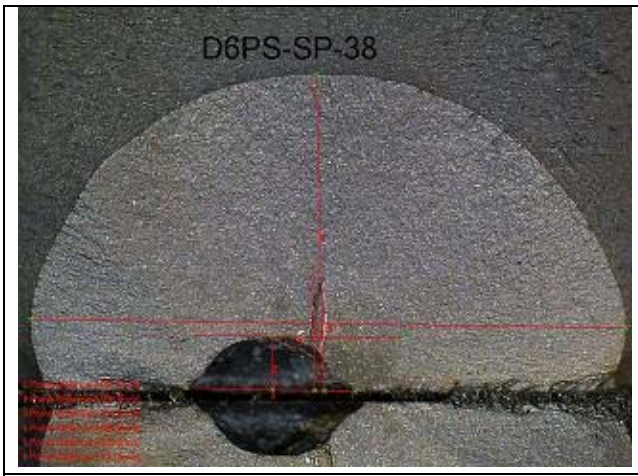	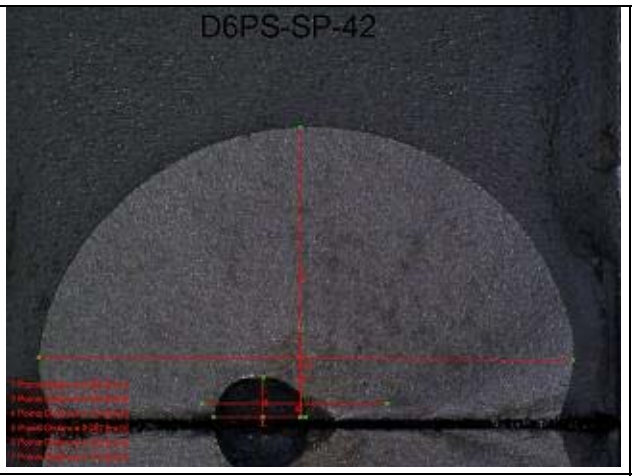
D6ACPS-SP-38	D6ACPS-SP-42

Figure A-13. Photographs of Shot-Peened D6AC Steel, $R = 0.1$ (Continued)

No Photograph D6ACPS-SP-14	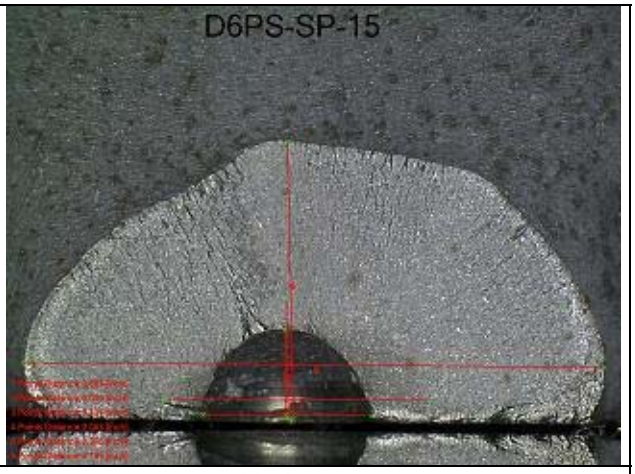
	D6ACPS-SP-15
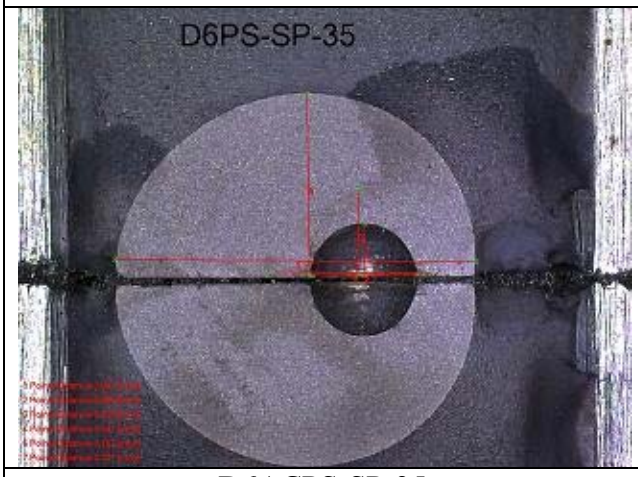	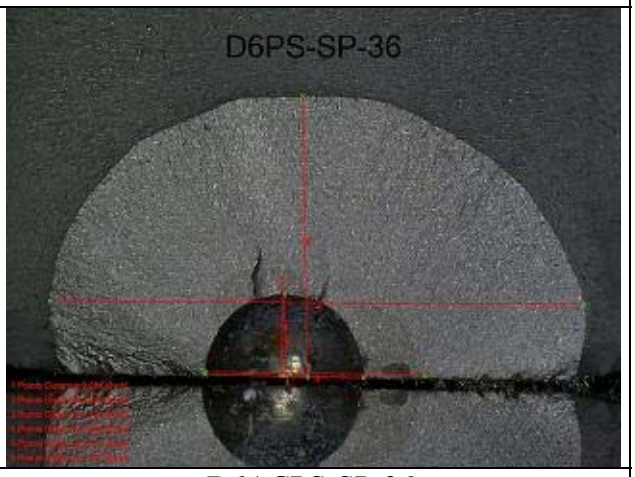
D6ACPS-SP-35	D6ACPS-SP-36

Figure A-14. Photographs of Shot-Peened D6AC Steel $R = 0.7$

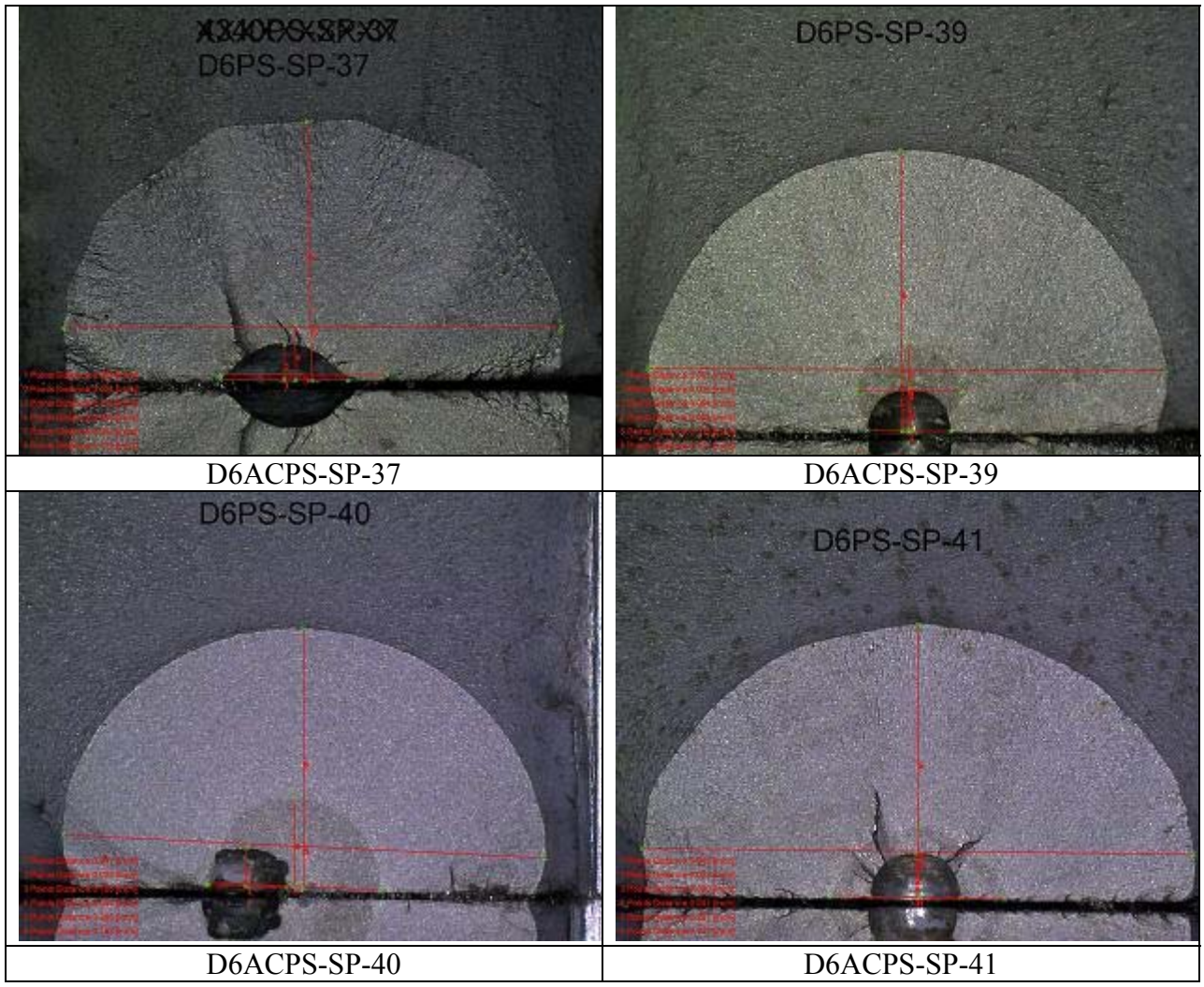

D6ACPS-SP-37	D6ACPS-SP-39
D6ACPS-SP-40	D6ACPS-SP-41

Figure A-14. Photographs of Shot-Peened D6AC Steel, R = 0.7 (Continued)

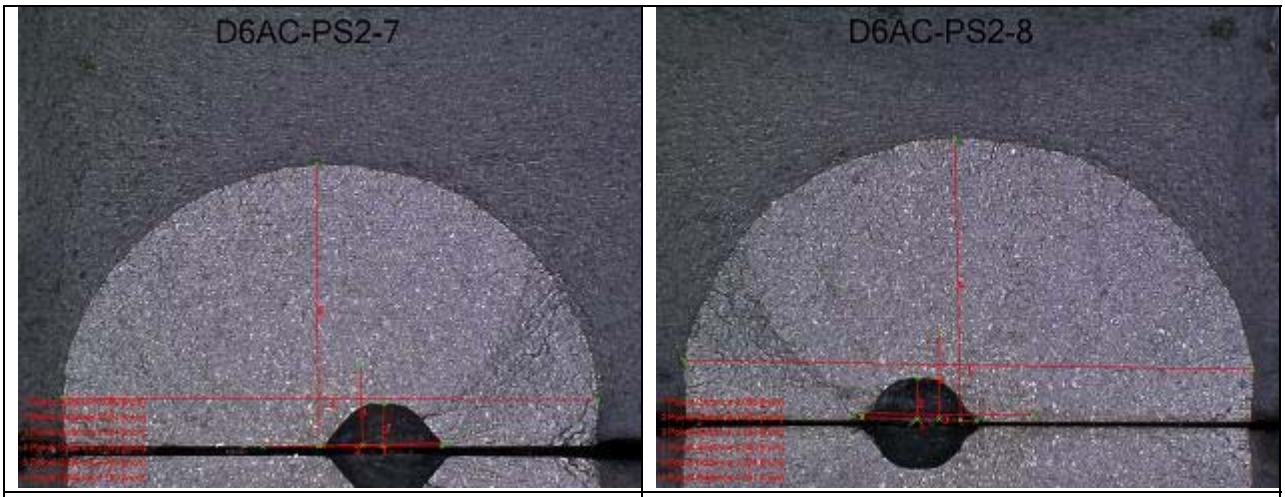

D6AC-PS2-7

D6AC-PS2-8

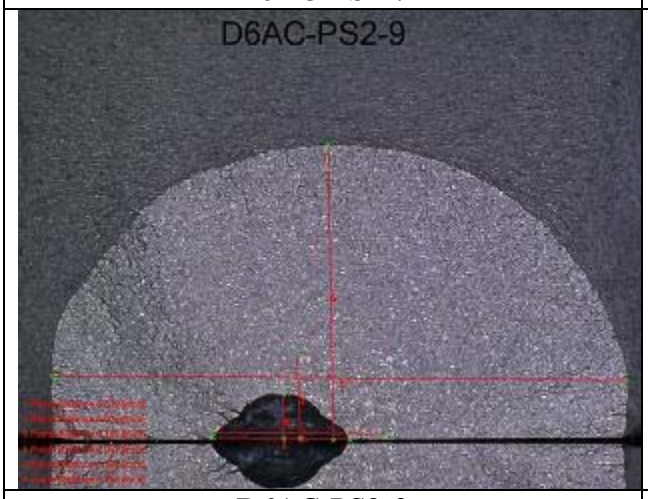

D6AC-PS2-9

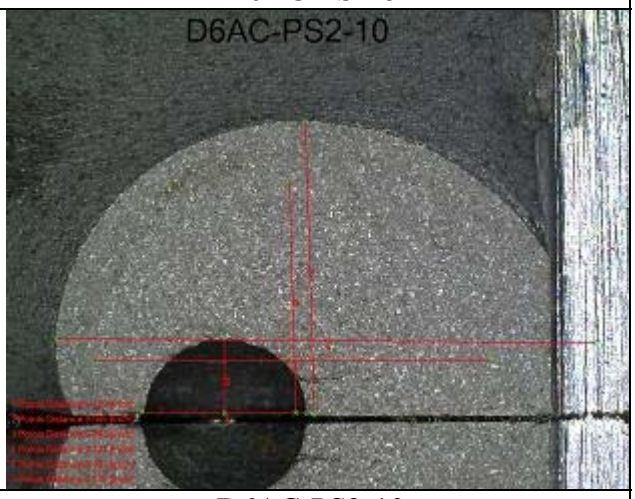

D6AC-PS2-10

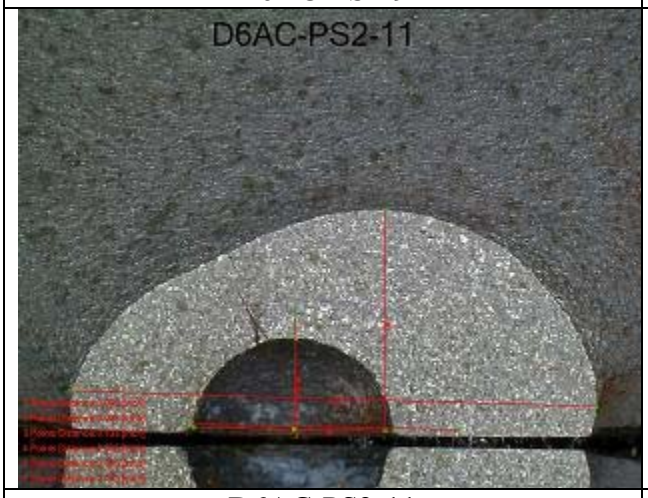

D6AC-PS2-11

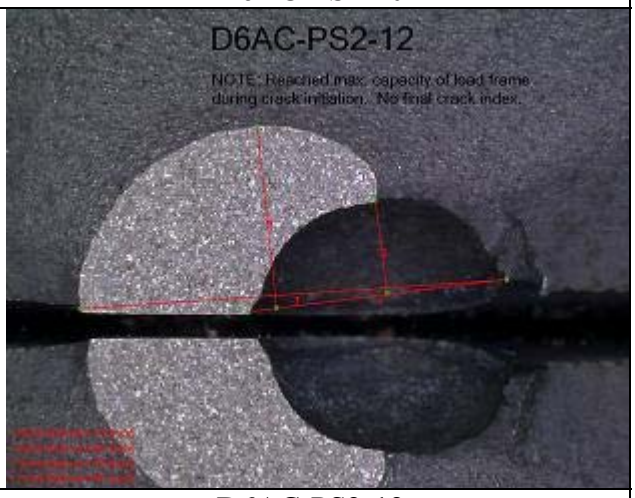

D6AC-PS2-12

Figure A-15. Photographs of Bare D6AC Steel, $R = 0.1$

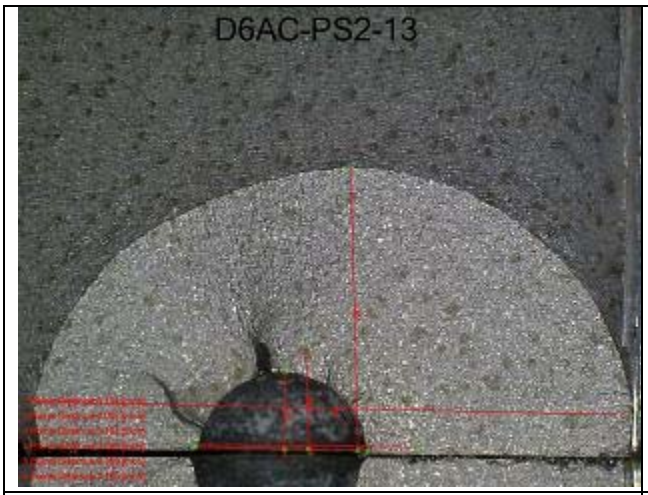

D6AC-PS2-13

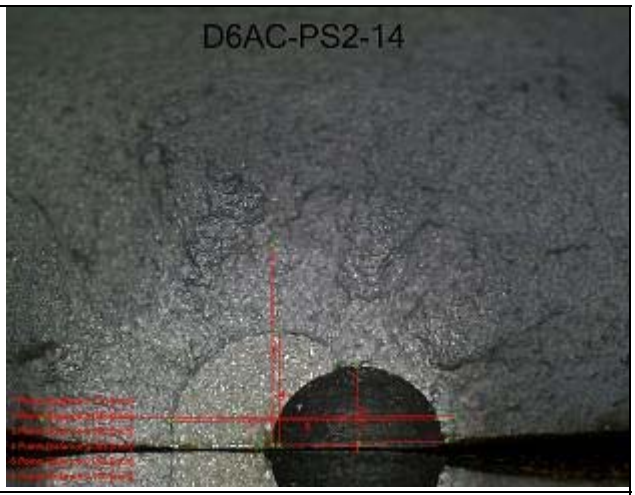

D6AC-PS2-14

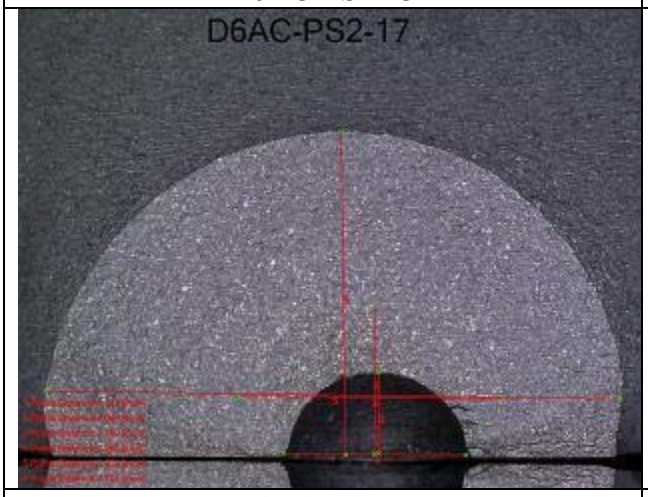

D6AC-PS2-17

Figure A-15. Photographs of Bare D6AC Steel, $R = 0.1$ (Continued)

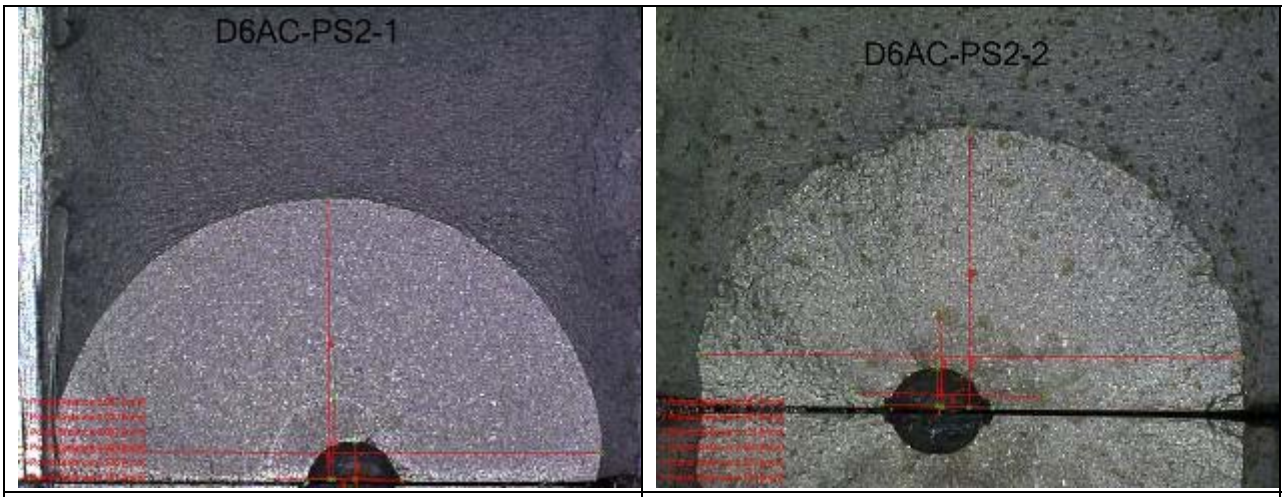

D6AC-PS2-1

D6AC-PS2-2

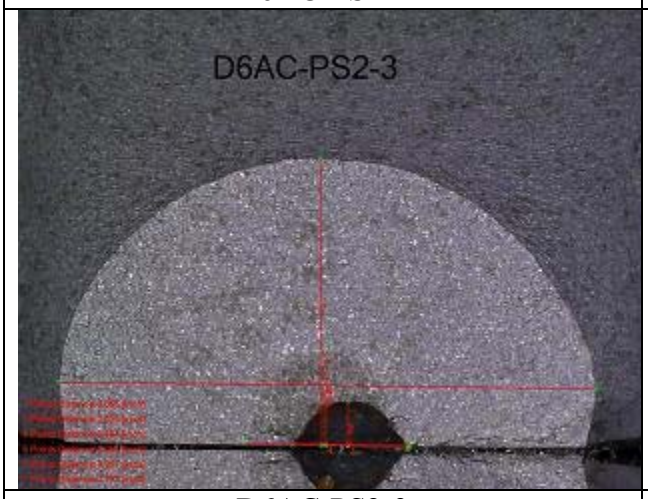

D6AC-PS2-3

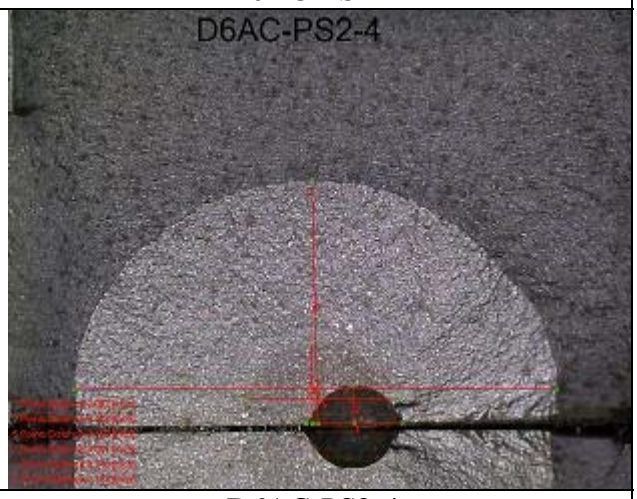

D6AC-PS2-4

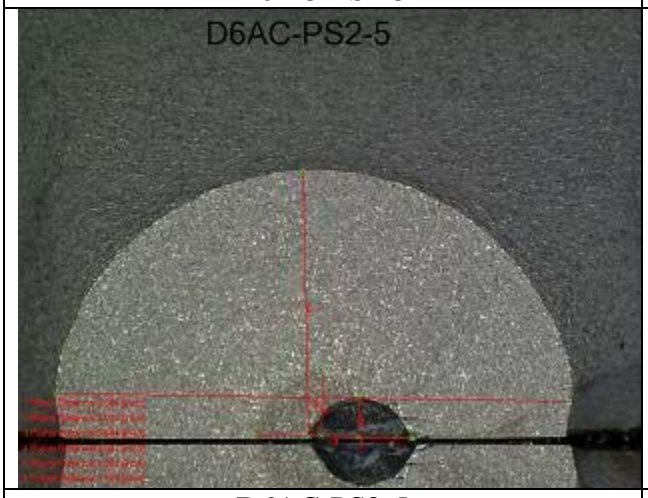

D6AC-PS2-5

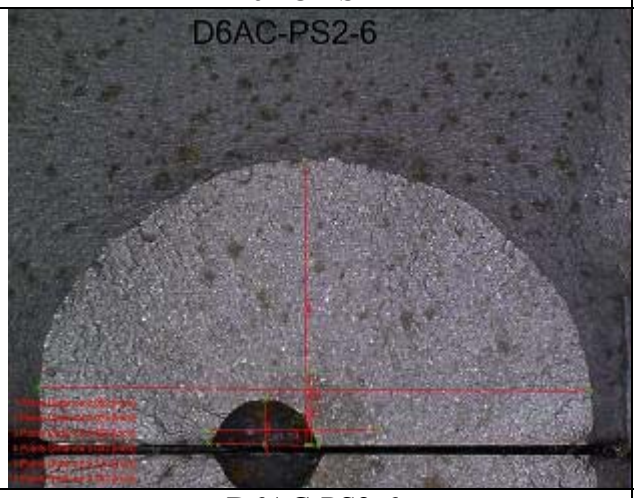

D6AC-PS2-6

Figure A-16. Photographs of Bare D6AC Steel, $R = 0.7$

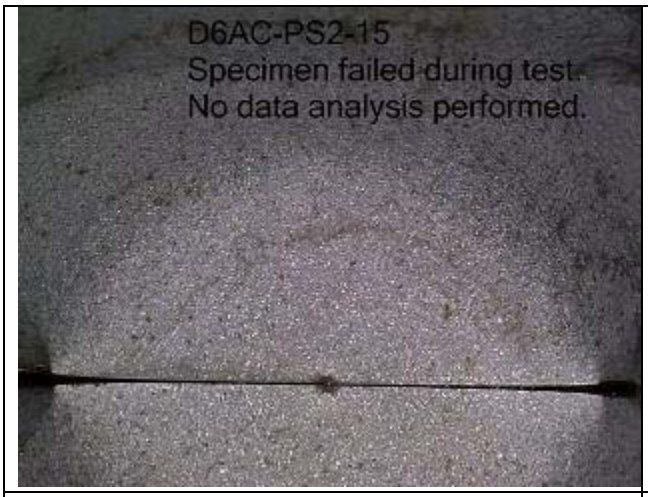

D6AC-PS2-15

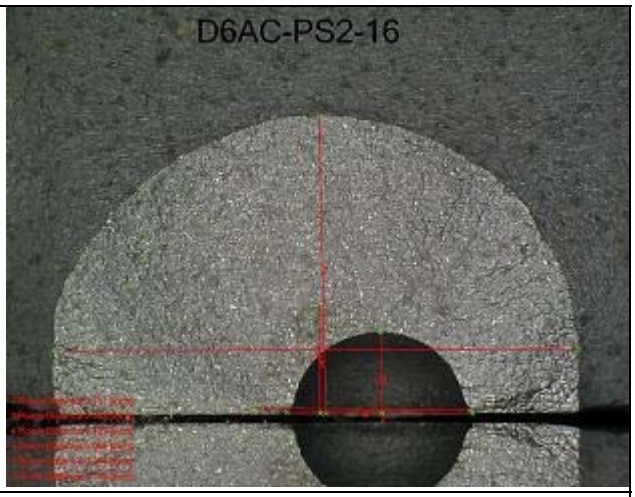

D6AC-PS2-16

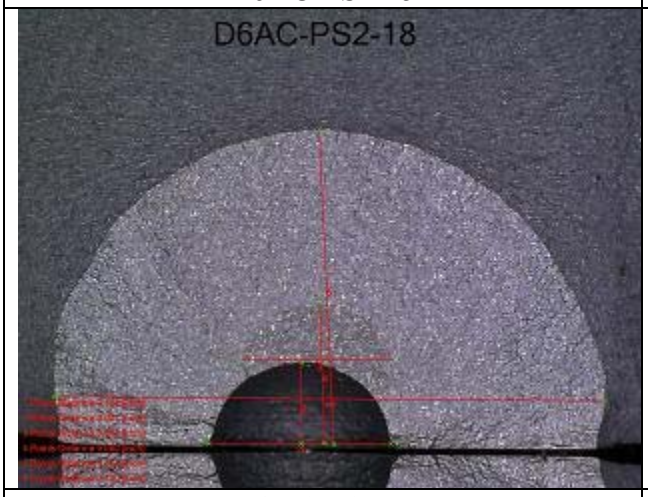

D6AC-PS2-18

Figure A-16. Photographs of Bare D6AC Steel, $R = 0.7$ (Continued)